Sialic acids reduction triggers complement C3-mediated microglial response and bipolar cell loss in the mouse retina

Doctoral thesis

to obtain a doctorate (PhD)

from the Faculty of Medicine

of University of Bonn

German Cuevas Rios

From Jalisco, Mexico

2025

Written with authorization of

the Faculty of Medicine of University of Bonn

First reviewer: Prof. Dr. Harald Neumann

Second reviewer: Prof. Dr. Herbert Hildebrandt

Day of oral examination: 17.12.2024

From the Institute of Reconstructive Neurobiology

Director: Prof. Dr. Oliver Brüstle

Table of Contents

List of abbreviations

AD	Alzheimer's disease
Aif1	Allograft inflammatory factor 1
AMD	Age-related macular degeneration
ANOVA	Analysis of Variance
ATP	Adenosine triphosphate
Brn3a	Brain-specific homeobox/POU domain protein 3A
BSA	Bovine serum albumin
C1q	Complement component 1 with q subcomponent
C3	Complement component 3
C4	Complement component 4
Casp-3, -8	Caspase 3, and 8
CD68	Cluster of differentiation 68, lysosomal associated membrane protein
CFB	Complement factor B
CFH	Complement factor H
CNS	Central nervous system
Col4a2	Collagen type IV alpha 2 chain
Col5a2	Collagen type V alpha 2 chain
Col6a3	Collagen type VI alpha 3 chain
Col16a1	collagen type XVI alpha 1 chain
CR3	Complement receptor 3
CT	Cycle threshold
Cy3	Cyanine 3
Cyba	Cytochrome B-245 alpha chain
Cybb	Cytochrome B-245 beta chain
DAPI	4',6-diamidino-2-phenylindole
ddH2O	Double-distilled water
DEGs	Differentially expressed genes
DEPC	Diethylpyrocarbonate
Derl3	Der1-like domain family, member 3

EMT	Epithelial–mesenchymal transition
EVs	Extracellular vesicles
FDR	False discovery rate
FC	Fold change
GAPDH	Glyceraldehyde-3-phosphate dehydrogenase
GCL	Ganglion cell layer
GFAP	Glial fibrillary acidic protein
GNE	UDP-N-acetylglucosamine-2-epimerase/N-acetylmannosamine kinase
GSEA	Gene set enrichment analysis
H2-eb1	Histocompatibility 2, class II antigen E beta
Iba1	Ionized calcium binding adaptor molecule 1
IHC	Immunohistochemistry
Il-1β	Interleukin 1 beta
INL	Inner nuclear layer
IPL	Inner plexiform layer
ITAM	Immunoreceptor tyrosine-based activation motif
Itgam	Integrin alpha M
ITIM	Immunoreceptor tyrosine-based inhibitory motif
Lcp1	Lymphocyte cytosolic protein 1
LPS	Lipopolysaccharide
NCAM	Cell-adhesion molecule
Neu	Neuraminic acid
Neu5Ac	N-acetylneuraminic acid
Neu5Gc	N-glycolylneuraminic acid
NF-KB	Nuclear factor kappa-light-chain-enhancer
NGS	Normal goat serum
NLRP3	NLR family pyrin domain containing 3
NOX2	NADPH oxidase 2
ns.	Not significant
ONL	Outer nuclear layer

OPL	Outer plexiform layer
Opn1sw	Opsin 1, short wave sensitive
P2ry10b	Purinergic receptor P2Y, G-protein coupled 10B
PBS	Phosphate buffer solution
PCA	Principal component analysis
PCR	Polymerase chain reaction
PFA	Paraformaldehyde
Pik3cd	Phosphatidylinositol 4,5-bisphosphate 3-kinase catalytic subunit delta isoform
PKCα	Protein kinase C alpha
PolySia	Polysialic acid
POS	Photoreceptors outer segments
PSA-NCAM	Polysialylated cell-adhesion molecule
RGC	Retinal ganglion cell
ROS	Reactive oxygen species
RPE	Retinal pigment epithelium
SEM	Standard error of the mean
SIGLECs	Sialic acid-binding immunoglobulin-like lectins
SHP	Src homology 2 domain-containing protein tyrosine phosphatases
SD	Standard deviation
STAT3	Signal transducer and activator of transcription 3
sqRT-PCR	Semi-quantitative real-time polymerase chain reaction
Tmem119	Transmembrane protein 119
Tnf	Tumor necrosis factor
TREM2	Triggering receptor expressed on myeloid cells 2
VEGF	Vascular endothelial growth factor
Vsx2	Visual system homeobox 2
WT	Wildtype

1. Introduction

1.1 Sialic acids

Sialic acids are negatively charged sugars that belong to an extensive family of 9-carbon backbone sugars. These sugars play important role in biological functions (Traving & Schauer, 1998). Sialic acids are usually found as the sugar component at the terminal branch of glycans in glycosphingolipids and glycoproteins at the cell surface. The most common types of sialic acids found in mammals (Fig. 1) are the N-acetylneuraminic acid (Neu5Ac), and their related forms with changes in the C-5 carbon, the N-glycolylneuraminic acid (Neu5Gc), and ketodeoxynononic acid (Lewis et al., 2022; Traving & Schauer, 1998).

Although sialic acids are present in humans and other mammals, other organism such as virus and bacteria also have sialic acids (Traving & Schauer, 1998). Increasing evidence suggest that fast evolution of the different glycans classes led to variances in the sialic acid distribution, or in their presence or absence across species (Bauer & Osborn, 2015; L. Deng et al., 2013).

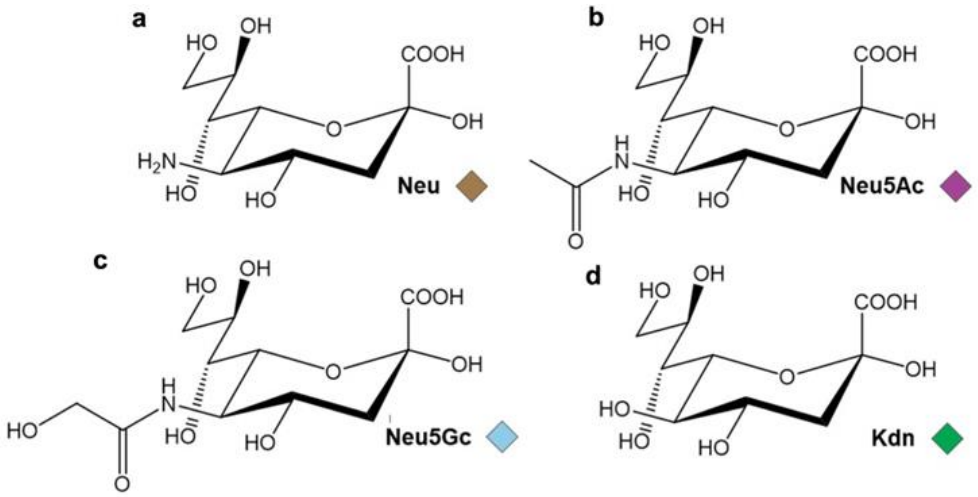

Figure 1. Common sialic acid types. The chemical structures of the four most common sialic acids in mammals are shown. The basic form of sialic acid is N-acetylneuraminic acid (Neu; a). Changes at C-5 carbon position results in N-acetylneuraminic acid (Neu5Ac; b), N-glycolylneuraminic acid (Neu5Gc; c), and ketodeoxynononic acid (Kdn, d). Image taken and modified from (Lewis et al., 2023).

1.2 Sialic acid biosynthesis and functions

The sialic acid synthesis involves several steps that occur in different cell structures, for instance, in the cytosol, nucleus, and Golgi apparatus. Reports suggest that alterations in the sialic acid synthesis and metabolism are related to human diseases, such as sialuria, muscular pathologies, and chronic inflammation associated with incorporation of non-human Neu5Gc into human tissues, a type of sialic acid present mostly in red meat (Y. Li & Chen, 2012; N. M. Varki et al., 2011). The biosynthesis of sialic acid initiates with four steps in the cytosol from the precursor UDP-N-acetylglucosamine. Two of the four cytosolic synthesis steps are catalized by the enzyme UDP-N-acetylglucosamine-2-epimerase/N acetylmannosamine kinase (GNE) (Gagiannis et al., 2007; Horstkorte et al., 1999). The resulting sialic acids are transferred to the nucleus to create the complex Cytidine-5′-monophospho-N-acetylneuraminic acid (CMP-Neu5Ac), which is then transported to the Golgi apparatus and used by sialyltransferases to create glycoconjugates, that are integrated later into the cell surface. These sialic acids incorporated into glycosphingolipids and glycoproteins can be recycled in the lysosomes in physiological conditions, but they also can be removed or degraded by sialidases (reviewed in Bhide & Colley, 2017; Y. Li & Chen, 2012; Schnaar et al., 2014; Traving & Schauer, 1998).

The sialic acids can undergo to different modifications such as methylation, acetylation, sulfation, and lactylation (Angata & Varki, 2002; Y. Li & Chen, 2012; Traving & Schauer, 1998). These sialic acid modifications on glycans provide a wide range of intracellular and extracellular functions. The negative charge and hydrophilicity provide sialic acids with their main functions, for instance, modulatory and structural roles (L. Deng et al., 2013; A. Varki, 2008). In more detail, sialic acids are involved in providing cell membrane stability, binding and transport of molecules, receptor-binding and signalling. In addition, due to their negative charge and hydrophilic hydration shell, sialic acids create a hydration shell that prevents non-specific interactions between neighbouring cells. Sialic acids facilitate cell motility and plasticity while also acting as a mask, covering membrane structures that, without their presence, could be exposed to cell receptors following desialylation by sialidases, also known as neuraminidases (Sato & Kitajima, 2013; A. Varki & Gagneux,

2012). Sialic acids also play important roles in the immune system, because their configuration on glycans can be used as a flag by immune cells to recognize self-structures, or the opposite, to react to pathogens missing the specific sialic acid structure. Sialic acids can be utilized not only by immune cells but also by viruses and bacteria to mimic sialylated structures and evade recognition by the immune system (A. Varki & Gagneux, 2012; Wißfeld et al., 2024).

1.3 Sialic acid-binding immunoglobulin-like lectin receptors

The sialic acids can be recognized on the glycocalyx by sialic acid-binding immunoglobulin-like lectin (SIGLEC) receptors, and therefore, act as ligands. SIGLECs are transmembrane receptors expressed on myeloid lineage cells, such as dendritic cells, monocytes, macrophages, neutrophils and microglia (Crocker et al., 2007; El Ali & Rivest, 2016). SIGLEC receptors can identify specific types of sialic acids, specifically N-acetylneuraminic acid (Neu5Ac), or N-glycolylneuraminic acid (Neu5Gc), as well as their O-acetylated derivatives (A. Varki & Gagneux, 2012; Wißfeld et al., 2024).

Alterations in the sialylated part of glycans can be recognized by SIGLECs, that upon stimulation, counteract activation and inflammatory responses of immune cells, such as microglial cells (Fig. 2). In more detail, cell surface sialylation is recognised mainly by SIGLEC receptors through the V-set Ig-like domain in their N-terminal domain (Crocker et al., 2007; Gianchecchi et al., 2021; Pillai et al., 2012; Wißfeld et al., 2024). In the majority of the SIGLECs the intracellular domain (C-terminal cytoplasmatic tail) contains immunoreceptor tyrosine-based inhibition motifs (ITIMs), that plays an important role in the inhibition of microglia pro-inflammatory responses. This SIGLEC-ITIM downstream signalling allows microglial cells to detect intact sialylation in the cell glycocalyx and leads to inhibition of responses activated by the immunoreceptor tyrosine-based activation motif (ITAM) signalling, which is carried on the SIGLECs intracellular domain with less frequency than ITIM motifs. The ITAM downstream signalling of the microglia receptors, such as complement receptor 3 (CR3) and triggering receptor expressed on myeloid cells 2 (TREM2), lead to microglia responses associated with activation, inflammation, reactive oxygen species (ROS) release, and phagocytosis (Fig. 2) (Neumann et al., 2010). The activatory downstream ITAM-signalling can be inhibited by ITIMs upon phosphorylation

by Src family kinases. Then, high affinity sites are created for Src homology region 2 domain-containing phosphatase (SHP)-1 and SHP-2, which in turn participate in dephosphorylation of tyrosine receptors, leading to blockade of downstream signalling of ITAM in microglia cells. Consequently, ITIM signalling helps maintain microglial tissue homeostasis in the presence of intact sialylation (Crocker et al., 2007; Linnartz & Neumann, 2013; Wißfeld et al., 2024).

The SIGLEC receptors expressed mainly on innate immune cells have immunoregulatory functions, mostly immunosuppressive. SIGLECs can be divided into two groups, depending on their evolutionary and sequence similarity. The conserved group of SIGLECs are SIGLEC-1 (sialoadhesin), SIGLEC-4 (myelin-associated glycoprotein; MAG), and SIGLEC-15. In humans, the encoding-genes of these SIGLECS are distributed on different chromosomes. On the contrary, CD33-related (CD33r) SIGLECs, which represents the main group, are encoded mostly in the chromosome 9, and include SIGLEC-5 to -11, -14, and -16 in humans, and in mice CD33 (Siglec-3) and Siglecs-E to -H (Duan & Paulson, 2020; Gianchecchi et al., 2021; Wißfeld et al., 2024). Some CD33r-SIGLECs possess both activating and inhibitory receptors in their cytoplasmic domains. It is hypothesized that this receptor pairing balances their effects, allowing SIGLECs with inhibitory functions to recognize a wide range of sialic acids on glycans and distinguish non-endogenous structures from self, and thereby preventing inappropriate activation of innate immune cells (Gianchecchi et al., 2021).

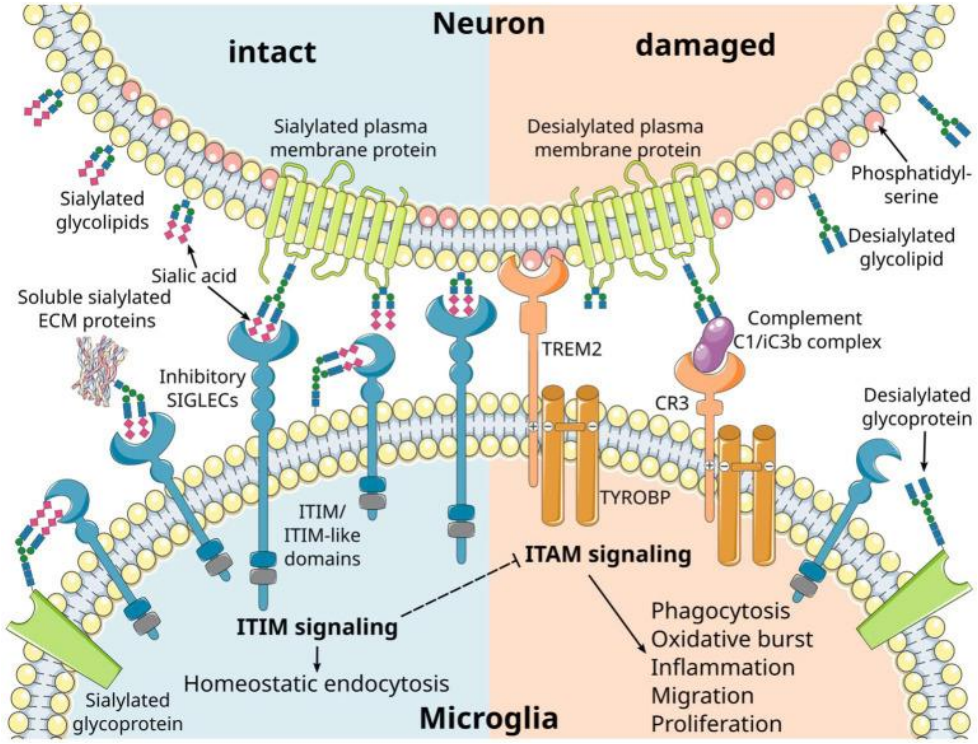

Figure 2. Sialic acid receptors in microglia. Residues or altered sialylation on the damage cell membranes can lead to activation of the triggering receptor expressed on myeloid cells 2 (TREM2), and to opsonization with complement C1, triggering responses mediated by signalling of the immunoreceptor tyrosine-based activation motif (ITAM). ITAM downstream-signalling responses include inflammation, oxidative burst, phagocytosis, as wells as cell migration and proliferation. On the contrary, the sialic acid-binding immunoglobulin-like lectin (SIGLEC) receptors on microglia recognize intact sialylation on neuronal glycans by the immunoreceptor tyrosine-based inhibition motif (ITIM) leading to inhibition of motif ITAM-signalling responses. Therefore, the interaction of sialic acids and ITIM/ITAM allows microglia cells to maintain balance in the microglia responses and tissue homeostasis. Image taken from (Wißfeld et al., 2024).

1.4 Complement system and sialic acids

Aside the capacity to bind to SIGLEC receptors, sialic acids can also have anti-inflammatory effects due to their role as ligands for inhibitory components of the complement system (Pillai et al., 2012). In more detail, complement factor H (CFH) can recognize and bind sialic acids of the host-cells (Schmidt et al., 2018). As result, this binding prevents the activation of the complement alternative pathway (Crocker et al., 2007; A. Varki & Gagneux, 2012) by interfering with the interaction of complement factor B (CFB) with the opsonin C3b, but also by recruiting the protease factor I that induces

disassembling and elimination of C3b (Pillai et al., 2012). In addition, sialic acids can also prevent the activation of the alternative complement pathway by attracting the positively charged protein properdin (Shahraz et al., 2022; Wißfeld et al., 2024). Evidence suggests that alterations in the sialylated portion of the glycans can lead to C1q opsonization, and to engagement of the CR3 (Linnartz et al., 2012), resulting in microglia activation. On the other side, sialic acids inhibit directly some complement component by binding to opsonin C3b, and by preventing the formation of C3-convertase, leading to complement downstream activation blockage. This complement blocking would otherwise lead to the formation of complement factor 4 (C4), complement factor 5 (C5), and finally to the membrane attack complex assembly.

1.5 The mammalian eye

The mammalian eye is an immune privileged organ, in which the light is processed by a complex neuronal circuit in order to create the perception of colour, shapes and proportions. Most of the sensory information that the human brain receives comes from the retina. It is estimated that retina is able to transmit 10 million bits per second to the brain (Koch et al., 2006). The basic structure of the mammalian eye can be divided into the anterior part with the cornea, pupil, iris, lens, and conjunctiva, and the posterior part that consist of sclera, choroid, optical nerve, and retina (McCaa, 1982).

1.5.1 Retina

The retina is a multi-layered tissue part of the central nervous system (CNS), which is attached in the posterior eye segment to the retinal pigment epithelium (RPE), and in the anterior eye segment to the iris and ora serrata (McCaa, 1982). The retina is rich in sialic acids, similar to other regions of the CNS (Karlstetter et al., 2017; Klaus et al., 2020).

Together with other structures, the retinal neurons form several histologic layers, listed from the inner to the outer parts of the eyeball: the internal limiting membrane, the nerve fiber, the ganglion cell layer (GCL), the inner plexiform layer (IPL), the inner nuclear layer (INL), the outer plexiform layer (OPL), and the outer nuclear layer (ONL). Furthermore, on its base can be found the RPE, choroid, and sclera (Fig. 3A). The cell bodies of the retinal

neurons form the retinal nuclear layers, while, the retinal synapses and processes are located in both plexiform layers (reviewed in Hoon et al., 2014; Vecino & Acera, 2015). The retina contains five different types of neurons; the photoreceptors (rods and cones), bipolar cells, horizontal cells, amacrine cells, and the ganglion cells. The photoreceptors cell bodies form the ONL and capture the light with their photopigments in their outer segments. The photoreceptors synapses contact the bipolar cells, that together with the horizontal and amacrine cells form the inner nuclear layer. The axons of the bipolar cells make contact with the ganglion cell in the inner plexiform layer (Fig. 3B). The ganglion cells are located mainly in the GCL and their long axons form the optic nerve, which transmits the retinal signals to the brain visual centres. The horizontal and amacrine cells are crucial for lateral interactions in the retina. The horizontal cells support the photoreceptor-bipolar cell interaction, while the amacrine cells are important for the communication between bipolar cells and ganglion cells (Purves et al., 2001). There are different subtypes of the five retinal neurons, and each subtype contributes to different characteristics of the sight, i.e., night and day vision, perception of different colours, shapes, and image depth. Despite the complexity of the visual circuitry, the interaction between photoreceptors, bipolar cells, and ganglion cells is considered the main route of information from the outer retina to the optic nerve (Purves et al., 2001).

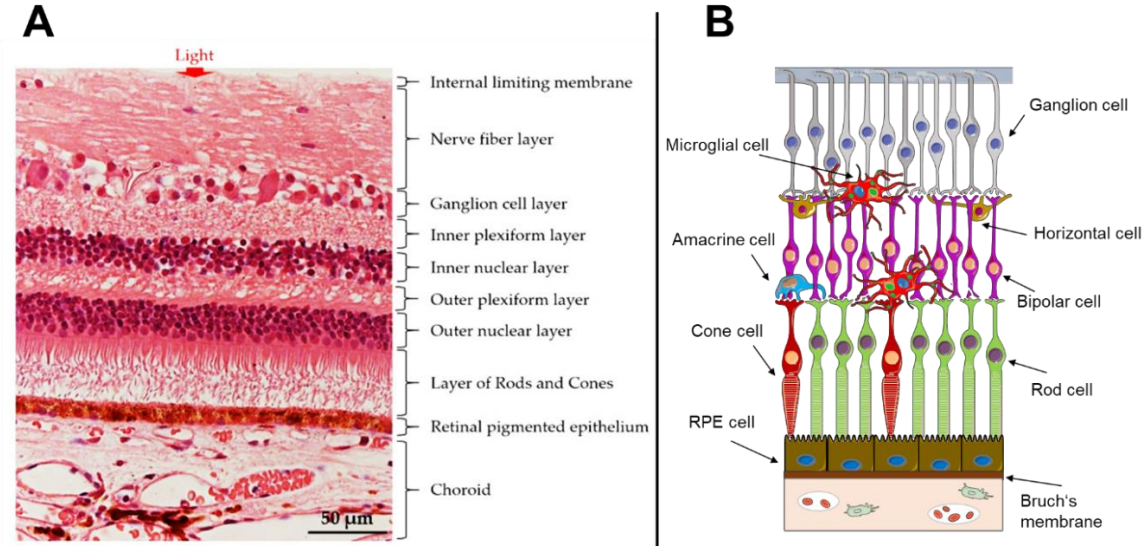

Figure 3. Histological retinal layers and retinal neurons. (A) The mammalian retina is composed of different layers, from the top to the bottom of the image; the internal limiting membrane, the nerve fiber, the ganglion cell layer (GCL), the inner plexiform layer (IPL), the inner nuclear layer (INL), the outer plexiform layer (OPL), the outer nuclear layer

(ONL), retinal pigment epithelium (RPE), and the choroid. (B) The main retinal neurons are the rod and cone photoreceptors, bipolar cells, amacrine cells, horizontal cells, and ganglion cells. In addition, the monolayer of RPE cells is located on the base of the neuroretina. The microglial cells are typically found in the plexiform layers. The Bruch's membrane connects the choroid with the RPE. Image A taken and modified from (Ding et al., 2017), and image B created using original or modified images from Servier Medical Art, licensed under CC BY 4.0. (https://creativecommons.org/licenses/by/4.0/)**.**

The macula is an important area of the central retina that contains the highest density of photoreceptors, and it is also known as the yellow spot due content of carotenoid pigments. The macula is crucial for sharp vision, and it is often affected in the elderly population (Beltran et al., 2014; Volland et al., 2015).

1.5.2 Retinal pigment epithelium

The retinal pigment epithelium (RPE) is located below the photoreceptors and contains only a single layer of pigmented and spheroidal-shape cells. The Bruch's membrane is located in the basement of RPE and it is also attached to the choroid (Claybon & Bishop, 2011; Ma et al., 2009). The Bruch's membrane is often the place of abnormal deposits of debris in pathological conditions of the retina. The core functions of the RPE cells in physiological conditions are to protect the retina from the excess of light due to their pigment, to act as blood-retinal barrier, to phagocytize sheds of old or damaged photoreceptors, and to provide nutritional and metabolic support to the underlying photoreceptors. Nevertheless, pathological conditions and the constant ingestion of photoreceptors' sheds can cause lipofuscin accumulation and dysfunction of the lysosomal enzymes of the RPE cells. These events can lead to oxidative stress, retinal inflammation, and photoreceptors loss (Al-Zamil & Yassin, 2017; Boatright et al., 2015; Kauppinen et al., 2016; Xin-Zhao Wang et al., 2012).

1.5.3 The glial cells in the retina

Three types of glial cells can be found in the mammalian retina, the microglia, and the two macroglia cells, Müller cells and astrocytes. The overall functions of the glial cells in the retina are to provide metabolic, nutritional and structural support, defence against pathogens, as well as tissue surveillance (reviewed in Reichenbach & Bringmann, 2020).

1.5.3.1 Retinal microglia

Microglia are the main resident immune cells in the CNS, including the retina. Earlier hypotheses suggested that microglia recruitment in the CNS occurred during embryonic and perinatal stages from bone marrow precursors, similar to bone-derived macrophages. However, recent evidence shows that microglia instead originate from myeloid progenitors in the yolk sac and migrate to the brain during embryonic development (Ginhoux et al., 2010). Then, microglia enter to the retina via the ciliary body and the fetal hyaloid vasculature through the optic nerve head. Later, microglia reach different retinal layers in the postnatal development (Provis et al., 1996).

In the CNS in general, microglial cells have the capacity of self-maintenance and -renewal, capable of expansion in response to insults or in degenerative conditions (Ajami et al., 2007). In the particular case of the retina, microglia contribute to some of the functions of glial cells, such as tissue surveillance and repair, defence against invading pathogens, neuronal and synaptic remodelling, vascularization, as well as phagocytosis of cellular debris and dying neurons (Karlstetter et al., 2015; Langmann, 2007; F. Li et al., 2019). Interestingly, microglia also contribute to synaptic pruning and remodelling during brain development with the involvement of complement components, such as component 3 (C3), and complement component 1q (C1q) (Paolicelli et al., 2011; Stevens et al., 2007). In physiological conditions microglia are located mainly in the inner part of the retina, in the retinal synaptic layers (IPL and OPL), but also in ganglion cells layer. Yet, microglia can migrate towards the photoreceptors in the outer retina, to the subretinal space, and even to the RPE, attracted towards degenerating neurons or to other danger signals (Chen et al., 2002; Usui-Ouchi et al., 2020).

1.5.3.2 Microglia types and morphology

Reports indicate that microglia exist in diverse populations, with their localization closely related to their primary functions and characteristics. For instance, microglia in the parenchyma are typically highly motile and ramified, playing key roles in neuron surveillance, synaptic refinement, and the removal of debris and metabolic waste. In contrast, perivascular microglia primarily regulate substances entering the brain through

blood vessels (Provis et al., 1996; Reichenbach & Bringmann, 2020). Microglia are also able to sense neuronal activity and modify its behaviour by detecting signals like Fractalkine ligand 1 (CX3CL1) and adenosine triphosphate (ATP) from retinal neurons (Eyo et al., 2014; Liang et al., 2009; Silverman & Wong, 2018). In addition, microglia can change their processes motility depending on the type of neurotransmission, to decrease it by γ-aminobutyric acid (GABA)ergic or to increased it with glutamatergic neurotransmission (Fontainhas et al., 2011; Reichenbach & Bringmann, 2020).

Microglial cells are highly dynamic and change their morphology and functions in response to the conditions of the surrounding tissue, but also depending on the retinal developmental stage. Despite a clear separation and distinction of microglial types is challenging, overall, they can be highly ramified or with amoeboid shape. However, microglia have the capacity to switch from one type to another. The functions of highly ramified microglia are neuronal surveillance, removal of metabolites, and support for neuronal survival by releasing neurotrophic factors (Silverman & Wong, 2018). In addition, these types of microglia are important for immunotolerance and for anti-inflammatory effects. On the other hand, upon danger signals, microglia can turn into more amoeboid shape, by retracting processes and enlarging their somas. These amoeboid microglia are classically considered as activated cells, responsible mainly for phagocytosis of axons, synapses, or even full neurons (Fan et al., 2022; Linnartz-Gerlach et al., 2016). A common characteristic of activated microglia is an increase in their number of phago- and lysosomes. Activation and proinflammatory profile of microglia are necessary for waste-clearance and for tissue repair, but if they are not able to stop these processes, microglia become neurotoxic and detrimental for retinal tissue (Rashid et al., 2019). In more detail, microglia can release proinflammatory cytokines such as IL-1β, TNFα, IL-6, as well as ROS, which could lead to chronic inflammation and tissue damage (Natoli et al., 2017; Rashid et al., 2019). Therefore, fine tuning of microglial responses is crucial to maintain healthy the retinal tissue.

1.5.3.3 Microglial receptors and supervision of sialylated glycocalyx

Microglial cells as the main immune cells in the retina are equipped with a wide range of receptors important for tissue surveillance and immune response modulation. The pattern

recognition receptors, e.g., the toll-like receptors, are able to recognize multiple danger-associated and pathogen molecules such as peptidoglycans, ATP, and nucleic acid molecules (El Ali & Rivest, 2016; Kumar et al., 2011). The specific microglial receptors that recognize sialic acids are the SIGLECs, which are able to identify intact glycocalyx in healthy neurons (described in the section 1.3). The activation of SIGLEC receptors is important to control microglia responses, while allowing for rapid responses in case of danger signals or altered sialylation (reviewed in Wißfeld et al., 2024). As mentioned before, pathological conditions can cause removal of sialic acids and engagement of the complement system that lead to neuronal removal by microglial cells. *In vivo* and *in vitro* studies, show that sialic acid administration prevent loss of neurons associated with complement activation (Karlstetter et al., 2017; Klaus et al., 2020; Linnartz-Gerlach et al., 2016; Linnartz et al., 2012). In humans, strategies to target SIGLECs with antibodies or with sialic acid structures are being tested in clinical trials for Alzheimer's disease (AD), and also for dry age-related macular degeneration (AMD) (clinical trials reviewed in Wißfeld et al., 2024).

1.5.3.4 Microglial markers

Microglia express some common markers for myeloid precursors, the CX3 chemokine receptor 1 (CX3CR1; Fractalkine), ionized calcium binding adaptor molecule 1 (Iba1), but also depending on their developmental stage they can express isolectins, CD45, CD11b, and the lysosomal marker CD68. The distinction of different microglia subsets, or specific markers that distinguish microglia from monocyte-derived macrophages remains unclear (Hume et al., 1983; F. Li et al., 2019; Silverman & Wong, 2018). Keiko Ohsawa and colleagues showed that Iba1 contributes with L-fimbrin to bind actin filaments, which provides motility to the cell surface. This surface motility is important to create cell protrusions that enable activated microglia to migrate, and to perform phagocytosis (Ohsawa et al., 2004). On the other hand, CD68 is expressed by the microglial and macrophages endosomes, and is an important component of the innate immune response. In addition, CD68 is also considered as phagocytic activation marker because their expression was found increased in intracellular uptake of oxidized low-density lipoprotein, and lipopolysaccharide (LPS) (Pearson, 1996; Ramprasad et al., 1996).

1.5.3.5 Microglia in retinal diseases

Despite microglia activation during acute injury can be beneficial, chronic and dysregulated responses are a common denominator of many retinal inflammatory and degenerative diseases. Microglia activation can lead to persistent inflammation by the direct or mediated release of pro-inflammatory cytokines, the apoptotic mediator TNF, but also production of ROS (reviewed in Colonna & Butovsky, 2017; Fan et al., 2022). The release of these factors can lead to neovascularization in the retina, dysfunction of the RPE cells, apoptosis of ganglion cells, and overall retinal degeneration (Kitaoka et al., 2006; Natoli et al., 2017). These inflammatory and degenerative phenomena can be seen in retinal diseases such as glaucoma, diabetic retinopathy, hereditary degeneration of photoreceptors, and AMD (Colonna & Butovsky, 2017; Rashid et al., 2019).

1.5.4 Macroglia; astrocytes and Müller cells

Astrocytes are part of the retinal macroglia cells, they are located mainly in the nerve fibre layer, and also in the GCL (Stone & Dreher, 1987). Together with Müller cells, astrocytes have important functions in regulating pH, extracellular fluids, and potassium (Newman, 1999). Astrocytes also play important roles in the overall retinal vascularization, and creation of a blood-barrier in the retina together with Müller cells, pericytes, and microglial cells (reviewed in Reichenbach & Bringmann, 2020). Under pathological conditions in the retina, astrocytes proliferate, turn activated, and upregulate the glial fibrillary acid protein (GFAP) (Luna et al., 2010), a common astrocytes and Müller cells marker (Iandiev et al., 2006; Stone & Dreher, 1987). While activation of astrocytes provide repair and protection effects in the injured retina, activation can also be toxic, contribute to oxidative stress, to vascular alterations, and to loss of ganglion cells (Guttenplan et al., 2020). For instance, retinal cell loss associated with astrocytic alterations have been observed in physiological aging of retinas, but also in age-related diseases such as AMD (Madigan et al., 1994).

The other type of macroglia are Müller cells, whose cell bodies are located in the inner nuclear layer. Their processes extend through all retinal layers, enveloping synapses and neuronal cell bodies (Bringmann et al., 2006). The functions of the Müller cells overlap with the astrocytes, but additional functions are neuronal activity modulation, retinal

structural support, and regulation of inflammatory and immune responses. The term gliosis refers to the reactivity of Müller cells and astrocytes. Similar to the other glial cells, Müller cells activation confer retinal support, but dysregulated responses are also associated with neuronal loss (Iandiev et al., 2006; Inman & Horner, 2007).

1.6 Age-related macular degeneration

Age-related macular degeneration (AMD) is a leading cause of central blindness in the elderly, particularly in industrialized countries, affecting primarily the macula. A key characteristic of the disease is the accumulation of proteins, lipids, waste materials, and auto fluorescent lipofuscin, collectively known as drusen. Drusen accumulate mainly in the Bruch's membrane and in the RPE, and can be visualized using fundoscopy. The presence of drusen and its components contributes to disease progression, which can advance to one of the two stages: 1) Wet or neovascular, characterized by the formation of abnormal blood vessels that leak and infiltrate the RPE and outer retina, causing structural and functional damage. 2) Dry or geographic atrophy, defined by progressive degeneration of the RPE, loss of the choriocapillaris, and eventual death of photoreceptors (reviewed in Rashid et al., 2019; Silverman & Wong, 2018).

Amoeboid retinal microglia have been found in humans with AMD around drusen in the RPE. In this area, activated microglia cells release factors such as IL-1β and NLR family pyrin domain containing 3 (NLRP3), which contribute to inflammation and degeneration not only of the retinal neurons, but also of RPE cells. Since RPE cells are important for nutritional and metabolic support for photoreceptors, damage of RPE cell can lead to a secondary death of cone and rod photoreceptors (Rashid et al., 2019; Tseng et al., 2013). Overall, microglia reactivity and NLRP3 expression can lead to apoptosis, and to retina degeneration (Wiedemann et al., 2018). In addition, studies show in mouse-models that activated microglia and RPE interactions alters the RPE autophagy capacity, their anatomical structure and the pro-inflammatory chemokine expression. Furthermore, microglial and bone-derived macrophages can also secrete vascular endothelial growth factor (VEGF) in early stages of wet AMD (Ishibashi et al., 1997; Reichenbach & Bringmann, 2020). Therefore, microglia are considered crucial players in the development and progression of AMD (Flamendorf et al., 2015; Ma et al., 2009).

Despite mice do not have macula, there are mouse-models to study AMD by inducing common signs of AMD, such as microglia activation, drusen formation, photoreceptor loss, and neovascularization (AMD animal models reviewed in Rashid et al., 2019). In addition, the central area of mouse retina shares some characteristics with the primate macula, i.e., a high photoreceptor cell density in a small area (Volland et al., 2015). Hence, mouse-models are an alternative to study retinal inflammation and degeneration.

1.7 Complement in age-related macular degeneration

Aside the classical risk factors such as advance age, smoking, cardiovascular diseases, family history of AMD, etc., the driving causes of AMD remains unclear. Recent evidence suggests the involvement of dysregulated innate immune system, such as uncontrolled microglial and complement activation. It has been reported that the gene mutation of the complement CFH, is one of the main gene or loci associated with AMD (Y. Deng et al., 2022; Haines et al., 2005; Klein et al., 2005). The incapacity of CFH to block C3 activation leads to uncontrolled complement activation. In addition, mutation in the C3 genes has also been reported in AMD development, but also fragments of C3a and C5b, which can induce the expression of VEGF, leading to increased risk of choroidal neovascularization (Y. Deng et al., 2022; Nozaki et al., 2006; Rashid et al., 2019). Furthermore, genetic polymorphisms of CFB, complement factor 2 (C2), and complement factor I, an inactivator of C3b, are linked either with higher risk, or, with protective effect for AMD (Y. Deng et al., 2022; Ennis et al., 2010; Kaur et al., 2010).

1.8 Mouse model for reduced sialylation

Previous data demonstrated that sialylation is important for homeostasis of the CNS and for regulation of innate immune responses. *In vitro* studies showed that sialic acid deletion from the neuronal glycocalyx lead to neuronal removal by microglia/macrophages in a CR3-dependent manner. Additionally, reports suggest that sialylation might be affected with age, particularly the sialic acid levels on gangliosides in the brains of elderly humans (Segler Stahl et al., 1983). To mimic hyposialylation that may occur with aging in the CNS,

particularly in the retina, I used 9- and 12-month-old mice deficient in one allele of the UDP-N-acetylglucosamine 2-epimerase/N-acetylmannosamine kinase (GNE).

As described above (section 1.2), the GNE enzyme is essential for the first two steps of sialic acid synthesis in the cytosol. Complete deletion of the *Gne* gene in mice induces embryonic death (Schwarzkopf et al., 2002). However, mice heterozygous for null mutant of enzyme GNE can live with no apparent phenotype defects. Depending on the tissue or organs, Gne+/- mice show an overall reduction of around 25 % membrane-bound sialic acids. Recently, Klaus et al., showed in Gne+/- mice neuronal loss in the brain associated with slight reduced sialic acids levels. Interestingly, the neuronal loss was prevented by *C3* deficiency (Klaus et al., 2020). Hence, data suggest that Gne+/- mice is a suitable model to investigate the effects of hyposialylation in nervous tissue such as retina.

1.9 Aims

Although the effects of hyposialylation have been described in various fields, it is not clear whether hyposialylation contributes to mouse retina inflammation and degeneration. Thus, in this study it was investigated and characterized the retinas of Gne+/- mice with the primary objectives to analyze sialic acid levels, assess microglia status, and determine neuronal cell density across retinal layers. Additionally, transcriptomic analysis was performed to investigate the mechanisms associated with hyposialylation, microglia activation, and neuronal loss. This study also aimed to investigate the role of the complement system in retinal inflammation and degeneration associated with hyposialylation, while exploring whether crossing Gne+/- mice with C3-/- mice could alleviate the retinal phenotype linked to hyposialylation. Overall, the study sought to examine the role of sialylation in retinal homeostasis.

2. Material and methods

2.1 Materials

2.1.1 Chemicals and Reagents

Name	Company
4',6-diamidino-2-phenylindole (DAPI)	Sigma, Germany
Ampuwa® water	Fresenius Kabi, Germany
AquaPoly/Mount	Polysciences Europe, Germany
Bovine serum albumin (BSA)	Sigma, Germany
UltraPure™ DEPC-Treated Water	Invitrogen, Thermo Fisher Scientific, Germany
Dulbecco's Phosphate Buffer Solution (PBS)	Gibco, Germany
Ethanol (C2H6O)	Roth, Germany
Ethidium Bromide (10g/l)	Roth, Germany
Hexanucleotide Mix (10x)	Roche, Germany
Isopropanol	Roth, Germany
Normal goat serum (NGS)	Sigma, Germany
O.C.T.™ Compound, Tissue Tek®	Sakura, USA
Paraformaldehyde (PFA)	Sigma, Germany
QIAzol Lysis Reagent	Qiagen, Germany
Sucrose	Roth, Germany
SuperScript® III Reverse Transcriptase	Invitrogen, Germany
SYBR® Green ERTM qPCR Super Mix	Invitrogen by Life Technologies, USA
Trichloromethane/chloroform	Roth, Germany
Triton X-100	Sigma, Germany
UltraPure™ DEPC-treated water	Invitrogen, Germany

2.1.2 Buffers and solutions

Name	Ingredients
1 % Agarose gel	0.6 g agarose 3 µl ethidium bromide 60 ml Tris/Borate/EDTA buffer (1x)
10x BSA	10 g BSA in 100 ml 1x PBS
30 % sucrose solution	30 g sucrose in 100 ml 1x PBS 0.1 % sodium azide
4 % paraformaldehyde (PFA), pH 7.3	20 g PFA + 30 ml NaOH + 50 ml PBS (1x), up to 1 litre ddH2O

2.1.3 Consumables

Name	Company
24-well plate Costar	Sigma-Aldrich, Germany
1 ml syringe	Braun, Germany
10 µl, 100 µl, 1000 µl pipette tips	StarLab, Germany
15 ml plastic tubes	Greiner, Germany
5 ml, 10 ml, 25 ml plastic pipettes	Costar, Germany
50 ml plastic tubes	Sarstedt, Germany
Disposable vinyl specimen molds (Cryomold®, 10 x 10 x 5 mm)	Tissue-Tek® Sakura Finetek, USA
Dumont #5 Forceps	Fine Science Tools GmbH, Switzerland
Examination gloves (Micro-Touch)	Ansell Healthcare, Belgium
Glass Anti-Roll Plate (Epredia)	Fisher scientific, Germany
Glass cover slips (24 x 60 mm)	Thermo Scientific, USA
Injection needles	Braun, Germany
Polymerase chain reaction (PCR) tubes, 500 µl	Biozym Scientific GmbH, Germany
QPCR Seal optical clear film	PeqLab, Germany

QPCR Semi-skirted 96 Well PCR Plate	PeqLab, Germany
Stainless steel beads (5 mm)	Qiagen, Germany
SuperFrost® Plus Adhesion Microscope Slides, white Tab (Epredia)	Fisher Scientific, USA
Vannas Spring Scissors - 2.5mm Cutting Edge	Fine Science Tools, GmbH, Switzerland

2.1.4 Mice

Mouse line	Mouse strain	Origin/Provider
C57BL/6J	C57BL/6J	Charles River, Sulzfeld, Germany
C3-/-	B6;129S4-C3tm1Crr/J	Charles River, Sulzfeld, Germany
Gne+/-	129/OLA and Balb/C mixed background mouse with heterozygous deletion of *Gne* gene (Schwarzkopf et al., 2002)	Animals were originally provided by Prof. Horstkorte (University of Halle-Wittenberg, Halle [Saale], Germany).
Gne+/+C3-/- Gne+/-C3-/-	Gne+/+ and Gne+/- mice crossed with C3-/- mice	University Hospital Bonn, Germany

2.1.5 Mouse primers (Oligonucleotides)

Genotyping		
Target	**Orientation**	**Sequence**
37	forward	5’ –CACCAGGCTCCACACGATTG– 3’
42	reverse	5’ –GATTGAAATATGCCCAATACTTTG– 3’
A541	forward	5’ –CGAAGGAGCAAAGCTGCTATTGGCC– 3’
C3geno	forward	5’ –ATCTTGAGTGCACCAAGCC– 3’
C3mt	reverse	5’ –GCCAGAGGCCACTTGTGTAG– 3’
C3wt	reverse	5’ –GGTTGCAGCAGTCTATGAAGG– 3’

sqRT-PCR		
Target	**Forward sequence (5’ – 3’)**	**Reverse sequence (5’ – 3’)**
Aif1	GAAGCGAATGCTGGAGAAAC	AAGATGGCAGATCTCTTGCC
C1qb	GACTTCCGCTTTCTGAGGACA	CAGGGGCTTCCTGTGTATGGA
C3	TAGTGCTACTGCTGCTGTTGGC	GCTGGAATCTTGATGGAGACGCTT
C4	TGGAGGACAAGGACGGCTA	GGCCCTAACCCTGAGCTGA
Casp3	CAGCCAACCTCAGAGAGACA	ACAGGCCCATTTGTCCCATA
Casp8	TGGAGAAGAGGACCATGCTG	AGTCACACAGTTCCGCCATT
Cd68	CAGGGAGGTTGTGACGGTAC	GAAACATGGCCCGAAGTATC
Cfh	AGAGCCTGAGACCCAACTTC	ACACATTTCCTGACGCATGG
Col4a2	ACAAGCTCTGGAGTGGGTAC	CAGTAGGACTTGTCGTTGCG
Col6a3	GGTATCTCCGGGGAAGATGG	TCTCCAGAAGAACCAGGCAG
Cyba	CCTCCACTTCCTGTTGTCGG	TCACTCGGCTTCTTTCGGAC
Cybb	GGGAACTGGGCTGTGAATGA	CAGTGCTGACCCAAGGAGTT
Gapdh	ACAACTTTGGCATTGTGGAA	GATGCAGGGATGATGTTCTG
Gfap	AAGGTTGAATCGCTGGAGGA	ACCACTCCTCTGTCTCTTGC
Gne	AAACTGGCCCCGATCATGTT	TCTACCATGGCCGCTTCATC
IL-1β	CTTCCTTGTGCAAGTGTCTG	CAGGTCATTCTCATCACTGTC
Itgam	AATTGGGGTGGGAAATGCCT	TGGTACTTCCTGTCTGCGTG
Opn1sw	CTGAACGGGAGGTGAGTCAT	CTCTTGGAAAAGAAGGCGGG
Pik3cd	GTCCACTCCTCCTCCATCCT	CAGCATTCACTTTTCGGCCC
Tmem119	GTGTCTAACAGGCCCCAGAA	AGCCACGTGGTATCAAGGAG
Tnf	GGTGCCTATGTCTCAGCCTC	TGAGGGTCTGGGCCATAGAA
Trpm1	GTCTGATCAAGGCTGCCATG	CTCAGAGGGTTGGACATGGT
Vegfa	CTCCACCATGCCAAGTGGTC	GCTGGCTTTGGTGAGGTTTG
Vsx2	ACAGTGGCCAAGAGTACCTC	AAGGTGGGCTGTGTGTAGAA

2.1.6 Antibodies

2.1.6.1 Primary antibodies

Antigen	Host	Company	Dilution
A2B5	mouse	Invitrogen, 433110	1:500
Brain-specific homeobox/POU domain protein 3A (Brn3a)	rabbit	Sigma-Aldrich, AB5945	1:2000
C1q	rabbit	Abcam, ab182451	1:200
CD68	rat	Bio-Rad, MCA1957	1:500
Cone arrestin	rabbit	Sigma-Aldrich, AB15282	1:500
Glial fibrillary acidic protein (GFAP)	rabbit	DAKO, #Z0334	1:1000
Ionized calcium binding adaptor molecule 1 (Iba1)	rabbit	Wako, #019-19741	1:500
Polysialylated neural cell adhesion molecule (PSA-NCAM), clone 2B	mouse	Millipore, MAB5324	1:500
Protein kinase C alpha H7 (PKCα)	mouse	Santa Cruz Biotechnology, sc-8393	1:250
Rhodopsin, Rho 4D2	mouse	Abcam, ab98887	1:1000

2.1.6.2 Secondary antibodies

Fluorophore	Reactivity	Host	Company	Dilution
Alexa Fluor® 488	mouse	goat	Invitrogen, A11001	1:500
Alexa Fluor® 488	rat	goat	Invitrogen, A11006	1:500
Alexa Fluor® 488	rabbit	goat	Invitrogen, A11008	1:500
Alexa Fluor® 647	mouse	goat	Jackson, 115-606-072	1:250
Alexa Fluor® 647	rabbit	goat	Dianova, 111-606-144	1:500-1:800
Cyanine 3 (Cy3)-conjugated F(ab')2	mouse	goat	Dianova, 115-166-072	1:500-1:800
Cyanine 3 (Cy3)-conjugated F(ab')2	rabbit	goat	Dianova, 111-167-003	1:500

2.1.7 Kits and markers

Name	Company
100 base pair DNA ladder	Invitrogen, Germany
KAPA mouse genotyping Hot Start Kit	PeqLab, Germany
RNase-Free DNase Set	Qiagen, Germany
RNeasy® Mini Kit	Qiagen, Germany
SuperScript First-Strand Synthesis System	Invitrogen, Germany
QuantSeq 3′ mRNA-Seq Library Prep Kit, Next Generation Sequencing (NGS) Core Facility, University Hospital Bonn	Lexogen, Austria

2.1.8 Technical equipment

Name	Company
Heraeus Megafuge, 8.0 R., centrifuge	Thermo Fisher Scientific, Germany
Freezer -20 °C ProfiLine	Liebherr, Germany
Freezer -80 °C Herafreeze	Heraeus, Germany
Fridge (4 °C)	Liebherr, Germany
GelDoc	BioRad, Germany
Leica SP8 resonant scanning with Lightning (Microscopy Core Facility of the Medical Faculty at the University of Bonn)	Leica Biosystems, Germany
Mastercycler realplex 4	Eppendorf, Germany
Megafuge, 1.0 R. (centrifuge)	Heraeus, Germany
Microm Cryo Star HM 560	Thermo Scientific, USA
NanoDrop 2000c spectrophotometer	Thermo Scientific, USA
NovaSeq 6000, Next Generation Sequencing (NGS) Core Facility, University Hospital Bonn	Illumina, Germany
NextSeq 500	Illumina, USA
Nutating mixer	VWR, USA
Perfect BlueTM Horizontal Midi/Mini Gel Systems	PeqLab, Germany

Stereo-Dissection Microscope (SMZ1500)	Nikon, Japan
Tapestation 2200 (NGS facility)	Agilent, USA
Thermocycler T3 (PCR machine)	Biometra, Germany
Tissue Lyser LT	Qiagen, Germany
Vortex Genie2	Scientific Industries Inc., USA

2.1.9 Softwares

Name	Company
Bioconductor package org.Mm.eg.db [v3.11.4]. (Carlson, 2019)	Bioconductor Core Team, USA
ClusterProfiler [v3.16.1]. (Yu et al., 2012)	Bioconductor Core Team, USA
FastQC (v0.11.8)	Babraham Institute, UK
FeatureCounts/Subread [v2.0.0]. (Y. Liao et al., 2014)	SUBREAD, Australia
GSEA Desktop [v4.2.2]. (Mootha et al., 2003; Subramanian et al., 2005)	Broad Institute, USA
Ggplot2 [v3.3.3]. (Wickham, 2016)	Hadley Wickham, USA
GraphPad Prism 8	GraphPad Software, USA
GraphPad QuickCalcs	GraphPad Software Inc., USA
ImageJ v2.1.0/1.53c	National Institute of Health, USA
LAS X v3.7.4.23463	Leica Microsystems CMS, Germany
Master cycler ep realplex	Eppendorf, Germany
Mendeley Desktop (v1.19.8)	Mendeley Ltd., USA
Microsoft Office 2019	Microsoft, USA
MultiQC (1.7)	SciLifeLab, Sweden.
NanoDrop 2000/2000c	Thermo Fisher Scientific, USA
R (v4.3.1; free software)	R Core Team, https://www.R-project.org
RStudio (v2023.6.2, build 531)	RStudio, http://www.rstudio.com/
MotiQ plugin	See reference (Hansen et al., 2022)

2.2 Methods

Elements of this methods section and the sequence of the mouse primers for sqRT-PCR (see above, section 2.1.5) were already published online in a pre-print version of the journal *GLIA* on September 3, 2024 (Cuevas-Rios et al., 2024).

2.2.1 Gne+/- mouse model

Mice heterozygous for null mutant of the bifunctional enzyme UDP-GlcNAc 2-epimerase/ManNAc kinase (referred as Gne+/-, or Gne+/-C3+/+ mice) were originally provided by Rüdiger Horstkorte (Schwarzkopf et al., 2002), and backcrossed for at least ten generations with C57BL/6J mice at the University Hospital Bonn. Additionally, mice homozygous for the C3 targeted mutation were obtained as B6; 129S4-C3^{tm1Crr}/J from Jackson Laboratory via Charles River (mentioned here as C3-/-), and were also backcrossed for at least ten generations in C57BL/6J mice. 9- and 12-months old mice were utilized with the following four genotypes: Gne+/+C3+/+ (wildtype; WT), Gne+/-C3+/+, Gne+/+C3-/-, and Gne+/-C3-/- mice. Retinas of 3-months-old mice were also used to investigate retinal sialylation of young mice. The animals were housed under a 12-hour light/dark cycle in a temperature-controlled facility, with free access to food and water. All experiments were conducted randomly using both male and female mice, in full accordance with animal care committee guidelines and legal regulations. The study was approved by the boards of the University Hospital Bonn and the local government. Every effort was made to minimize the number of animals used and to reduce their suffering.

2.2.2 Genotyping of mice

Ear tissue was obtained after ear puncture for first genotyping of the mice at the weaning time (postnatal day 21). The genotype was confirmed with tail tissue obtained at the moment of mice sacrification at 3, 9, and 12 months of age. A fragment of 2-3 mm^3 of ear or tail tissue was used to extract the genomic DNA using the KAPA mouse genotyping Hot Start Kit following the manufacture's protocol (Table 1). The genomic DNA material was diluted in ddH2O and polymerase chain reaction (PCR) with the primers listed below (Table 2, and section 2.1.5 for the primers sequences) was performed using the

Genotyping Mix of the KAPA2G Fast Hot Start kit (Table 3). A thermocycler was used for the genotyping using different programs for the specific mouse-genotypes (Table 4).

Table 1. DNA extraction with KAPA kit

DEPC treated H_2O	88 µl
KAPA extraction enzyme	2 µl
10X kapa Express Buffer	10 µl

Table 2. Genotyping primers mix

Mouse line	**Primer mix**	**Expected product length**
Gne+/-	- A541 10 µM - 37 10 µM - 42 20 µM modified from (Weidemann et al., 2010)	- knockout allele (A541/42) – 750 bp - wildtype allele (37/42) – 500 bp - heterozygous: both bands
C3-/-	- C3mt 4.46 µM - C3wt 7.8 µM - C3geno 7.8 µM	- knockout allele – 500 bp - wildtype allele – 350 bp - heterozygous: both bands
Gne/C3-/-	Combination of primers for Gne+/- and for C3-/-	

Table 3. Genotyping polymerase chain reaction mix

Master mix per reaction		
	Gne	**C3-/-**
KAPA Genotyping mix	10 µl	10 µl
ddH_2O	1 µl	6 µl
Primer mix	4 µl	3 µl
DNA	5 µl	1 µl

Table 4. Genotyping programs for thermocycler

Step	Temperature	Time (minutes)
Gne PCR		
Initial denature	94 °C	4:00
*Denature	94 °C	0:30
*Annealing	58 °C	0:45
*Elongation	72 °C	0:60
Final elongation	72 °C	7:00
Hold	4 °C	
* 32 cycles		
C3 PCR		
Initial denature	94 °C	3:00
*Denature	94 °C	0:20
*Annealing	64 °C	0:30
*Elongation	72 °C	0:35
**Denature	94 °C	0:20
**Annealing	58 °C	0:30
**Elongation	72 °C	0:35
Final elongation	72 °C	7:00
Hold	4 °C	
* 12 cycles, ** 25 cycles		

Next, the resulting PCR products were loaded onto 1 % agarose gel which contains ethidium bromide. DNA ladder of 100 base pair (bp) was used as reference marker. The samples were then run at 100 V and 150 mA for 45 minutes. Finally, the gels were scanned and visualized using GelDoc with QuantityOne software in order to determine the genotype results (Fig. 4). The genotype of the mice was determine using bands in the gel at different base pairs. The wildtype mice (Gne+/+) show only a wildtype allele with a band at 500 bp, while, the heterozygous mice (Gne+/-) displayed the wildtype allele at 500 bp and one knockout allele at 750 bp (Fig. 4).

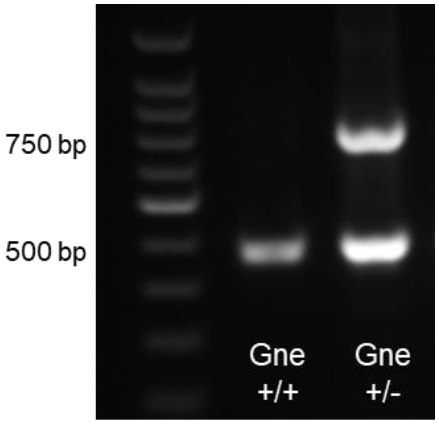

Figure 4. Gne mouse genotype example. Representative image of 1 % agarose gel loaded with the polymerase chain reaction products of both mice genotypes. The Gne+/+ genotype was determine by the presence of a band at 500 bp, and the Gne+/- genotype with bands at 500 bp and 750 bp.

2.2.3 Retina isolation and dissection

To collect retinal tissue, mice were euthanized and then perfused transcardially with ice-cold phosphate-buffered saline (PBS). Both eyes were enucleated and utilized either for retinal homogenates in RNA isolation, or for immunohistochemistry (IHC) on eye cryosections or retinal whole-mounts (Fig. 5). After enucleation, the eyes assigned to be used for IHC were incubated in 4 % paraformaldehyde (PFA) for 2-3 hours at room temperature (RT), washed with PBS and transferred to 30 % sucrose (Roth, Germany) in PBS until further processing. On the other hand, the eyes designated for RNA isolation of retina were placed in cold PBS. The retina dissection was performed as previously described (Völgyi et al., 2005) in order to prepare retinal whole-mounts either for IHC or for RNA isolation. Briefly, the eyes were dissected in cold PBS under a binocular microscope and extraocular tissue including optic nerve were removed. The eyeballs were cut along the limbus/ora serrata and the anterior segment, lens and vitreous body were discarded. From the remaining posterior eyecup, the neuroretina was gently separated from the retinal pigment epithelium (RPE) and was further cut into four-petal-like form to achieve a flat tissue (Fig. 5).

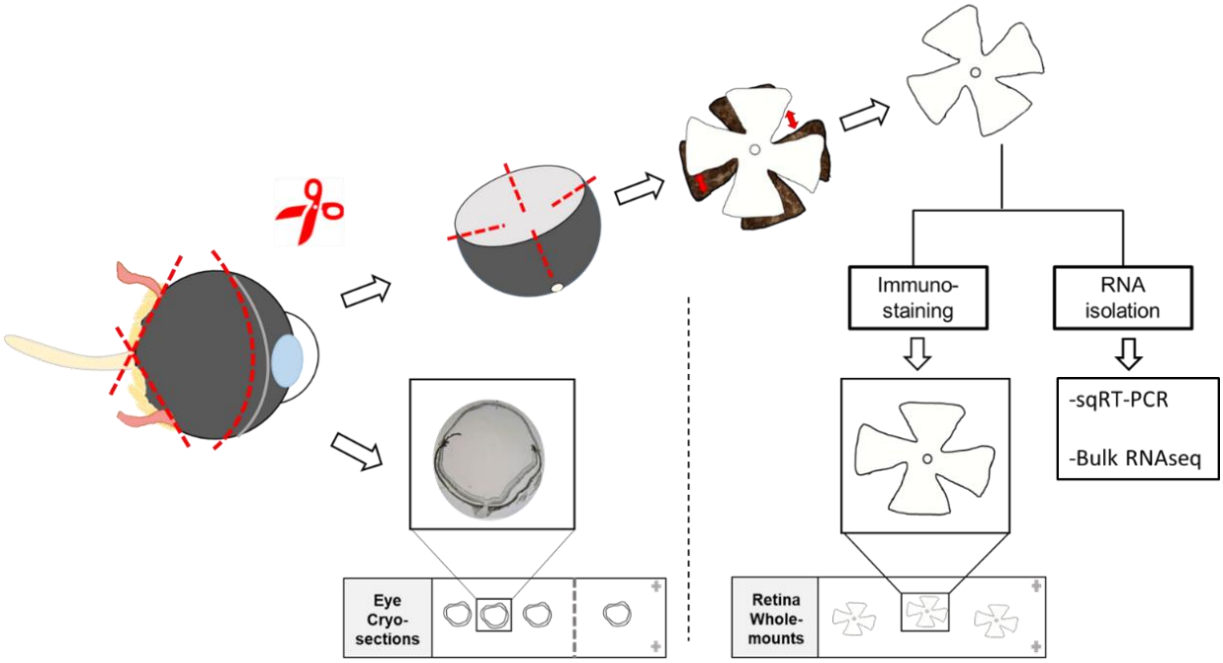

Figure 5. Whole-mount retina and eye cryosections preparation. The scheme shows the general eye dissection. First, the extraocular tissue is removed from the eyeball, and an incision is made behind the limbus/ora serrata (grey semicircle). Then, one mouse eye is used for cryosections (bottom), while the contralateral eye is used to prepare retinal whole-mounts (top). To prepare whole-mounts, the anterior part of the eye is removed and the posterior eye cup is further cut into four quarters. The neuroretina (white) is separated from the retinal pigment epithelium (brown). Finally, retinal whole-mounts are either used for RNA isolation or for immunostainings.

2.2.4 Semi-quantitative real-time polymerase chain reaction (sqRT-PCR)

After the dissection, retinal whole-mounts were homogenized in QIAzol Lysis reagent (Qiagen) and stored at -80 °C until further processing. Then, chloroform was used to separate the RNA phase and isopropanolol to precipitate the RNA material. Afterwards, the material was washed with 70 % ethanol and the final pellet was resuspended in ultra-pure DEPC treated water. RNA concentration and quality were measured using a NanoDrop 2000c spectrophotometer (Thermo Scientific, Germany). The reverse transcription of the obtained RNA material was performed with SuperScript III First-Strand Synthesis System (Invitrogen, Germany) and a mixture of random hexanucleotides (Invitrogen, Germany) according to the manufacturer's protocol. Semi-quantitative real-time polymerase chain reaction (sqRT-PCR) for the designed oligonucleotides listed in section 2.1.5 was performed using SYBR GreenER qPCR SuperMix Universal (Invitrogen,

Germany) on the Mastercycler epigradient S (Eppendorf, Germany) using the program in the table 5. The housekeeping gene glyceraldehyde-3-phosphate dehydrogenase (GAPDH) was used as internal control for all mouse-retina samples. The melting curves were analyzed to confirm amplification specificity for all primers.

The results were analyzed using the Mastercycler ep realplex software (Eppendorf, Germany), with values normalized to the corresponding GAPDH levels of each mouse sample and compared to WT animals. For the quantification of relative gene transcription, the delta delta CT (cycle threshold) method was applied.

Table 5. sqRT-PCR program for Mastercycler epigradient S

Step	Temperature	Time (minutes)
Initial denaturation	95 °C	10:00
*Amplification: Denaturation	95 °C	00:15
Annealing	60 °C	00:30
Elongation	72 °C	00:30
*Amplification for 40 cycles		
Inactivation	95 °C	00:15
Melting curve	60 °C – 95 °C	20:15
Final denaturation	95 °C	00:15
Ramp rate		20:00
Pause	4 °C	pause

2.2.5 RNA sequencing analysis.

The RNA of mouse retina for RNA sequencing (RNAseq) was extracted from 9-month-old mice as previously described. Library preparation was performed using the QuantSeq 3′ mRNA-Seq Library Prep Kit (Lexogen) with an input of 100 ng total RNA, followed by quality control (Tapestation 2200, Agilent). RNAseq was conducted at the NGS Core Facility, University Hospital Bonn, generating 2×10^7 single-end reads per sample on the NovaSeq 6000 platform (Illumina). RNAseq analysis was performed with the support of Tawfik Abou Assale and Annemarie Burgartz, under the supervision of Dr. Jannis Wißfeld.

Quality control of raw reads was performed using FastQC (v0.11.8) and MultiQC (v1.7), and samples with abnormally high GC (guanine-cytosine) content (>2 standard deviations) were excluded. Adapter trimming was done using Bbmerge/BBDUK (pmid: 29073143). Reads were aligned to the mouse reference genome mm10 (GRCm38) with ensemble gene annotation version 101, using STAR [v2.7.3a] (Dobin et al., 2013) under standard parameters. Read counts were generated using featureCounts/Subread [v2.0.0] (Liao et al., 2014), excluding multimapping reads. Quality control was repeated as previously described.

Differential expression analysis was conducted in R [v4.3.1] (RStudio Team, 2020) using DESeq2 [v1.42.0] (Love et al., 2014), with group contrasts defined for the analysis. Transcript annotations were obtained using the Bioconductor package org.Mm.eg.db [v3.11.4] (Carlson, 2019), and visualizations were created with ggplot2 [v3.3.3] (Wickham, 2016). Pathway enrichment analyses were performed using clusterProfiler [v3.16.1] (Yu et al., 2012) and GSEA Desktop [v4.2.2] (Mootha et al., 2003; Subramanian et al., 2005) with a threshold of log2FC ≥ 1 and adjusted P-value <0.05. Gene transcripts from all four groups (Gne+/+C3+/+, Gne+/-C3+/+, Gne+/+C3-/-, and Gne+/-C3-/-) were included in the analyses, unless otherwise specified in the results section, to extract differential gene expression (DEG), hallmarks, and enriched pathways for the groups of interest.

2.2.6 Immunohistochemistry of mouse retina

2.2.6.1 Retinal whole-mounts

The retinal whole-mounts dissected from eyes that were previously fixed with 4 % PFA and stored in 30 % sucrose (described in section 2.2.3) were stained to analyse microglia density and morphology.

Retinas were washed with PBS and incubated with blocking solution; 5 % normal goat serum (NGS), 0.2 % bovine serum albumin (BSA), and 0.3 % Triton X-100 overnight at 4 °C. Retinas were incubated for 24 hours at 4 °C with primary antibodies against Iba1 (1:500, Wako, 019-19741) and the lysosomal marker CD68 (1:500, Bio-Rad, MCA1957), both diluted in the previously mentioned blocking solution. After washing with PBS, the retinas were incubated for 2 h at RT with secondary antibodies: Alexa Fluor 647 goat anti-

rabbit (1:800; Jackson ImmunoResearch, 111-606-144) for Iba1, and Cy3 goat anti-rat (1:800, Jackson ImmunoResearch, 112-166-072) for CD68, diluted in washing solution (PBS + 0.3 % Triton X-100).

Following PBS washes, nuclei were stained with 4',6-diamidino-2-phenylindole (DAPI; 1:10,000, Sigma-Aldrich, Germany) for 1 minute. The incubation and washing steps were performed on a nutating mixer (VWR, USA). Finally, the stained retinas were flattened onto microscope slides (Epredia, Germany), mounted with Aqua/Polymount (Polysciences Inc., Germany), and covered with a glass coverslip.

2.2.6.2 Retina cryosections

Retinal cryosections were used to investigate sialylation, the cell density of various retinal neurons, complement factor C1q, glial marker expression (including microglia, Müller cells, and astrocytes). Eyes were fixed in 4 % PFA, embedded and frozen in O.C.T. Compound Tissue Tek (Sakura/Fisher Scientific, Germany). Sagittal sections (20 µm) were cut with a cryostat (Microm, HM 560, Thermo Scientific, Germany), starting laterally and including the optic nerve head for reference during imaging. After drying and PBS washing, sections were blocked for 1 hour at RT in a solution containing 5 % NGS, 10 % BSA, and 0.1–0.3 % Triton X-100.

Three retinal sections per mouse were incubated overnight at 4 °C with primary antibodies diluted in the blocking solution. To assess sialylation in retinal layers, an anti-polysialic acid antibody (PSA-NCAM; clone: 2-2B; 1:500; Millipore, MAB5324) and an anti-trisialic acid antibody (A2B5, 1:500; Invitrogen, 433110) were used. Microglia distribution and activation were examined using antibodies against Iba1 (1:500; Wako, 019-19741) and the lysosomal marker CD68 (1:500; Bio-Rad, MCA1957). To label Müller cells and astrocytes, antibodies against glial fibrillar acidic protein (GFAP; 1:1000, Agilent/Dako, Z0334) and glutamine synthetase (1:500, Invitrogen, PA5-28940) were applied. Glutamine synthetase antibody was also used for improved Müller cell visualization in a co-staining with PSA-NCAM. Complement opsonization was analyzed using an anti-C1q antibody (1:200; Abcam, ab182451).

For retinal neuron identification and quantification, I used anti-cone arrestin (1:500; Millipore, AB15282) for cone photoreceptors, anti-rhodopsin (Rho 4D2; 1:1000, Abcam, ab98887) for rod outer segments, anti-protein kinase C alpha (PKCα, H-7; 1:250, Santa Cruz Biotechnology, sc-8393) for rod bipolar cells, and anti-Brn3a (1:2000; Sigma-Aldrich, AB5945) for ganglion cells. To visualize all retinal nuclei, including those in the outer nuclear layer (ONL), the nuclear marker DAPI (1:10,000; Sigma-Aldrich, Germany) was utilized.

As a negative control, one retinal cryosection per mouse was incubated with only secondary antibodies to account for background fluorescence during intensity analysis. After PBS washes (4 x 5 minutes), secondary antibodies diluted in blocking solution were used to incubate sections for 2 hours at RT: Alexa Fluor 647-conjugated goat anti-mouse (1:500; Jackson ImmunoResearch, 115-606-072) for PSA-NCAM, A2B5, and PKCα; Alexa Fluor 647-conjugated goat anti-rabbit (1:500–1:1000; Jackson ImmunoResearch, 111-606-144) for C1q, cone arrestin, GFAP, and Iba1; Alexa Fluor 488-conjugated goat anti-rat (1:500; Invitrogen, A-11006) for CD68; Alexa Fluor 488-conjugated goat anti-rabbit (1:500; Invitrogen, A11008) for glutamine synthetase; Alexa Fluor 488-conjugated goat anti-mouse (1:500; Invitrogen, A11001) for rhodopsin; and Cy3-conjugated goat anti-rabbit (1:500; Jackson ImmunoResearch, 111-167-003) for Brn3a.

After incubation, the sections were washed and nuclei were stained with DAPI (1:10,000; Sigma-Aldrich, Germany) for 1 minute. All steps were performed in a dark, humidified chamber. The stained sections were mounted with Aqua/Polymount (Polysciences Inc., Germany) and covered with a glass coverslip.

2.2.6.3 Microscope imaging

All images of retinal whole-mounts or retina cryosections were taken using a Leica SP8 resonant scanning confocal microscope and the LAS-X software (Leica Biosystems, Germany) with 40x and 63x objective lenses at the microscopy Core Facility of the Medical Faculty at the University of Bonn.

For retinal whole-mounts stained for Iba1 and CD68, the images were taken from the outer plexiform layer (OPL), a usual location of microglial cells which provided in the staining

clearer images comparing to the inner plexiform layer (IPL). For each mouse retina, six z-stack images were acquired, consisting of 10 optical sections at 1 µm intervals. These images were taken from central, middle, and peripheral regions of both contralateral retina sides, yielding a total of 6 images per mouse.

For retina cryosections all images were taken with 40x objective lens, except for sections stained for C1q, which were taken using a 63x objective lens to better visualize C1q deposits. The images were taken covering all retinal layers, from the photoreceptor's outer segments until the ganglion cell layer. All the images were taken as z-stacks at 2 µm intervals, except for C1q that images were taken at 1 µm intervals, with 10 optical sections for all retina sections. The optic nerve head for most of the stainings, or, the middle point of the full retina length was used as reference and central point to take images at consistent distance (Fig. 6). For all stainings, a total of six images were taken per mouse retina from the central, middle and peripheral areas from the left and right side of the retina cryosection (Fig. 6). Three additional images were collected from negative control sections (stained only with secondary antibodies) covering central, middle and peripheral retina areas, to be used to subtract the background signal for the fluorescence intensity analysis (Fig. 6).

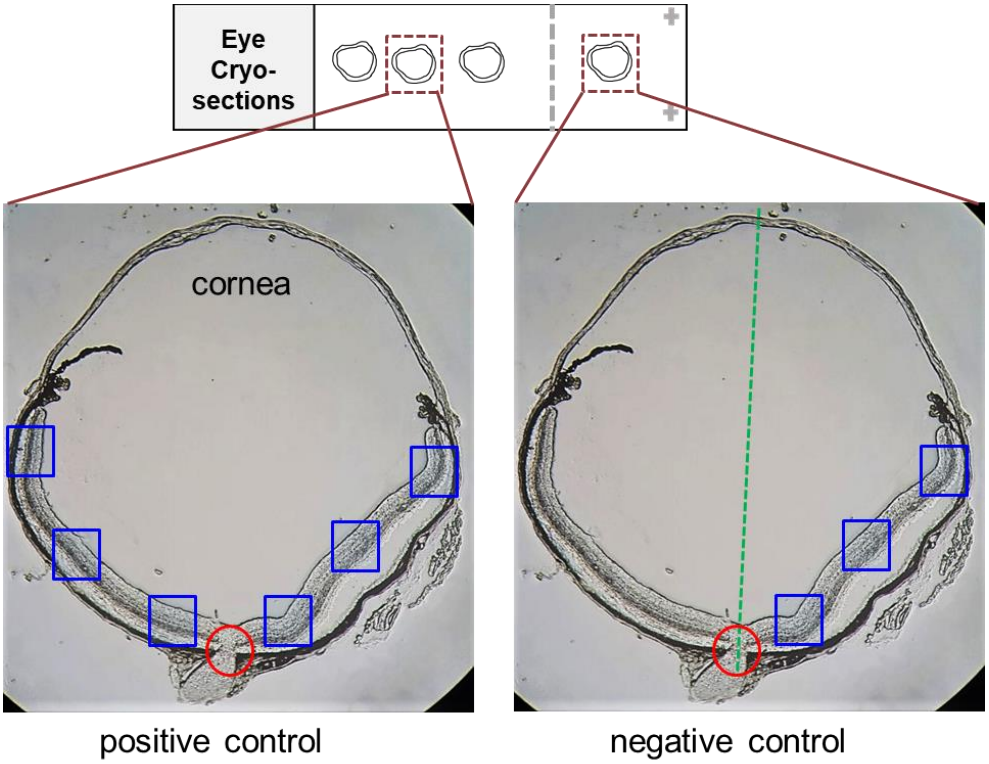

Figure 6. Confocal microscopy imaging scheme. Images of retinal cryosections were taken from both, left and right side of the retinal section for positive control (6x images), and only from one side of the retina section for the negative control (3x images). The images were taken from central, middle, and peripheral retinal areas, using the optic nerve head as reference (red circle), or, the middle point of the full cryosection length (greed dotted line). Images taken using a Samsung 20 smartphone under binocular microscope.

For all stained retinal sections, single images were converted to maximum projections of z-stacks (10 optical sections), except for those stained for PKCα, which were overlaid with only 3 optical sections, and for cone arrestin images that were overlaid just with 8 optical sections to avoid cell overlapping and better visualization. The images were saved with the LAS-X software (Leica Biosystems, Germany, v3.5.5) as tag image file format (TIFF) multichannel before being used for different analysis.

2.2.7 Image analysis

The analysis of the images was conducted using the ImageJ software (v2.1.0/1.53c, NIH, USA) by measuring the fluorescence integrated density (mean gray value per area) after subtracting the mean background fluorescence from negative control images. For all staining analyses, the mean fluorescence intensity and cell density of each mouse were

normalized to the average values of the WT mice group. DAPI-stained nuclei were used to identify the main retinal layers: ganglion cell layer (GCL), inner plexiform layer (IPL), inner nuclear layer (INL), outer plexiform layer (OPL), and outer nuclear layer (ONL).

2.2.7.1 Measurement of sialic acids, glial and complement markers

The expression of polysialic and trisialic acids (detected using antibodies PSA-NCAM and A2B5, respectively) was assessed throughout the entire retinal thickness. Additionally, the expression levels of microglia markers Iba1 and the lysosomal marker CD68 were quantified across all retinal layers. The Müller cell and astrocyte marker GFAP was also measured in every retinal layer. For the fluorescence intensity analysis of Iba1/CD68 and GFAP, the ganglion cell layer (GCL) and the inner plexiform layer (IPL) were combined, as microglial cells and astrocytes are frequently located between these two layers. Quantification of C1q was conducted only in the OPL due to its strongest staining signal in this layer compared to the other retinal layers, which exhibited very weak C1q signals.

2.2.7.2 Analysis of microglia distribution, density, and morphology

The distribution of microglia across retinal layers was examined using cryosection images of the retina stained for Iba1 and CD68. The count of double-positive cells for Iba1 and CD68 was primarily focused on the OPL, and the IPL including the GCL.

Microglial cell density was quantified using the images taken from the OPL of retinal whole-mounts by counting manually the somas of Iba1 positive cells. The number of cells were divided by the selected area to calculate the relative cell density.

The microglial skeleton was analyzed using the MotiQ plug-in in ImageJ (for details see Hansen *et al.*, 2022). A minimum of 8 microglial cells per mouse retina were randomly selected from three different images using the ImageJ polygon tool, ensuring that both the microglial soma and its processes were included in the selection. After cropping and saving the images as single-cell files, a 2-dimensional reconstruction was performed, and several parameters were measured: number of branches, number of tips, number of junctions, the ramification index, spanned area (total area covered by the cell), and tree length. Lower values of these skeleton parameters suggest that microglia transition from a highly ramified to amoeboid shape (Stence et al., 2001; Young & Morrison, 2018).

2.2.7.3 Analysis of neuronal cell density in the retina

To calculate the density of different retinal neurons, images of retinal cryosections stained for cone arrestin (for cone photoreceptors), PKCα (for rod bipolar cells), and Brn3a (for ganglion cells) were analyzed. The density was determined by dividing the number of positive cells by the selected area, using the DAPI signal to identify the corresponding neuron areas.

Additionally, the thickness or width of the ONL, which contains the photoreceptor cell bodies, was measured to indirectly assess potential photoreceptor loss. As mentioned above, images of retinal cryosections stained with DAPI for nuclei were captured from the central, middle, and peripheral regions of the retina. The optic nerve head was used as a reference to ensure consistent image acquisition across all mice and to minimize discrepancies in retinal thickness measurements. The ONL width was measured using the freehand line tool in ImageJ, with three measurements taken per image across all nine images for each mouse, resulting in a total of 27 measurement points per mouse.

2.2.8 Statistical analysis

All experimental data are presented as mean ±, or, + SEM (standard error of the mean), unless otherwise specified. For all analyses, results were normalized to the mean of the WT mice within each age group to obtain relative values. Extreme outliers were identified and removed using Grubbs' test using the outlier calculator from GraphPad QuickCalcs. Statistical comparisons between two groups were performed using an unpaired Student’s t-test, while comparisons of 4 genotype groups were made using Welch ANOVA with Welch's correction. Statistical analysis and graph creation were conducted using GraphPad Prism (v8.0.2). Lastly, statistically significant differences are depicted as *$p < 0.05$, **$p < 0.01$, ***$p < 0.001$, and ****$p < 0.0001$.

3. Results

Elements of the results section, along with all figures within this section with modifications, except for figures 17 and 24, were already published online in a pre-print version of the journal *GLIA* on September 3, 2024 (Cuevas-Rios et al., 2024).

3.1 Reduced levels of sialic acids in the Gne+/- mouse retinas

Complete *Gne* knock out mice (Gne-/-) leads to embryonic lethality, however, Gne+/- mice can live with no apparent phenotype defects. It was previously shown that Gne+/- mice has reduced levels of sialic acid in different brain regions, particularly at 12 months of age (Klaus et al., 2020). Despite retina is a part of the CNS, it is not known whether hyposialylation can also be observed in the retinas of Gne+/- mice.

After PCR determination of the mice genotypes (Fig. 4), sqRT-PCR was performed to confirmed transcription of the *Gne* gene in the retinas of Gne+/- at 9 months of age. The analysis showed a significant decreased of *Gne* mRNA levels of 29 % compared to wildtype (WT) mice (Fold change; FC 1.02 ± 0.08 vs. 0.73 ± 0.03, p= 0.02; Fig. 7A).

To investigate whether the lower transcription of *Gne* translates into alteration in the sialic acid expression in the mouse retina, the sialylation status of retinal layers was screened with IHC for oligosialic (trisialic) acid on gangliosides (A2B5; Fig. 7B), and for long-chain sialic acids on NCAM (PSA-NCAM; Fig. 7D) using retina cryosections of 3-, 9- and 12-months old mice.

Analysis of retinal images revealed that the localization and expression pattern of both, trisialic and polysialic acids were similar in Gne+/- and WT animals at 3, 9 and 12 months. Nevertheless, the expression pattern within groups was not uniform across the retinal layers, with higher intensity in the ganglion cell layer (GCL), followed by the inner and outer plexiform layers (IPL and OPL), the outer nuclear layer (ONL) and the inner nuclear layer (INL). Additionally, trisialic acid showed stronger staining intensity in the photoreceptor outer segments (POS) compared with polysialic acid signal (Fig. 7B, D).

The analysis of the fluorescence intensity revealed a trisialic acid level reduction of 35.1 ± 6.07 % (p= <0.0001) compared to WT mice at 9 months of age, while at 12 months

of age showed just a slight trend for decreased levels from 100 ± 10.09 % in Gne+/+ mice to 87.70 ± 9.87 % in Gne+/- animals (p= 0.40; Fig. 7C). On the other hand, levels of polysialic acid showed at 9 months of age a significant decrease of 24.2 ± 6.41 % (p= 0.01) in Gne+/- mice compared to WT Gne+/+ mice. Moreover, 12 months mice also displayed a tendency for reduced polysialic acid expression, from 100 ± 7.76 % in Gne+/+ mice to 74.87 ± 9.18 % in Gne+/- animals (p= 0.06; Fig. 7E). There was no significant decrease in trisialic and polysialic acids levels in the retinas of Gne+/- mice at 3 months of age (Fig. 7C, E), indicating that the reduction in retinal sialylation may occur progressively in middle-aged mice.

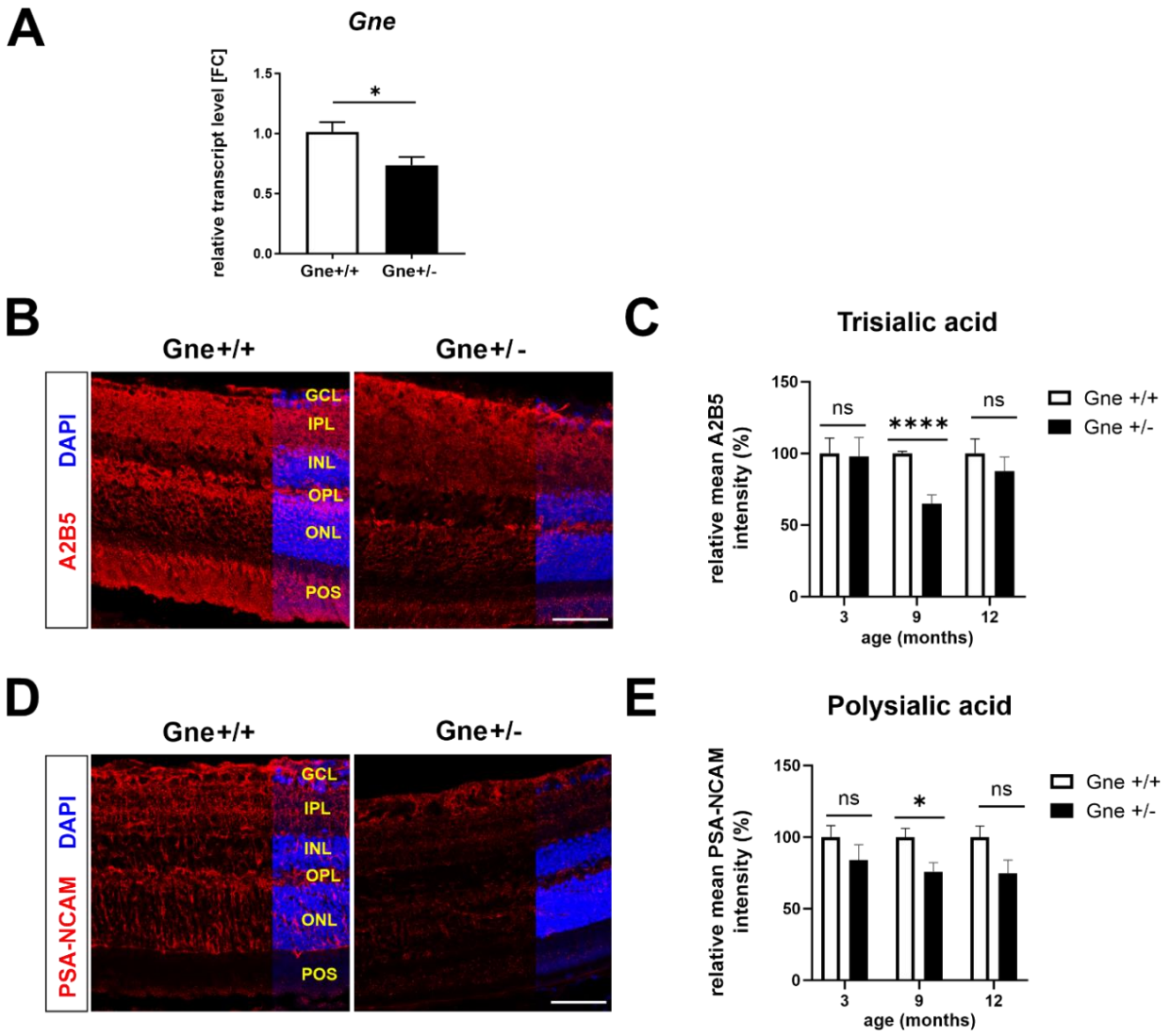

Figure 7. Reduced sialic acids levels in the retinas of Gne+/- mice. (A) Transcriptional analysis of retinas from 9-month-old mice revealed reduced *Gne* mRNA levels in Gne+/- mice compared to wildtype (Gne+/+) mice; n= 6. (B) Representative images of retinal

cryosections co-stained for trisialic acid on gangliosides (A2B5, red) and the nuclear marker DAPI (blue). (C) Quantification of A2B5-immunofluorescence in mouse retinas showed comparable trisialic acid intensity at 3 and 12 months of age, but a significant reduction at 9 months in Gne+/- mice compared to wildtype (Gne+/+) mice. (D) Representative images of retinal cryosections co-stained for polysialic acid on neuronal cell adhesion molecule (PSA-NCAM; red) and DAPI (blue). (E) Fluorescence intensity analysis of PSA-NCAM-immunostaining in the retinas indicated comparable polysialic acid expression at 3 months, a significant decrease at 9 months, and a tendency toward reduced expression at 12 months in Gne+/- mice compared to wildtype mice; n= 4–9. Both scale bars: 50 µm. FC: fold change; GCL: ganglion cell layer; IPL: inner plexiform layer; INL: inner nuclear layer; OPL: outer plexiform layer; ONL: outer nuclear layer. POS: photoreceptors outer segments. All data shown as mean + SEM; normalized to wildtype mice within age group; *$p \leq 0.05$, ****$p \leq 0.0001$. Elements of this figure were already published online in *GLIA* on September 3, 2024 (Cuevas-Rios et al., 2024).

A co-staining for PSA-NCAM and glutamine synthetase (Fig. 8) was also performed to examine whether the polysialic acid staining pattern is linked to a specific retinal cell type, particularly Müller cells, as the signal staining appeared to align with the Müller cells arrangement. The images revealed partial co-localization of polysialic acid with Müller cells, particularly around the GCL. However, polysialic acid is also observed outlining other retinal structures across all layers (Fig. 8).

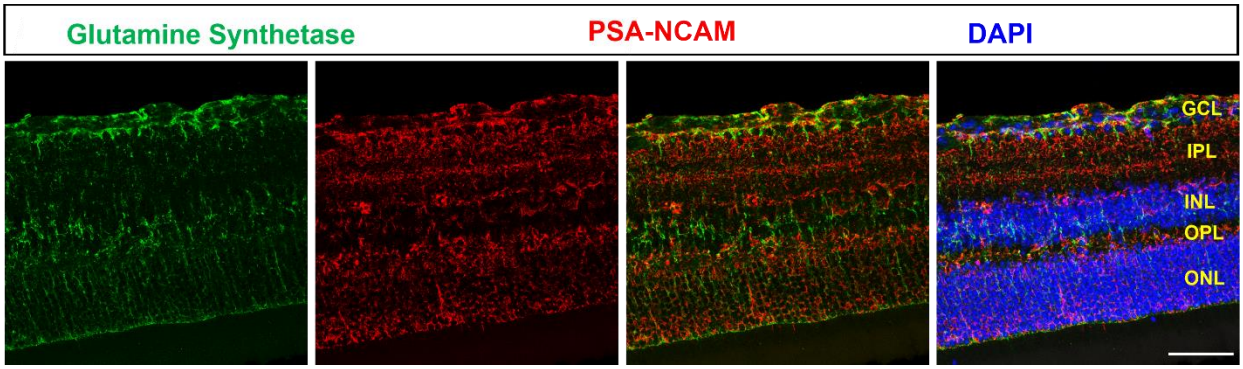

Figure 8. Partial co-localization of polysialic acid with Müller cells. Representative images of retinal cryosections from 9-month-old wildtype Gne+/+ mice co-stained with antibodies against glutamine synthetase (green) for Müller cells and PSA-NCAM (red) for polysialic acid, with nuclei counterstained using DAPI (blue). The images of stained retina demonstrate partial co-localization between polysialic acid and Müller cell structures. Scale bar: 50 µm. GCL: ganglion cell layer; IPL: inner plexiform layer; INL: inner nuclear layer; OPL: outer plexiform layer; ONL: outer nuclear layer. Modified figure was already published online in *GLIA* on September 3, 2024 (Cuevas-Rios et al., 2024).

Overall, the analysis of Gne+/- mouse retinas revealed reduced transcription of the *Gne* gene and a significant decrease in trisialic and polysialic acids at 9 months, with a lesser extent of reduction at 12 months of age.

3.2 Increased microglial CD68 expression but no microglial density or morphology changes in the retinas of Gne+/- mice

Evidence suggest that sialylation might act as check-point for the innate immune system in the mouse retina (Klaus et al., 2021; Lünemann et al., 2021). To examine microglial activation, immunostaining on retinal cryosections was performed using antibodies targeting the microglial markers Iba1 and CD68 (Fig. 9A). The analysis of Iba1-positive cells showed that the majority of microglial cells were concentrated in the GCL, with additional presence in the INL and OPL. In contrast, only a few microglial cells were observed in the ONL or subretinal space in both Gne+/- and WT animals (Fig. 9A). The analysis of retina cryosections showed similar microglial cell density in the GCL/IPL and OPL in both, Gne+/- and WT mice at 9 and 12 months of age (data not shown).

Analysis of the fluorescence was also performed to include microglia processes that extend to the different retinal layers (Fig. 9B). The results showed similar Iba1 intensities in all retinal layers between the Gne+/- and Gne+/+ WT mice at 9 months of age, and a tendency for higher Iba1 expression at 12 months of age. For instance, in the retinal nuclear layers, Iba1 intensity showed a tendency for an increase of 19.5 % ± 5.34 (p= 0.05) in the INL compared to WT mice. Similarly, 12 months Gne+/- mouse retinas displayed trend for higher Iba1 staining intensity in the ONL compared to the WT mice (120.3 ± 7.89 vs. 100 ± 7.59, p= 0.09). In contrast, the expression of the microglial lysosomal protein CD68 was elevated across nearly all retinal layers in Gne+/- mice compared to Gne+/+ mice at 9 and 12 months of age. Notably, the outer plexiform layer, a typical location for microglia, showed a 44.17 % increase in fluorescence intensity in Gne+/- mice at 9 months of age compared to WT animals. (144.17 ± 7.48 % vs. 100 ± 14.8 %, p= 0.01; Fig. 9B).

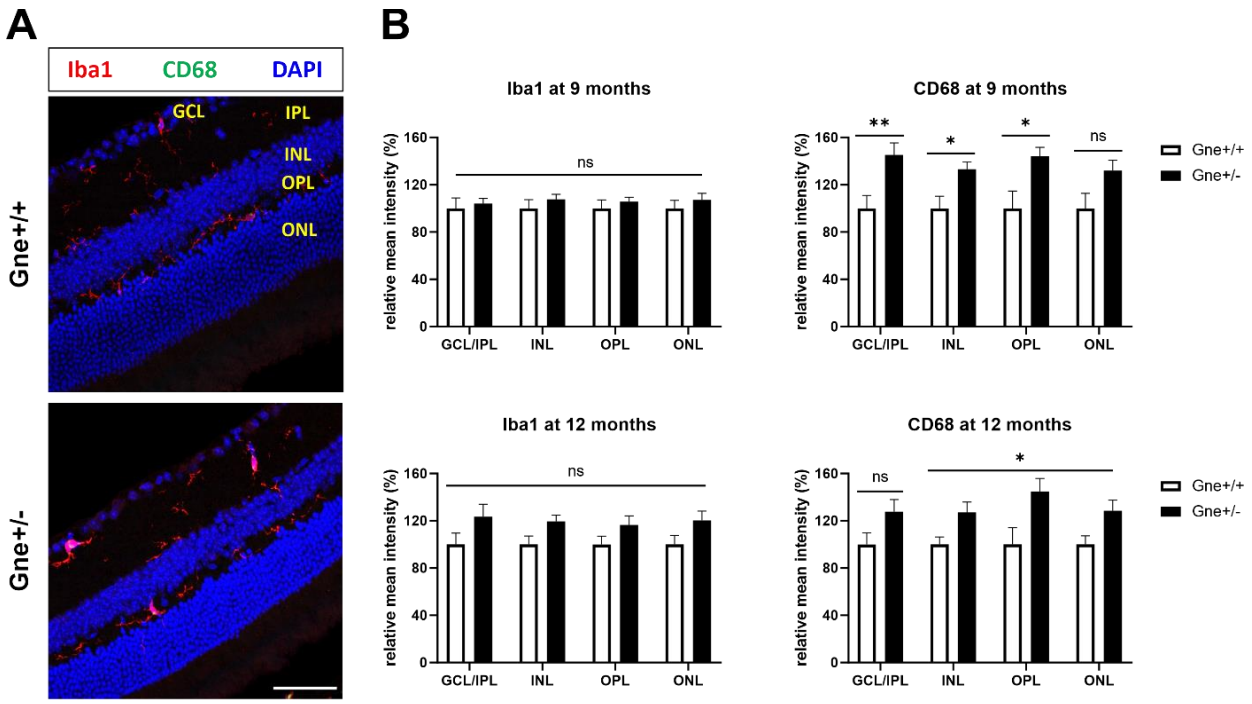

Figure 9. Increased expression of lysosomal CD68 in retinal microglia of Gne+/- mice. (A) Representative images of retinal cryosections from 12-month-old Gne+/- and Gne+/+ mice stained with antibodies against the microglial markers, ionized calcium binding adaptor molecule 1 (Iba1; red) and antigen CD68 (green), along with the nuclear marker DAPI (blue). (B) Fluorescence intensity analysis indicated a slight trend towards higher Iba1 expression in the inner nuclear layer (INL) and in outer nuclear layer (ONL) of 12-month-old Gne+/- mice. In contrast, CD68 levels were elevated in most retinal layers of Gne+/- mice at both 9 and 12 months of age; n= 7–10. Scale bar, 50 µm. GCL: ganglion cell layer; IPL: inner plexiform layer; INL: inner nuclear layer; OPL: outer plexiform layer; ONL: outer nuclear layer. All data shown as mean + SEM; normalized to wildtype mice; ns= not significant, **p* ≤ 0.05, ***p* ≤ 0.01. Modified figure already published online in *GLIA* on September 3, 2024 (Cuevas-Rios et al., 2024).

Since microglial can expand and increased its number in response to retinal alterations or insults, the relative density of Iba1-positive cells was determined using retinal whole-mounts co-stained for Iba1 and CD68 (Fig. 10A). The results showed similar retina cell density in 9 and 12 months Gne+/- mice compared to WT animals (Fig. 10B). Next, to investigate potential morphological changes in microglia due to hyposialylation, microglia shape and arborization was assessed using ImageJ software with the MotiQ plugin, which quantifies various microglial skeleton parameters (Hansen et al., 2022) (Fig. 10C). The analysis revealed highly ramified microglia, with no detectable differences in morphological parameters between 9-month-old Gne+/- and WT mice (Fig. 10D).

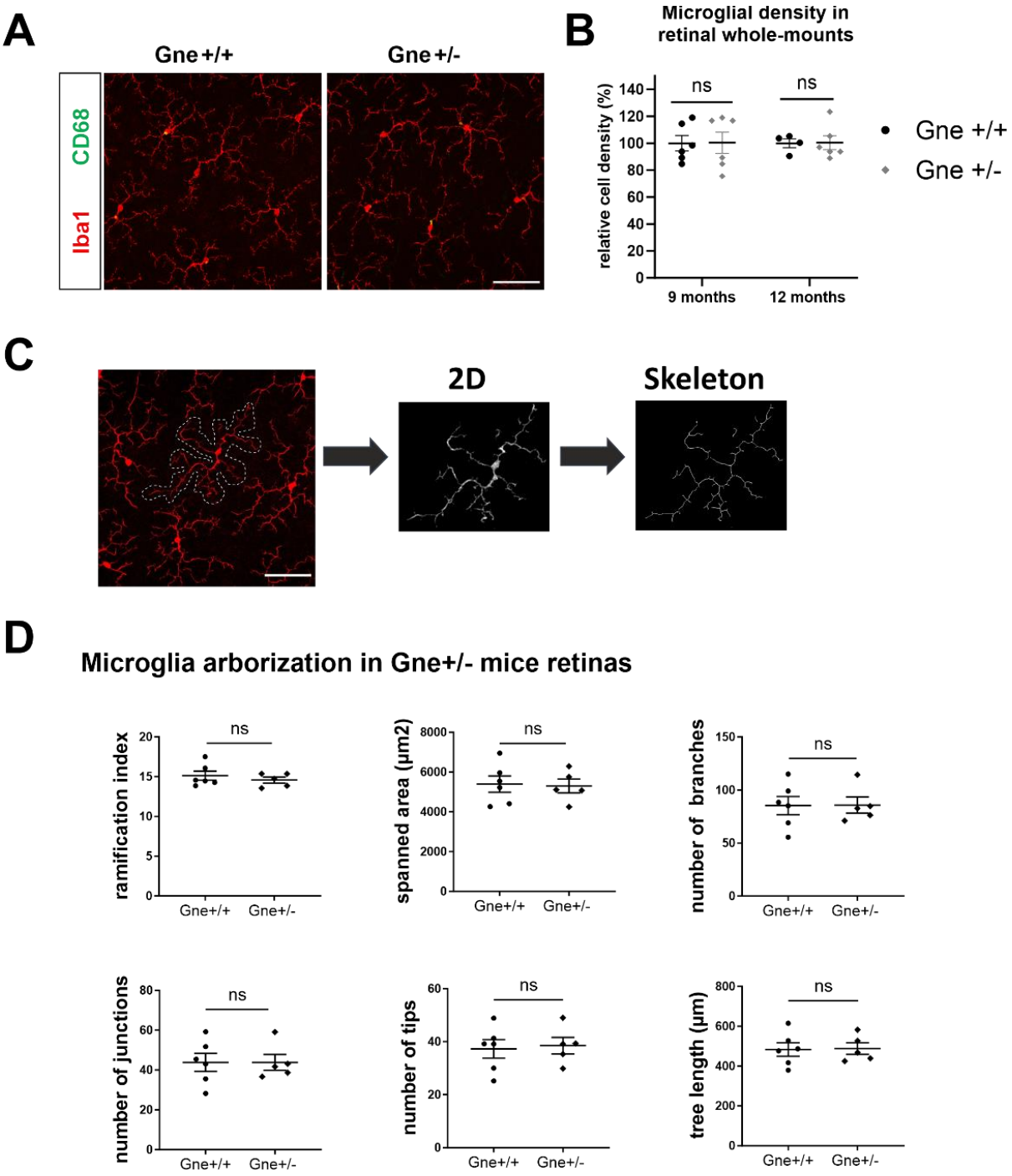

Figure 10. No microglial density or morphology changes in Gne+/- mouse retina. (A) Representative images of retinal whole-mounts from 9-month-old Gne+/- and Gne+/+ mice stained with antibodies against ionized calcium binding adaptor molecule 1 (Iba1; red) and antigen CD68 (green), alongside the nuclear marker DAPI (blue). (B) Cell density analysis showed no difference in the number of microglia between Gne+/- and Gne+/+ mice at 9 and 12 months of age; n= 4-6. (C) Microglial skeletons were analyzed using the MotiQ plugin in ImageJ, with representative images showing a 2-dimensional (2D) reconstruction of a selected microglial cell (white dotted line) and its skeleton. (D) The analysis of microglial cytoskeletons revealed no significant differences in arborization

parameters between Gne+/- and Gne+/+ mice; n= 5-6. Both scale bars, 50 µm. The data are shown as mean ± SEM; normalized to wildtype mice; ns= not significant. Slightly modified figure already published online in *GLIA* on September 3, 2024 (Cuevas-Rios et al., 2024).

Hence, despite no changes in the microglia morphology or cell density were observed in retinas of Gne+/- mice at 9 months of age, there is a clear increase in the expression of the lysosomal microglial marker CD68 in several retinal layers at 9 and 12 months of age.

3.3 Macroglial cell reactivity in Gne+/- retinas

It has been shown that reduced levels of sialic acid led to neuroinflammation and degeneration. Activation of retinal Müller cells and astrocytes, and gliosis in general, has been linked to inflammation and various retinal diseases (Guttenplan et al., 2020; Iandiev et al., 2006; Inman & Horner, 2007; Nadal-Nicolás et al., 2018; Yang et al., 2019). Therefore, Müller cells and astrocytes were investigated in the retina using an antibody against glial fibrillary acidic protein (GFAP; Fig. 11). GFAP staining was primarily localized in the GCL, with a gradual decrease in intensity towards the OPL. In some mouse retinas, GFAP expression extended into the ONL (Fig. 11A). Quantitative analysis revealed an overall increase in GFAP fluorescence intensity in 9-month-old Gne+/- mice, with a smaller increase observed at 12 months. Specifically, the relative GFAP signal in the ganglion cell layer/inner plexiform layer (GCL/IPL) was significantly elevated at 9 months (p= 0.03), rising from 100 ± 8.85 % in WT to 123.37 ± 4.47 % in Gne+/- mice (Fig. 11B). In contrast, the other retinal layers showed only a mild trend towards higher GFAP expression in Gne+/- mice, particularly at 9 months of age (Fig. 11B).

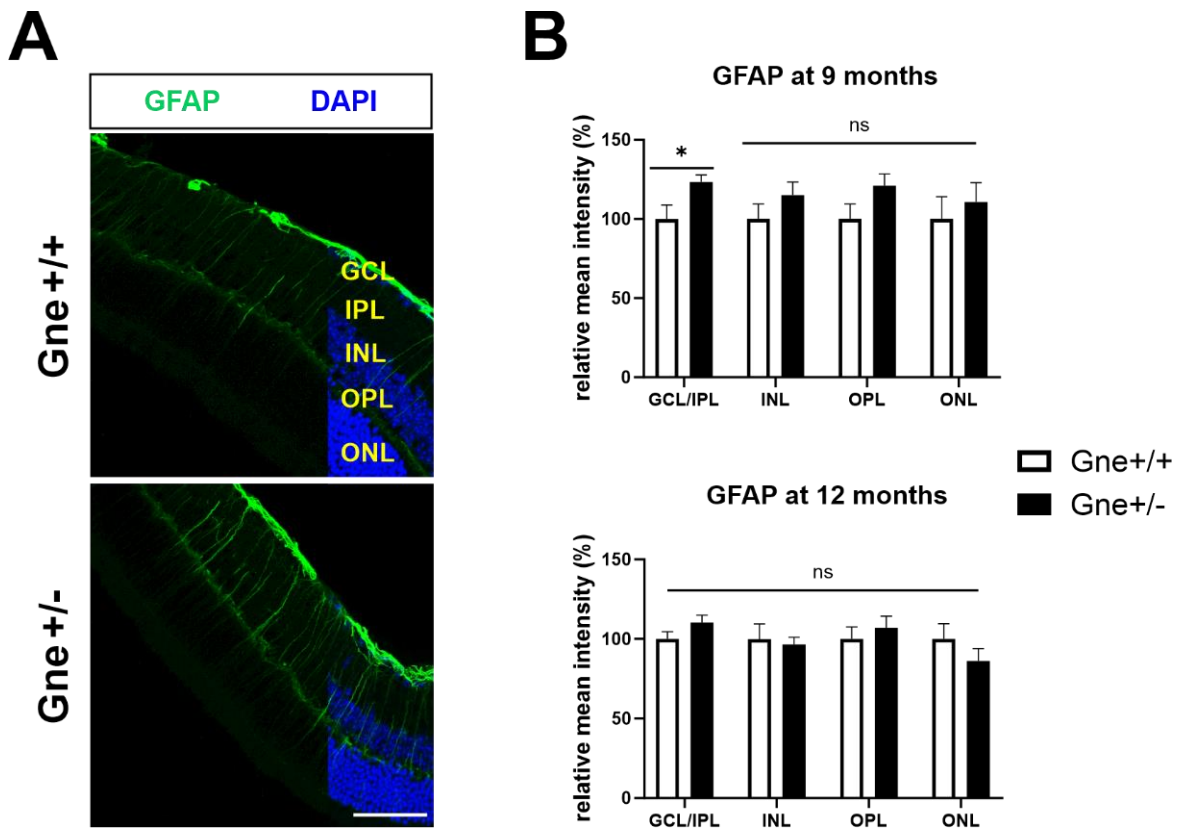

Figure 11. Increased expression of macroglial marker in the retinas of Gne+/- mice. (A) Representative images of retinal cryosections from 12-month-old Gne+/- and Gne+/+ mice co-stained with antibodies against glial fibrillary acidic protein (GFAP; green) and the nuclear marker DAPI (blue). (B) Fluorescence intensity quantification showed an increased expression of GFAP in the ganglion cell layer/inner plexiform layer (GCL/IPL) of 9-month-old Gne+/- mice; n= 7-10. Scale bar: 50 µm. GCL: ganglion cell layer; IPL: inner plexiform layer; INL: inner nuclear layer; OPL: outer plexiform layer; ONL: outer nuclear layer. All data shown as mean + SEM; normalized to wildtype mice; ns= not significant, $*p \leq 0.05$. Slightly modified figure already published online in *GLIA* on September 3, 2024 (Cuevas-Rios et al., 2024).

Thus, the data indicate an increased expression of the astrocyte and Müller cell marker GFAP in the retinas of 9-month-old Gne+/- mice, with the most pronounced changes observed in the inner retinal layers.

3.4 Bipolar cell loss in retinas of 12 months old Gne+/- mice

Sialylation in the CNS is crucial for a wide range of functions such as regulation of neurotransmission, synaptic plasticity, and prevention of unwanted neuronal-removal (Hildebrandt & Dityatev, 2013; H. Liao et al., 2020; Linnartz-Gerlach et al., 2016).

Previously, it was reported that hyposialylation is associated with neuronal and synaptic loss in the substantia nigra and hippocampus of middle-aged mice (Klaus et al., 2020). To assess potential changes in photoreceptor neuronal density, I examined the thickness of ONL using DAPI staining as a nuclear marker (Fig. 12A). Additionally, the cellular density of key retinal neurons was investigated by staining for cone photoreceptors (cone arrestin; Fig. 12C), rod bipolar cells (PKCα; Fig. 12E), ganglion cells (Brn3a; Fig. 12G), and the outer segments of rod photoreceptors (rhodopsin; Fig. 13A).

Analysis of ONL thickness revealed no significant differences between Gne+/- and WT mice at 9 and 12 months of age (Fig. 12B). To further investigate photoreceptors, the relative cell density of cone cells was calculated using cone arrestin staining. The results indicated similar cell densities for both Gne+/- and WT mice at 9 and 12 months (Fig. 12D). Rod bipolar cells, which transmit light signals from rod photoreceptors to ganglion cells, were stained with PKCα antibody. Analysis revealed no changes in the density of rod bipolar cells at 9 months, however, at 12 months, the relative cell density decreased (p= 0.02) from 100 ± 1.42 % in WT mice to 92.54 ± 2.58 % in Gne+/- mice (Fig. 12F). Finally, I assessed ganglion cell density, which is responsible for sending visual stimuli to the brain, using Brn3a staining of retinal cryosections. The analysis showed no significant changes in ganglion cell density at either 9 or 12 months of age (Fig. 12H).

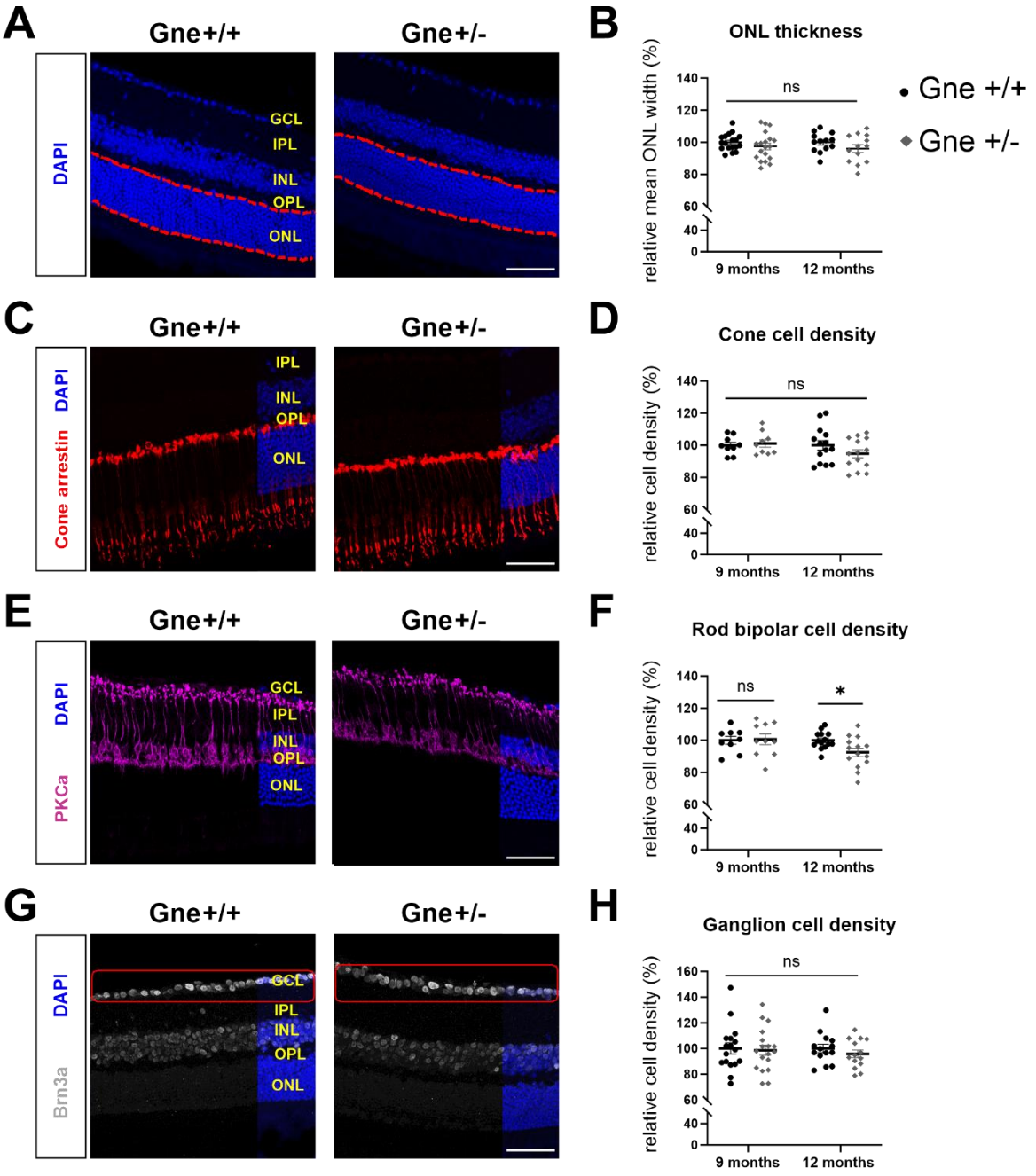

Figure 12. Loss of rod bipolar cells in retinas of 12 months Gne+/- mice. (A) Representative images of retinal cryosections from 12-month-old Gne+/- and Gne+/+ mice stained with the nuclear marker DAPI (blue). (B) Analysis of the outer nuclear layer (ONL; indicated by red dotted line) showed no significant differences in thickness between 9- and 12-month-old Gne+/- and wildtype Gne+/+ mice; n= 13-19. (C) Retinal cryosections from 12-month-old mice stained with cone arrestin antibody (red). (D) Quantification of cone arrestin-positive cells revealed similar cell densities in 9- and 12-month-old Gne+/- mice and Gne+/+ mice; n= 9-14. (E) Images showing rod bipolar cells stained with the PKCα antibody (magenta) in retinal cryosections from 12-month-old Gne mice. (F) Analysis of rod bipolar cell density showed a decrease in Gne+/- mice at 12 months compared to Gne+/+ mice; n= 9-14. (G) Representative images of retinal cryosections

from 12-month-old Gne mice stained with the Brn3a antibody (gray). (H) Cell counting of Brn3a-positive ganglion cells indicated no significant differences between Gne+/- and Gne+/+ mice at 9 or 12 months; n= 14-18. All scale bars; 50 µm. GCL: ganglion cell layer; IPL: inner plexiform layer; INL: inner nuclear layer; OPL: outer plexiform layer; ONL: outer nuclear layer. All data shown as mean ± SEM; normalized to wildtype mice; ns= not significant, *$p \leq 0.05$. Slightly modified figure already published online in *GLIA* on September 3, 2024 (Cuevas-Rios et al., 2024).

Additionally, fluorescence intensity analysis showed no differences of rhodopsin levels in the rod photoreceptors outer segments (POS) in 9 and 12 months Gne+/- mice compared to WT animals (Fig. 13B).

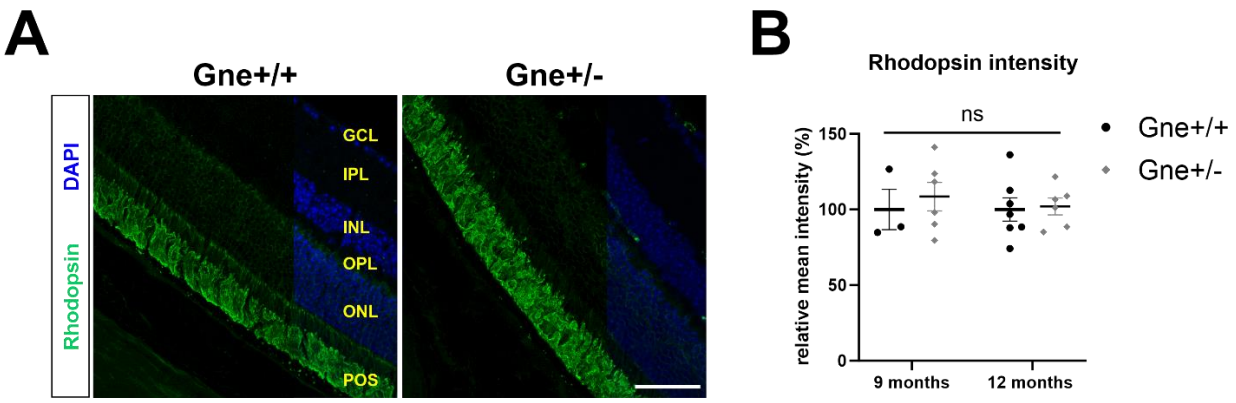

Figure 13. No changes in the rhodopsin expression in the retinas of Gne+/- mice. (A) Representative images of retinal cryosections from 12-month-old Gne+/- and Gne+/+ mice stained for rhodopsin in the rod cell outer segments (green) and the nuclear marker DAPI (blue). (B) Quantification of fluorescence intensity showed comparable levels of rhodopsin in Gne+/- and Gne+/+ mice at both 9 and 12 months of age; n= 3-7. Scale bar: 50 µm. GCL: ganglion cell layer; IPL: inner plexiform layer; INL: inner nuclear layer; OPL: outer plexiform layer; ONL: outer nuclear layer; POS: photoreceptors outer segments. The data are shown as mean ± SEM; normalized to wildtype mice; ns= not significant. Slightly modified figure already published online in *GLIA* on September 3, 2024 (Cuevas-Rios et al., 2024).

Overall, the data demonstrate that the cell density of retinal neurons was not affected at 9 months of age, nonetheless at 12 months, Gne+/- mouse retinas showed a significant loss of rod bipolar cells.

3.5 No changes in C1q expression in Gne+/- mice retinas

Neurons with hyposialylation or undergoing degeneration are often opsonized by complement factors, such as C1q, before being cleared by microglial phagocytosis (Hong et al., 2016; Werneburg et al., 2020). To investigate this, I analyzed C1q deposition in the retinas of 9- and 12-month-old mice (Fig. 14). C1q was detected predominantly in the OPL, with only minimal staining observed in the GCL in both Gne+/- and WT control mice (Fig. 14A). Consequently, fluorescence intensity quantification was concentrated on the OPL. The results revealed similar levels of C1q expression between Gne+/- and Gne+/+ WT mice at both 9 and 12 months of age (Fig. 14B). Interestingly, in some retinal images, C1q expression appeared to exhibit patterns resembling microglial cells (Fig. 14A, magnified images).

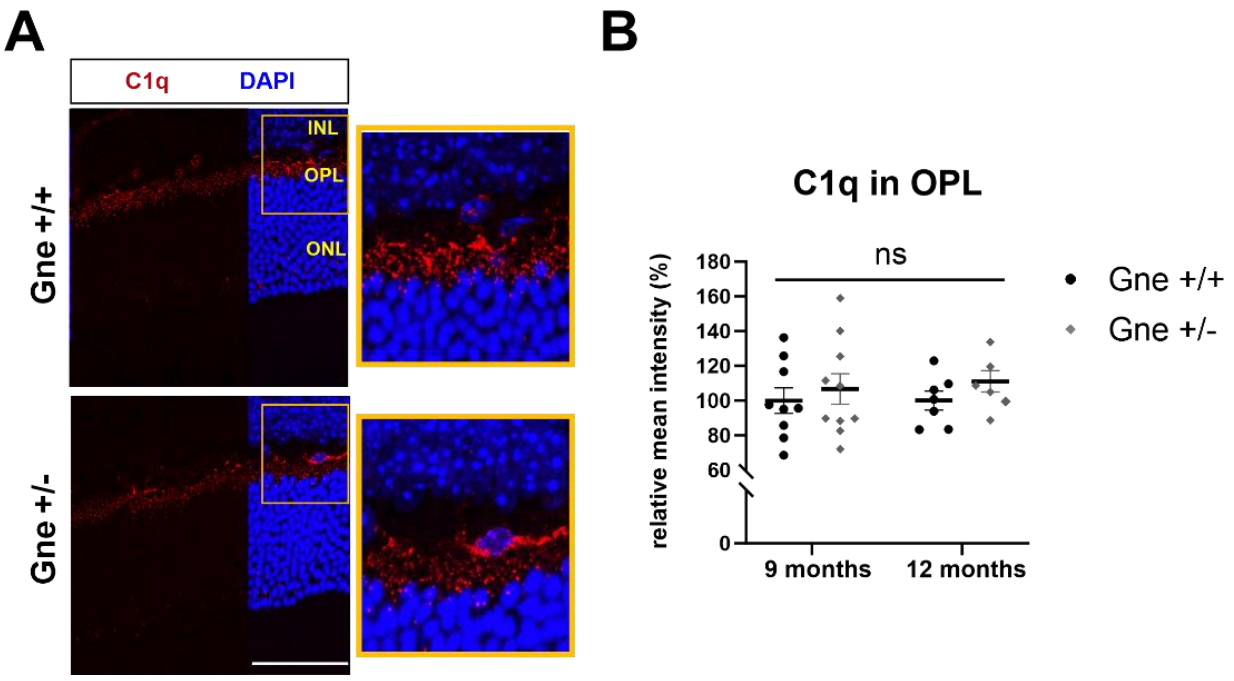

Figure 14. No change in the C1q expression in Gne+/- mouse retinas. (A) Images of retinal cryosections from 12-month-old Gne+/- and Gne+/+ mice co-stained with an antibody against complement component 1q (C1q; red) and the nuclear marker DAPI (blue). (B) Fluorescence intensity analysis in the outer plexiform layer (OPL) revealed comparable C1q expression levels between Gne+/- and Gne+/+ wildtype mice at both 9 and 12 months of age; n= 6-10. Scale bar; 50 µm. INL: inner nuclear layer; OPL: outer plexiform layer; ONL: outer nuclear layer. The data are shown as mean ± SEM; normalized to wildtype mice; ns= not significant. Modified figure already published online in *GLIA* on September 3, 2024 (Cuevas-Rios et al., 2024).

Thus, these data demonstrate that the observed loss of bipolar cells at 12 months is independent of C1q expression in the retinas of Gne+/- mice.

3.6 Transcriptional changes in the retina of Gne+/- mice

Bulk RNAseq analysis was conducted on retinas from 9-month-old Gne+/- and WT mice to investigate the mechanisms underlying microglia activation and the loss of rod bipolar cells in this hyposialylation model. The goal was to identify early transcriptional changes that may precede alterations in protein expression and cellular loss. While principal component analysis (PCA) did not reveal a distinct separation between the Gne+/- and WT control groups (Fig. 15A), differentially expressed genes (DEGs) indicated a significant reduction in *Gne* gene transcripts in Gne+/- mice (p adj. 5.93e-19). Additionally, several novel gene transcripts were found to be differentially expressed between the two mice groups (Fig. 15B). Notably, transcripts for crystallin alpha B (*Cryab*) and beta-crystallin B1 (*Crybb1*) were upregulated in Gne+/- mice. These genes encode crystallin proteins essential for maintaining lens transparency and refractivity. Furthermore, the transcription of the HORMA domain containing 2 (*Hormad2*) gene, which is crucial for meiotic prophase (Kogo et al., 2012), was also upregulated (Fig. 15B).

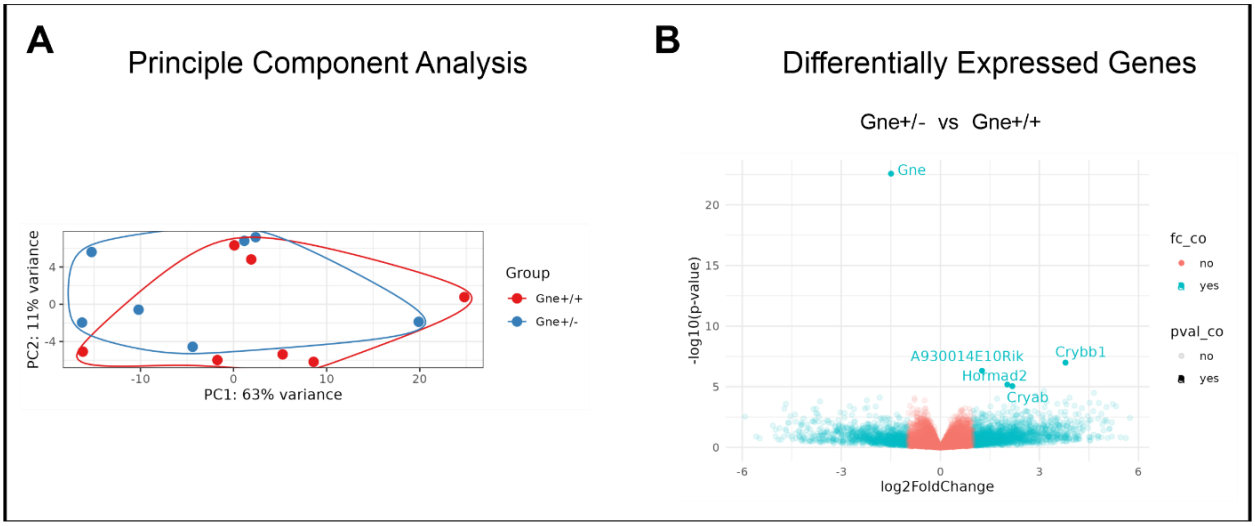

Figure 15. RNAseq analysis of retinas from 9 months old Gne+/- mice. (A) Principal component analysis (PCA) of retinal RNA sequencing data showing the distribution of Gne+/- (blue) and wildtype (Gne+/+; red) mice. Each dot represents an individual mouse. Although there is some clustering, indicated by ellipses, there is no clear separation between the two groups. (B) The volcano plot displays differential gene expression between Gne+/- and wildtype mice (Gne+/+). Genes with a *p*-value below 0.05 (depicted

by clear dots) and a log2 fold change greater than 1 (depicted by blue dots) are highlighted. The *Gne* gene is the most significantly downregulated in Gne+/- mice compared to wildtype mice, while beta-crystallin B1 (*Crybb1*), crystallin alpha B (*Cryab*), and HORMA domain containing 2 (*Hormad2*) are notably upregulated; n= 7. Images A and B were adapted from the original graphs provided by Tawfik Abou Assale. Modified figure already published online in *GLIA* on September 3, 2024 (Cuevas-Rios et al., 2024).

Subsequently, gene set enrichment analysis (GSEA) was conducted (Fig. 16A). Notably, several hallmark gene sets were upregulated in Gne+/- mice. These included gene sets associated with UV responses, epithelial/mesenchymal transition (EMT), the p53 pathway, angiogenesis, apoptosis, KRAS signaling, IL6/JAK/STAT3 signaling, TNFA signaling via NF-kB, coagulation, and complement pathways (Fig. 16A).

Then, using sqRT-PCR, key upregulated gene transcripts identified by GSEA in retinas of 9-months old Gne+/- were verified, particularly the complement system, inflammation, apoptosis, EMT, oxidative stress markers, as well as those related to retinal functions. Thus, I investigated the gene transcript levels of complement components *C3*, *C4*, and *C1q*, and the complement regulatory factor H (*Cfh*). The pro-inflammatory cytokines interleukin-1 beta (*Il-1β*) and tumor necrosis factor (*Tnf*) were also analyzed, along with the oxidative stress markers cytochrome b-245 alpha chain (*Cyba*) and beta chain (*Cybb*) (Fig. 16B).

The sqRT-PCR results revealed significant upregulation of mRNA levels for *C3* (p= 0.03), *C4* (p= 0.02), and *Il-1β* (p= 0.01) in the retinas of 9-month-old Gne+/- mice compared to WT mice (Fig. 16B). Moreover, elevated gene transcript levels were observed for retina-associated markers, visual system homeobox 2 (*Vsx2*; p= 0.022) and vascular endothelial growth factor A (*Vegfa*; p= 0.04) in Gne+/- mice. On the contrary, no significant changes were detected in *Tnf* levels or in the oxidative stress markers *Cyba* and *Cybb* (Fig. 16B).

A

Hallmark Gene Set	NOM p-val	FDR q-val
UV RESPONSE UP	0.0000	0.0263
EPITHELIAL MESENCHYMAL TRANSITION	0.0050	0.0605
P53 PATHWAY	0.0052	0.1352
ANGIOGENESIS	0.0067	0.0225
ESTROGEN RESPONSE EARLY	0.0101	0.1503
APOPTOSIS	0.0131	0.1183
KRAS SIGNALING UP	0.0192	0.1623
IL6 JAK STAT3 SIGNALING	0.0199	0.0629
TNFA SIGNALING VIA NFKB	0.0204	0.1184
CHOLESTEROL HOMEOSTASIS	0.0275	0.1225
COAGULATION	0.0344	0.1497
COMPLEMENT	0.0508	0.2129
UV RESPONSE DN	0.0695	0.1741
PROTEIN SECRETION	0.0988	0.1954
ANDROGEN RESPONSE	0.1032	0.1995
PEROXISOME	0.1157	0.1889

B

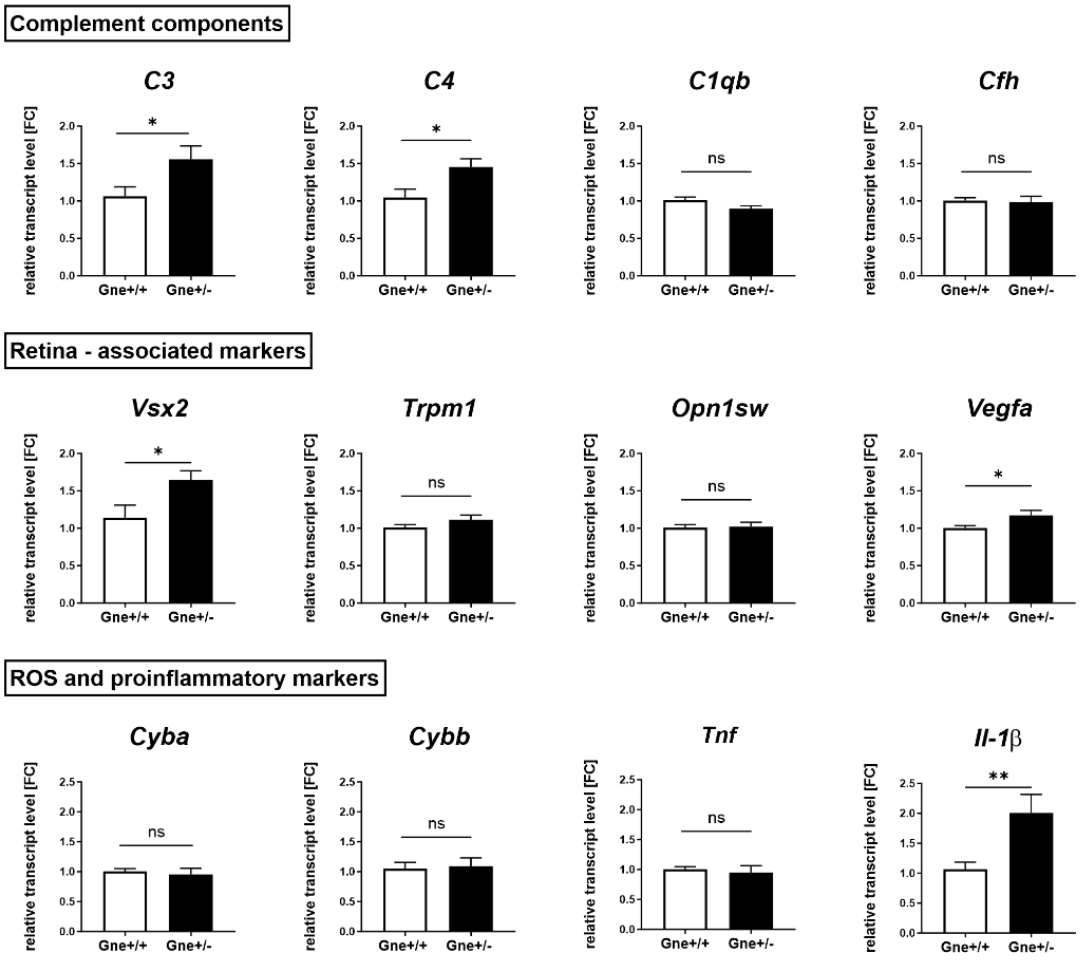

Figure 16. Top up-regulated hallmarks, increased gene transcription of pro-inflammatory and retina-associated markers in 9 months old Gne+/- mice retinas. (A) The top upregulated hallmarks in the retinas of Gne+/- mice compared to wildtype

(WT) controls were identified using gene set enrichment analysis (GSEA) in 9-month-old mice. (B) Semi-quantitative real-time polymerase chain reaction (sqRT-PCR) analysis of retinas from 9-month-old Gne+/- mice revealed a significant increase in the transcript levels of complement component 3 (*C3*) and complement component 4 (*C4*). In contrast, no differences were observed in the expression of complement component 1, q subcomponent, beta polypeptide (*C1qb*), and complement factor H (*Cfh*) between Gne+/- and WT mice. Additionally, the transcript levels of visual system homeobox 2 (*Vsx2*) and vascular endothelial growth factor A (*Vegfa*) were elevated, while the expression of transient receptor potential cation channel subfamily M member 1 (*Trpm1*) and opsin 1 short-wave-sensitive (*Opn1sw*) remained unchanged in Gne+/- mice at 9 months of age. Similarly, the expression levels of cytochrome b-245 alpha chain (*Cyba*), cytochrome b-245 beta chain (*Cybb*), and tumor necrosis factor (*Tnf*) showed no significant differences between Gne+/- and WT mice, whereas interleukin-1 beta (*Il-1β*) was found to be elevated in Gne+/- mice at 9 months; n= 10-13. NOM p-val: nominal *p* value; FDR q-val: false discovery rate q value; ROS: reactive oxygen species; FC: fold change. All data shown as mean + SEM; normalized to wildtype mice; ns= not significant, **p* ≤ 0.05, ***p* ≤ 0.01. Image A was created from the original graph provided by Tawfik Abou Assale. Slightly modified figure already published online in *GLIA* on September 3, 2024 (Cuevas-Rios et al., 2024).

In addition to the analyzed genes in 9 months old mice to confirm findings identified in the RNAseq analysis, retinal homogenates of 12 months mice were also used to investigate some gene transcription of common complement, microglia, oxidative stress markers, and *Il-1β* (Fig. 17). However, aside the very mild tendency for increased transcript levels of complement factors *C3* (FC: 1.14 ± 0.16 in WT vs. 1.45 ± 0.29 in Gne+/- mice, *p*= 0.37), and *C4* (FC: 1.10 ± 0.13 in WT vs. 1.37 ± 0.25 in Gne+/- mice, *p*= 0.36), the transcript levels of *Itgam*, the microglia markers (*Aif1*, *Cd68*, and *Tmem119*), the reactive oxygen species (*Cyba* and *Cybb*), and *Il-1β* showed no differences in Gne+/- mice retinas at 12 months of age compared to WT mice (Fig. 17).

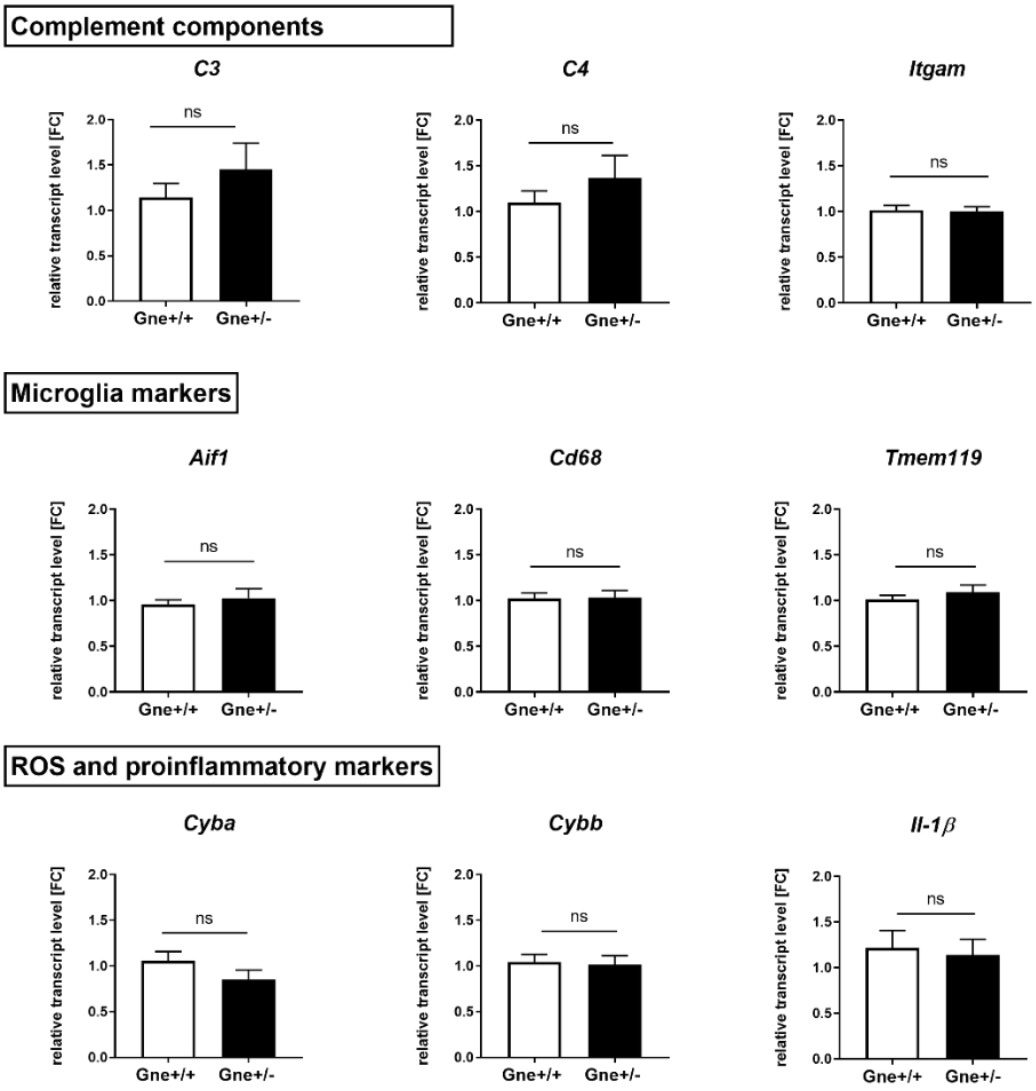

Figure 17. Mild transcriptional changes in retinas of 12 months old Gne+/- mice. Transcriptional analysis with semi-quantitative real-time polymerase chain reaction (sqRT-PCR) of 12 months old mouse retinas showed only a mild tendency for elevation of the complement factor 3 (*C3*) and complement component 4 (*C4*) in Gne+/- mice at 12 months of age, whereas, the transcript levels of the integrin subunit alpha M (*Itgam*) showed no differences. The transcript levels of allograft inflammatory factor 1 (*Aif1*), the *Cd68* antigen, and the transmembrane protein 119 (*Tmem119*), as well as cytochrome b-245 alpha chain (*Cyba*), cytochrome b-245 beta chain (*Cybb*), and interleukin 1 beta (*Il-1β*) were similar in Gne+/- and wildtype mice at 12 months of age. n= 11-13. FC; fold change. All data shown as mean + SEM; normalized to wildtype mice; ns= not significant.

Overall, the transcriptome data indicate a mild pro-inflammatory *Il-1β* profile, along with increased complement components *C3* and *C4*, as well as increased expression of retina-associated *Vsx2* and angiogenesis-related *Vegfa* in retinas of 9 months old mice with

hyposialylation. These findings also suggest that transcriptional changes in the retinas of Gne+/- mice are more pronounced at 9 months than at 12 months of age.

3.7 Prevention of retinal phenotype in Gne+/- mice by *C3* deficiency

The complement system is important for neuronal remodelling and immunosurveillance. However, removal of hyposialylated neurons also occurs in a complement-dependent manner (Klaus et al., 2020; Linnartz-Gerlach et al., 2016; Linnartz et al., 2012). The initiation of any complement pathway results in the activation of C3, which induces strong inflammatory response (Zarantonello et al., 2023). Hence, based on the finding of increased *C3* transcription in 9 months Gne+/- mice retinas and also with the aim to investigate the role of complement system in retinal hyposialylation, Gne+/- mice were crossed with C3 knock-out mice (C3-/-). The deficiency of *C3* was verified by genotyping and by retinal transcriptomic analysis (section 2.2.2 and 3.7.3).

Overall, 12-month-old Gne+/- mice exhibited a more pronounced retinal phenotype, characterized by an enhanced microglial response and neuronal loss, compared to 9-month-old mice. To investigate this further, I analyzed retinal cryosections from 12-month-old Gne+/- mice (referred hereafter as Gne+/-C3+/+) and C3-deficient Gne+/- mice (Gne+/-C3-/-). The focus was on the key IHC findings in Gne+/-C3+/+ retinas, particularly microglial activation and bipolar cell loss.

3.7.1 Prevention of increased CD68 expression in Gne+/- mice by *C3* deficiency

Previous data highlighted the importance of the complement system in microglial activation in the brains of Gne+/- mice, and the possibility of deleting the key complement factor C3 as demonstrated by Klaus et al. (Klaus et al., 2020). Accordingly, I examined retina cryosections stained for Iba1 and CD68 of 12-month-old Gne+/- mice crossed with *C3*-deficient mice to decipher the role of the complement system in the microglial response associated with hyposialylation. The analysis of the stained retina cryosections for microglia markers (Fig. 18A) revealed that the fluorescence intensity of the both microglial markers Iba1 and CD68 was decreased in Gne+/- mice crossed with *C3*-deficient mice (Gne+/-C3-/-) in all retinal layers in comparison to the Gne+/-C3+/+ mice (Fig. 18B). For instance, in the ONL the Iba1 intensity showed a trend for an increase in

Gne+/-C3+/+ mice to 120.33 ± 7.89 % (*p*= 0.088) compared to Gne+/+C3+/+ WT animals (100 ± 7.59 %), while it was reduced in the retinas of Gne+/-C3-/- mice to 46.70 ± 3.58 % (*p*= <0.0001). The intensity of the lysosomal marker CD68 in the ONL of Gne+/- mouse retinas was 128.52 ± 8.96 %, but decreased significantly in Gne+/-C3-/- mice to 68.21 ± 16.51 % (*p*= 0.01). A similar reduction was seen across other retinal layers (Fig. 18B). Additionally, no differences in the fluorescence intensity of Iba1 and CD68 were observed between *C3*-deficient mice crossed with either Gne+/- or WT mice (Gne+/-C3-/- vs. Gne+/+C3-/-), suggesting that, despite reduced sialylation, there was no observed microglial response in the absence of *C3* (Fig. 18B).

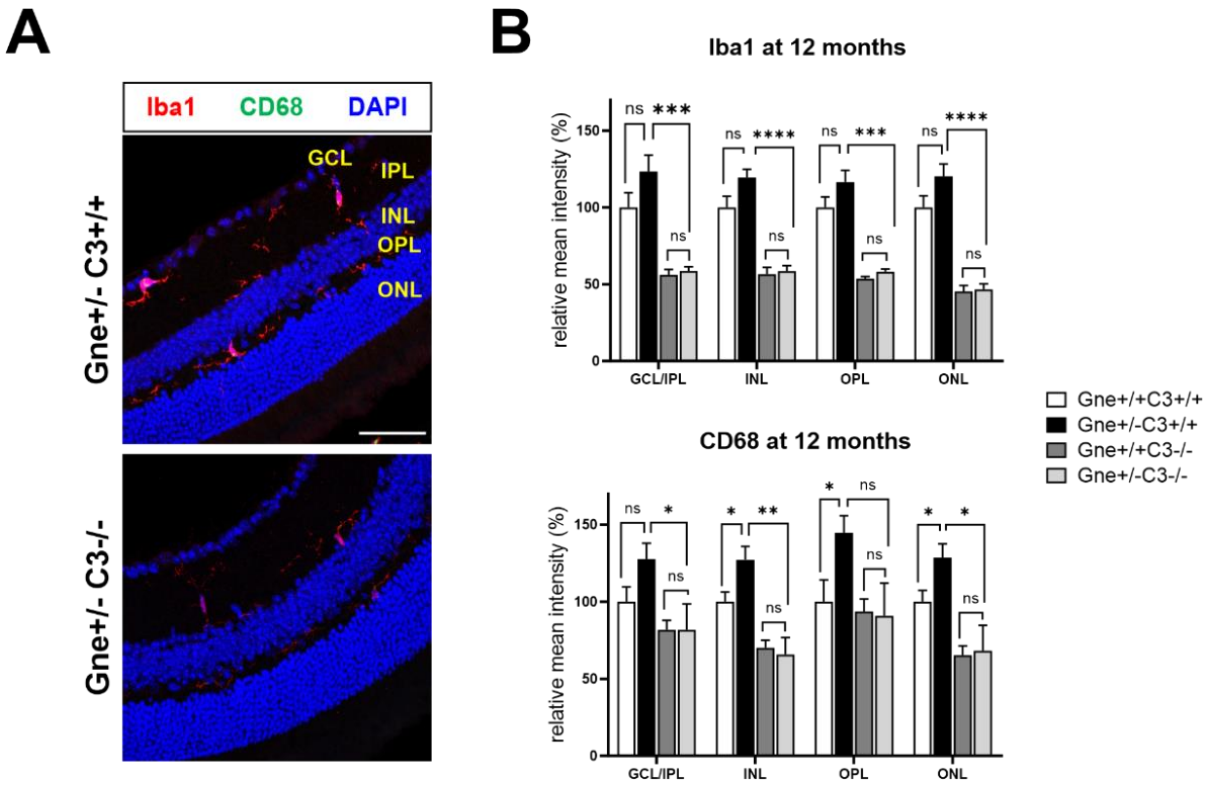

Figure 18. Prevention of increased CD68 expression in Gne+/- mice by *C3* deficiency. (A) Images of retinal cryosections from Gne+/-C3+/+ and Gne+/-C3-/- mice at 12 months of age stained with ionized calcium-binding adaptor molecule 1 (Iba1; red), CD68 (green), and the nuclear marker DAPI (blue). (B) Fluorescence intensity analysis showed a reduction in Iba1 and CD68 signal across most retinal layers in 12-month-old Gne+/-C3-/- mice compared to Gne+/-C3+/+ mice; n= 7. Scale bar, 50 µm. GCL: ganglion cell layer; IPL: inner plexiform layer; INL: inner nuclear layer; OPL: outer plexiform layer; ONL: outer nuclear layer. Welch ANOVA with Welch's correction. All data shown as mean + SEM; normalized to Gne wildtype mice (Gne+/+C3+/+); ns= not significant, **p* ≤ 0.05, ***p* ≤ 0.01, ****p* ≤ 0.001, *****p* ≤ 0.0001. Slightly modified figure already published online in *GLIA* on September 3, 2024 (Cuevas-Rios et al., 2024).

Taken together, *C3* deficiency suppressed the microglial activation markers Iba1 and CD68, and reversed the elevated levels of the lysosomal marker CD68 in hyposialylated retinas of 12-month-old Gne+/- mice.

3.7.2 Prevention of bipolar cells loss in Gne+/- mice by *C3* deficiency

I also investigated whether the loss of rod bipolar cells observed in 12-month-old Gne+/- mice could be mitigated by deleting *C3*. To address this, the bipolar cell density was analyzed in Gne+/- mice that were crossed with *C3*-deficient mice (Fig. 19A, B).

The deletion of *C3* had a significant effect, leading to an increased density of rod bipolar cells in *C3*-deficient mice compared to those with an intact *C3*. Specifically, the reduction in bipolar cells seen in 12-month-old Gne+/- mice was no longer visible in the absence of *C3*. Gne+/-C3-/- mice exhibited a higher bipolar cell density compared to Gne+/-C3+/+ mice (110.13 ± 3.96 % vs. 92.54 ± 2.58 %, p= 0.001), suggesting that *C3* deficiency offers a protective effect on rod bipolar cells (Fig. 19B).

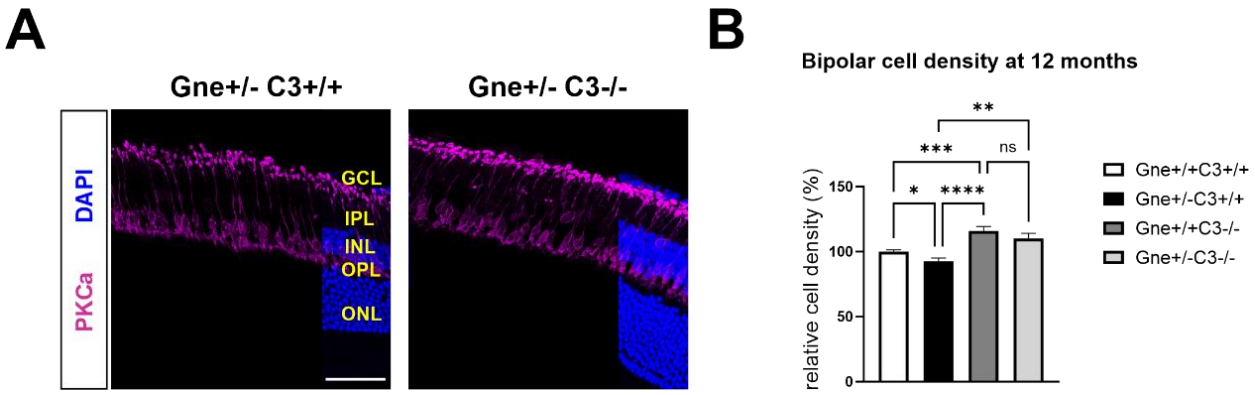

Figure 19. Prevention of bipolar cell loss of Gne+/- mice retinas by *C3* deficiency. (A) Illustrative images of retinal cryosections from 12-month-old Gne+/-C3+/+ and Gne+/-C3-/- mice co-stained with an antibody against protein kinase C-alpha (PKCα; magenta) to label rod bipolar cells, along with the nuclear marker DAPI (blue). (B) Cell density analysis revealed higher rod bipolar cells density in 12 months old Gne+/-C3-/- mice compared to Gne+/-C3+/+ mice; n= 12-14. Scale bar, 50 µm. GCL: ganglion cell layer; IPL: inner plexiform layer; INL: inner nuclear layer; OPL: outer plexiform layer; ONL: outer nuclear layer. Welch ANOVA with Welch's correction. Data shown as mean + SEM; normalized to Gne wildtype mice (Gne+/+C3+/+); ns= not significant, *$p \leq 0.05$, **$p \leq 0.01$, ***$p \leq 0.001$, ****$p \leq 0.0001$. Slightly modified figure already published online in *GLIA* on September 3, 2024 (Cuevas-Rios et al., 2024).

Overall, these results suggest that the absence of *C3* plays a protective role in preserving rod bipolar cells in the 12 months Gne+/- mouse retinas with decreased sialylation.

3.7.3 Prevention of transcriptional changes in Gne+/- mice by *C3* deficiency

Contrasting with the stronger retinal phenotype observed at protein level in 12 months old Gne+/-C3+/+ mice with the IHC analysis, transcriptional changes were more pronounced at 9 months of age. Therefore, I focused in the transcriptomic analysis of Gne+/- mice crossed with *C3*-deficient mice (Gne+/-C3-/- and Gne+/+C3-/-) in comparison to the mice with intact *C3*, including the WT mice (Gne+/+C+/+) at 9 months of age.

The PCA plot obtained from the RNAseq analysis revealed a distinct separation between the mouse groups with intact *C3* (C3+/+) and those with *C3* deletion (C3-/-). However, no clear separation was observed between *Gne* heterozygous (Gne+/-) and WT (Gne+/+) mice (Fig. 20A). The DEG analysis between Gne+/-C3+/+ and Gne+/-C3-/- mice identified several genes that were differentially expressed following the deletion of *C3* (Fig. 20B).

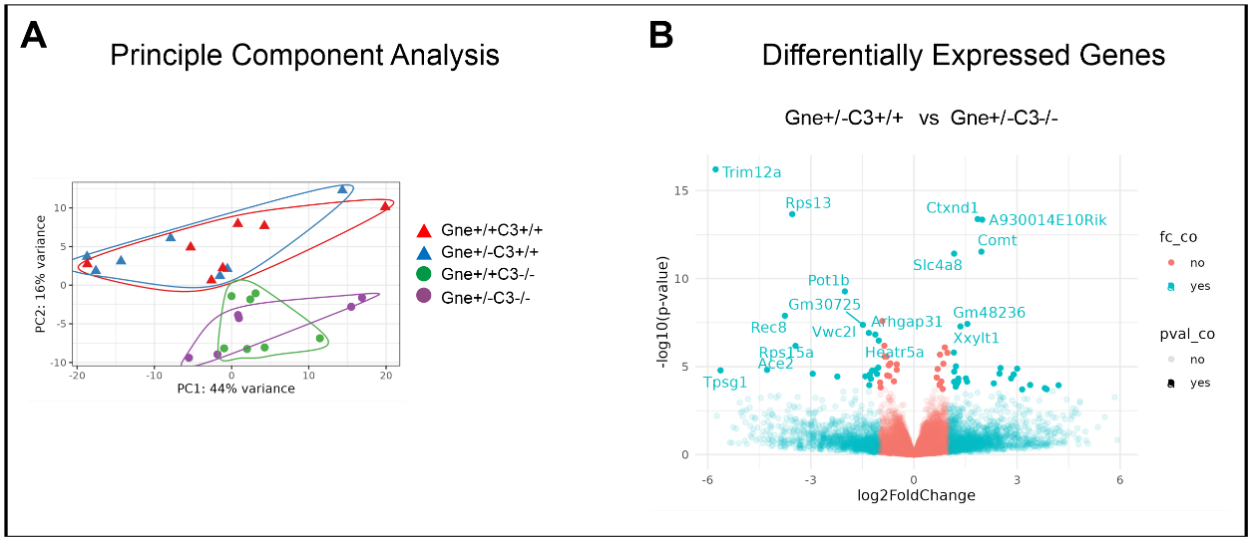

Figure 20. RNAseq analysis of retinas from 9-month-old *C3*-deficient Gne+/- mice. Principal component analysis (PCA) of retinal RNA sequencing data shows the multivariate distribution of wildtype (Gne+/+C3+/+; red triangles), Gne+/-C3+/+ (blue triangles), Gne+/+C3-/- (green dots), and Gne+/-C3-/- mice (purple dots), with each point representing an individual mouse. The clustering of samples, outlined by ellipses, highlights the separation between groups. A distinct separation is evident between the C3+/+ genotypes (Gne+/+C3+/+ and Gne+/-C3+/+) and the C3-/- genotypes (Gne+/+C3-/- and Gne+/-C3-/-). (B) A volcano plot illustrates the differential gene expression analysis between Gne+/-C3+/+ and Gne+/-C3-/- mice. Genes with a *p*-value of less than 0.05 (shown by clear dots) and a log2FoldChange greater than 1 (shown by blue dots) are

considered significantly differentially expressed; n= 6-7. Images A and B were adapted from the original graphs provided by Tawfik Abou Assale. Modified figure already published online in *GLIA* on September 3, 2024 (Cuevas-Rios et al., 2024).

To further investigate the impact of *C3* knock-out, GSEA was performed to identify the top 50 most up- and down-regulated genes and visualized in a heatmap (Fig. 21). The heatmap highlighted several immune-related genes, such as histocompatibility 2 class II antigen E beta (*H2-EB1*), purinergic receptor P2Y, G-protein coupled 10B (*P2ry10b*), and lymphocyte cytosolic protein 1 (*Lcp1*), that were highly expressed in the retinas of Gne+/-C3+/+ mice. Additionally, collagen genes including collagen type V alpha 2 (*Col5a2*) and type XVI alpha 1 (*Col16a1*), which were upregulated in Gne+/-C3+/+ mice, were restored to WT levels in C3-/- mice. Notably, downregulation of der1-like domain family, member 3 (*Derl3*) in Gne+/-C3+/+ retinas, responsible for clearing misfolded glycoproteins, was reversed in C3-/- mice. The heatmap also confirmed downregulation of *Gne* transcription in both Gne+/-C3+/+ and Gne+/-C3-/- mice. Thus, many of the transcriptional changes observed in Gne+/-C3+/+ retinas were partially mitigated by the deletion of *C3* (Fig. 21).

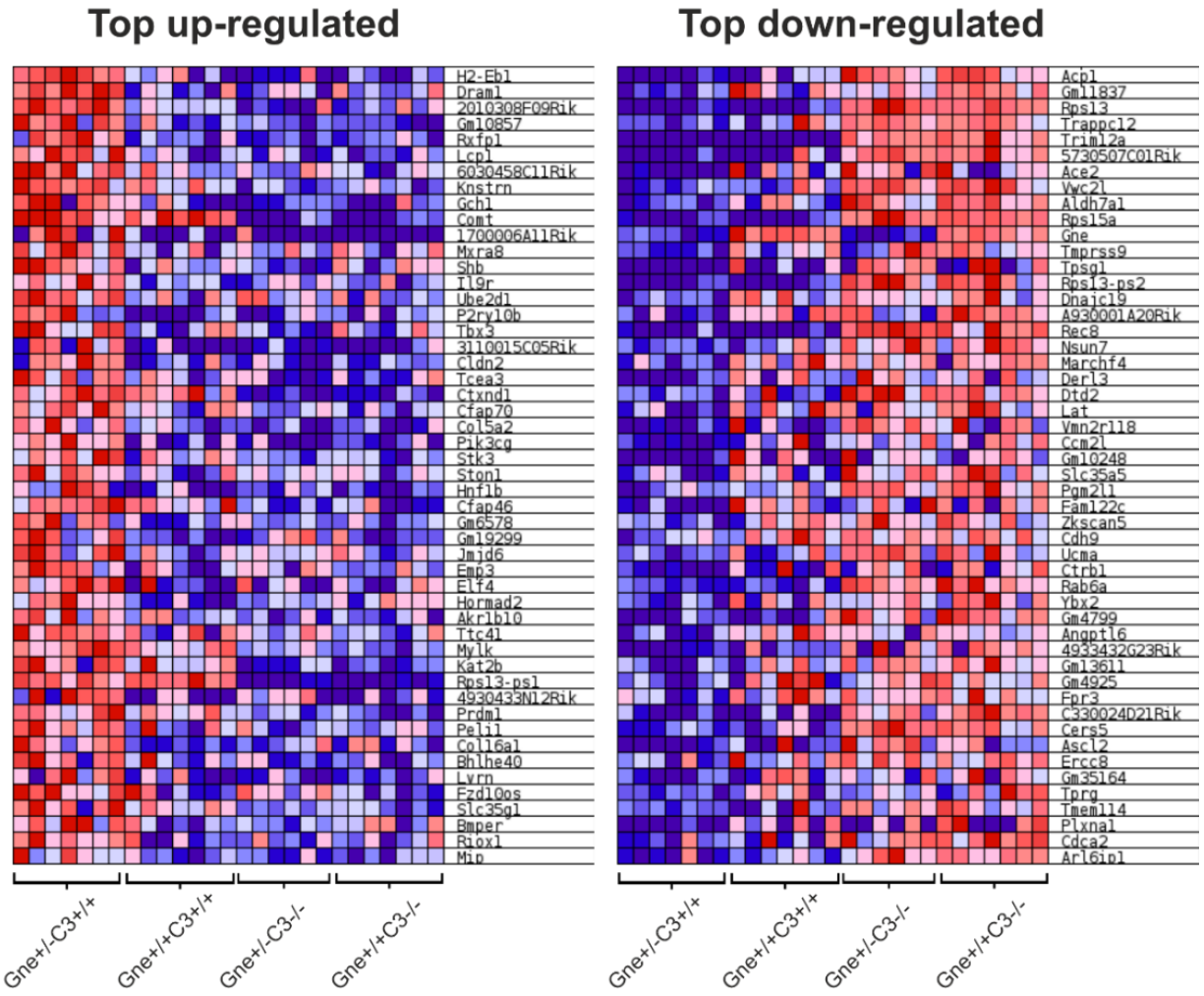

Figure 21. Heatmap with top 50 up- and down-regulated genes of 9 months old Gne+/-C3+/+ compared to all other genotypes. Top up- and down-regulated genes in the retinas of 9-month-old Gne+/-C3+/+ mice compared to the rest of genotype groups identified with the gene set enrichment analysis (GSEA). The data show that the transcriptomic alterations in Gne+/-C3+/+ retinas are largely neutralized following the deletion of complement factor *C3*; n= 6-7 mice per group. Heatmap image was modified from the original image provided by Tawfik Abou Assale. Figure already published online in *GLIA* on September 3, 2024 (Cuevas-Rios et al., 2024).

In addition to the RNAseq-identified gene transcripts, further genes were examined using sqRT-PCR to assess whether *C3* deficiency prevents retinal transcriptomic changes. The elevated *C4* levels observed in the retinas of 9-month-old Gne+/-C3+/+ mice were significantly reduced in Gne+/-C3-/- mice (FC: 1.454 ± 0.11 vs. 0.352 ± 0.14, $p< 0.0001$, Fig. 22). In contrast, the transcription levels of *C1qb* and *Cfh* remained consistent across all genotypes, including *C3*-deficient mice (Fig. 22). While the observed increase in *Il-1β*

expression in Gne+/-C3+/+ mice showed a trend towards normalization in *C3*-deficient mice (Gne+/-C3-/-), approaching Gne+/+C3+/+ WT levels (FC: 2.007 ± 0.31 vs. 1.223 ± 0.21, *p*= 0.054), no significant differences were observed in the transcript levels of *C3*, *C4*, or *Il-1β* between Gne+/+C3-/- and Gne+/-C3-/- mice (Fig. 22).

Regarding retina-associated markers, the elevated gene expression of *Vsx2* in Gne+/-C3+/+ mice was significantly reduced in Gne+/-C3-/- mice (FC: 1.647 ± 0.12 vs. 0.607 ± 0.12, *p*= <0.0001, Fig. 22). However, *Vegfa* transcript levels in Gne+/-C3-/- mice did not show a significant change compared to Gne+/-C3+/+ mice (Fig. 22). On the contrary, *Trpm1* transcript levels were lower in Gne+/-C3-/- mice compared to Gne+/-C3+/+ mice (FC: 0.750 ± 0.02 vs. 1.115 ± 0.06, *p*= <0.0001, Fig. 22). On the other hand, gene expressions of *Opn1sw* and *Tnf* remained unchanged across all mouse groups (Fig. 22). Notably, the transcription levels of oxidative stress markers *Cyba* and *Cybb* were significantly lower in 9 months old Gne+/-C3-/- mice compared to Gne+/-C3+/+ mice (*Cyba*: *p*= 0.018, *Cybb: p*= 0.007; Fig. 22).

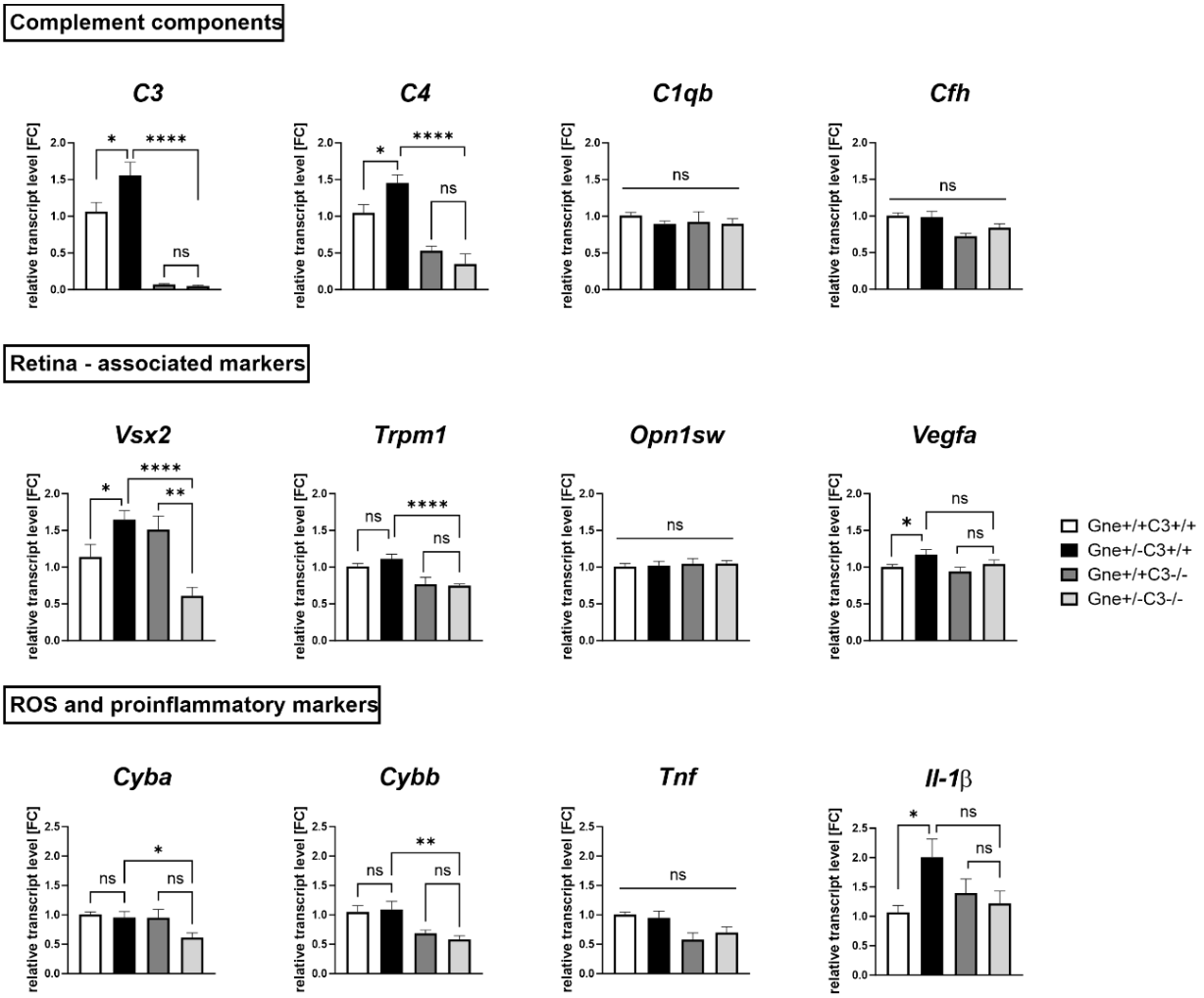

Figure 22. Partial prevention of transcriptional changes in the retinas of 9 months old Gne+/- mice by deletion of *C3*. Transcriptional analysis with semi-quantitative real-time polymerase chain reaction (sqRT-PCR) of 9 months old Gne+/+C3-/- and Gne+/-C3-/- mice retinas showed nearly undetectable transcript levels of complement component 3 (*C3*). The elevated transcript levels of complement component 4 (*C4*) and visual system homeobox 2 (*Vsx2*) observed in Gne+/-C3+/+ mice were reduced in the Gne+/-C3-/- mice. While the increased gene transcription of interleukin-1 beta (*Il-1β*) in Gne+/-C3+/+ mice showed a tendency to revert levels in Gne+/-C3-/- mice, vascular endothelial growth factor A (*Vegfa*) levels did not show a significant decrease in Gne+/+C3-/- compared to Gne+/-C3+/+ mice. Additionally, transcript levels of transient receptor potential cation channel, subfamily M, member 1 (*Trpm1*), cytochrome b-245 alpha chain (*Cyba*), and cytochrome b-245 beta chain (*Cybb*) were significantly reduced in Gne+/-C3-/- mice compared to Gne+/-C3+/+ mice at 9 months. Gene expression of complement component 1, q subcomponent, beta polypeptide (*C1qb*), complement factor h (*Cfh*), opsin 1, short wave-sensitive (*Opn1sw*), and tumor necrosis factor (*Tnf*) remained unchanged; n= 6-13. ROS: reactive oxygen species; FC; fold change. Welch ANOVA with Welch's correction. All data shown as mean + SEM; normalized to wildtype mice (Gne+/+C3+/+); ns= not significant, *$p \leq 0.05$, **$p \leq 0.01$, ****$p \leq 0.0001$. Slightly modified figure already published online in *GLIA* on September 3, 2024 (Cuevas-Rios et al., 2024).

Transcript levels of glial markers, apoptosis and necroptosis, as well as epithelial and mesenchymal markers were also investigated in retinas of 9 months mice (Fig. 23). Results showed only a very slight increase of *Cd68* gene transcription in the Gne+/-C3-/- mice compared to Gne+/-C3+/+ (FC; 1.16 ± 0.06 vs. 0.89 ± 10, p= 0.039), and significant decrease of *Itgam* in Gne+/-C3-/- mice compared to Gne+/-C3+/+ mice (FC; 0.72 ± 0.08 vs. 1.03 ± 0.08, p= 0.015; Fig. 23). The rest of microglia markers *Aif1* and *Tmem119* showed no differences. Interestingly, the *Gfap* gene transcription showed lower values in Gne+/-C3+/+ compared to Gne+/+C3+/+ WT mice (FC; 0.75 ± 0.08 vs. 1.01 ± 0.04, p= 0.014). The transcripts of collagen type IV alpha 2 chain (*Col4a2*) showed only a tendency for increased in Gne+/- compared to WT mice, while collagen type VI alpha 3 chain (*Col6a3*) showed a significant decrease in Gne+/-C3-/- mice compared to Gne+/- mice (FC; 0.65 ± 0.04 vs. 1.21 ± 0.11, p= 0.0003). No changes were observed in the apoptosis and necroptotic markers; caspase 3 (*Casp3*), caspase 8 (*Casp8*), or phosphatidylinositol 4,5-bisphosphate 3-kinase catalytic subunit delta isoform (*Pik3cd*) (Fig. 23).

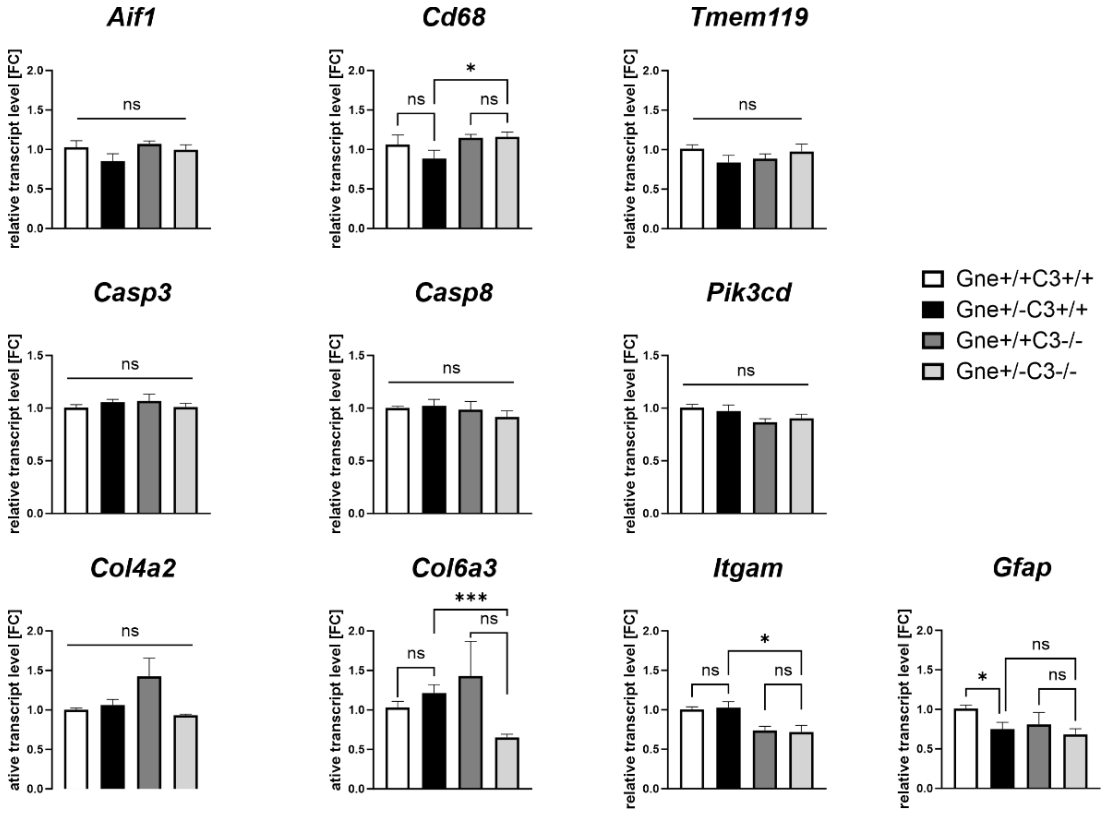

Figure 23. Minor transcriptional changes of collagen and glial cell markers in retinas of 9 months Gne+/- mice deficient for *C3.* Transcriptional analysis with semi-

quantitative real-time polymerase chain reaction (sqRT-PCR) showed that transcriptional levels of the CD68 antigen (*Cd68*) were slightly elevated in Gne+/-C3-/- mice compared to Gne+/-C3+/+ mice at 9 months of age. No significant differences were observed in the gene transcripts for allograft inflammatory factor 1 (*Aif1*), transmembrane protein 119 (*Tmem119*), caspase 3 (*Casp3*), caspase 8 (*Casp8*), or phosphatidylinositol-4,5-bisphosphate 3-kinase catalytic subunit delta (*Pik3cd*) between the genotype groups at 9 months. In contrast, transcription levels of collagen type VI alpha 3 (*Col6a3*) and integrin alpha M/complement receptor 3 (*Itgam/CR3*) were reduced in Gne+/-C3-/- mice compared to Gne+/-C3+/+, while no significant changes were observed in collagen type IV alpha 2 (*Col4a2*) levels. Glial fibrillary acidic protein (*Gfap*) transcript levels were lower in 9-month-old Gne+/-C3+/+ mice relative to Gne+/+C3+/+ wildtype mice; n= 6-13. FC; fold change. Welch ANOVA with Welch's correction was performed. All data shown as mean + SEM; normalized to wildtype mice (Gne+/+); ns= not significant, *$p \leq 0.05$, ***$p \leq 0.001$. Slightly modified figure already published online in *GLIA* on September 3, 2024 (Cuevas-Rios et al., 2024).

Despite there were only minor transcriptional changes in the retinas of Gne+/-C3+/+ mice at 12 months of age, retinas of Gne+/- mice crossed with *C3*-deficient mice were also utilized to investigate further the effect of *C3* deficiency in the mouse retinas at 12 months of age (Fig. 24). The results showed very low transcript levels of *C3*, and significantly lower *C4* gene transcription in Gne+/-C3-/- mice compared to Gne+/-C3+/+ mice animals (FC; 0.63 ± 0.07 vs. 1.37 ± 0.25; p= 0.013). On the other hand, despite the slight decrease *Cd68* expression in Gne+/+C3-/- mice compared to Gne+/-C3-/-, no differences were observed in the gene transcription of the microglia markers (*Aif1*, *Cd68*, and *Tmem119*), the oxidative stress markers (*Cyba* and *Cybb*), *Il-1β* and *Itgam* between Gne+/-C3-/- mice and Gne+/-C3+/+ mice (Fig. 24).

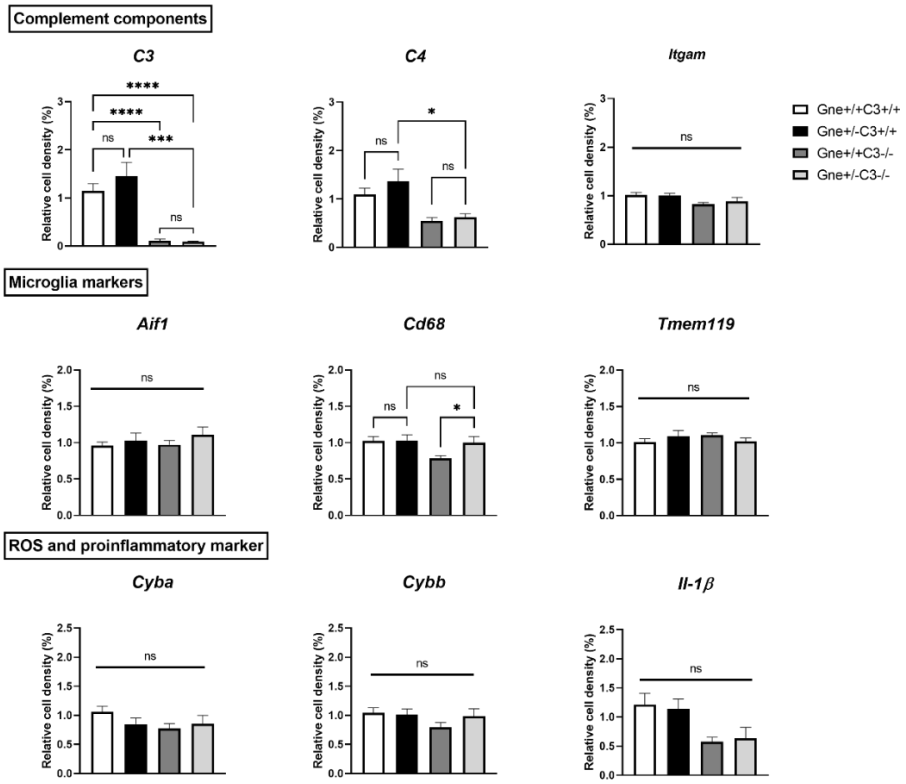

Figure 24. Minor transcriptional changes in 12-month-old *C3*-deficient Gne+/- retinas. Analysis with semi-quantitative real-time polymerase chain reaction (sqRT-PCR) showed almost undetectable transcription of complement factor 3 (*C3*), and significant decreased complement factor 4 (*C4*) in 12 months old Gne+/-C3-/- mice retinas. Transcript levels of integrin subunit alpha M (*Itgam/CR3*), allograft inflammatory factor 1 (*Aif1*), transmembrane protein 119 (*Tmem119*), cytochrome b-245 alpha chain (*Cyba*), and cytochrome b-245 beta chain (*Cybb*), and interleukin-1 beta (*Il-1β*) showed no differences in 12 months old Gne+/-C3-/- mice compared to Gne+/-C3+/+; n= 6-13. FC; fold change. Welch ANOVA with Welch's correction. All data shown as mean ± SEM; normalized to wildtype mice; ns= not significant, **p* ≤ 0.05, ****p* ≤ 0.001, *****p* ≤ 0.0001.

The RNAseq and sqRT-PCR analysis showed that the main transcriptional changes in the Gne+/-C3+/+ mouse retinas occur at 9 months compared to 12 months of age. These data also indicate prevention of the increased transcription levels of *C4* by deficiency of *C3* in Gne+/-C3+/+ mice at 9 months of age, accompanied by a slight reduction of transcripts associated with inflammation and retina-associated markers.

Taken together, *C3* deficiency prevented the increased expression of microglial markers at the protein level, transcriptional changes primarily related to immune responses, and the loss of rod bipolar cells, corroborating the involvement of the complement system in retinal changes associated with hyposialylation.

4. Discussion

Elements of this section were already published online in a pre-print version of the journal *GLIA* on September 3, 2024 (Cuevas-Rios et al., 2024).

Sialylation plays several important roles in the organs and tissues of mammals. It contributes to the structural integrity of the cell surface, functions as ligands, and facilitates cell adhesion and cell-to-cell interactions (L. Deng et al., 2013; Traving & Schauer, 1998; A. Varki, 2008; A. Varki & Gagneux, 2012). Another crucial function of sialic acids is their role in the innate immune system, where they help to identify intact sialylated structures as self-components. This recognition prevents unwanted removal of whole cells or their structures (revised in Klaus et al., 2021; H. Liao et al., 2020).

Sialylation can be recognized by SIGLEC receptors on microglia cells, which serve as the primary line of defence in the central nervous system (CNS), particularly in the retina. Microglia are crucial for retinal surveillance and, together with other glial cells such as Müller cells and astrocytes, they also provide metabolic support to the retina (Reichenbach & Bringmann, 2020). Microglial responses are essential for maintaining tissue homeostasis, but excessive or chronic activation has been shown to be detrimental to neuronal survival in both the brain and retina. Previous studies have demonstrated that microglia and macrophages remove neurons with reduced levels of sialic acid in a complement-dependent manner (Klaus et al., 2020; Linnartz-Gerlach et al., 2016). Interestingly, human studies have revealed that sialylated brain gangliosides decrease with age (Segler Stahl et al., 1983). In this context, advanced age is a significant risk factor for neurodegenerative diseases such as Alzheimer's disease (AD) and age-related macular degeneration (AMD) (reviewed in Hersi et al., 2017; L. S. Lim et al., 2012). Therefore, it can be hypothesized that decreased sialylation may be an underlying mechanism responsible for, or associated with neurodegenerative pathologies. In this study, I used Gne+/- heterozygous mice to model reduced levels of sialic acid in the retina. The results revealed decreased sialylation across all retinal layers, which were linked to a microglial response, increased transcription of complement factors, pro-inflammatory and retina-associated markers, epithelial-mesenchymal transition (EMT), and notably, the loss of bipolar cells.

Due to the involvement of complement in the removal of hyposialylated structures, I also performed analysis of Gne+/- mice crossed with *C3*-deficient mice to determine whether *C3* depletion could prevent the hiposialylation-associated retinal phenotype. The results showed that the increased microglia response, bipolar cell loss and transcriptome retinal profile were all prevented in the Gne+/- mice deficient for C3.

Thus, the data of this study demonstrate that hyposialylation in the mice retina leads to mild microglia response, to pro-inflammatory profile, and bipolar cell loss. The findings also indicated that retinal changes due to hyposialylation were associated with the upregulation of the complement system.

4.1 Gne+/- mouse model for reduced retinal sialylation

Given the essential biological functions of sialylation, for this study Gne+/- mice were utilized to investigate the effect of decreased sialylation in the mouse retina. Complete knock-out of the *Gne* gene, which encodes for the enzyme GNE, is incompatible with life and leads to embryonic death around day 10. To circumvent this embryonic lethality, Gne+/- heterozygous can be used (Schwarzkopf et al., 2002). The membrane-bound sialic acid levels in Gne+/- mice have been studied across various organs and tissues (Gagiannis et al., 2007). However, the effect of these reduced levels of sialic acids on different organs and tissues were not determine in the initial studies. Recently, Klaus et al., characterized the brains of Gne+/- mice, revealing decreased levels of both short- and long-chain sialic acids in the hippocampus and substantia nigra, which led to complement-dependent neuronal loss, particularly at 9 and 12 months of age (Klaus et al., 2020). Since the retina, as part of the CNS, is also rich in sialic acids, and based on the findings of Klaus and colleagues (Klaus et al., 2020), this study focused on analyzing the retina of Gne+/- mice at 9 and 12 months of age. The aim was also to target an age in mice that might correspond to the period when sialylation possibly begins to decline in humans.

4.2 Confirmation of reduced retinal sialylation of Gne+/- mice

All the mice used in this study were genotyped to confirm the knock-out of one allele of the *Gne* gene. After confirmation of the correct genotype, sqRT-PCR was performed to asses *Gne* transcription and I found that the mouse retinas of 9 months old Gne+/- mice

showed reduced *Gne* transcription. Subsequent, I performed immunostaining of retina to visualize the distribution and expression of short chain sialic acids, typically covering gangliosides (Trisialic acids), and long chain sialic acid attached to the neural cell adhesion molecule (NCAM). The results revealed that both types of sialic acids were decreased in most retinal layers, particularly in 9 months old mice compared to those at 12 months of age. Given that the staining pattern of polysialic acid resembled that of Müller cell marker staining, I performed co-staining with glutamine synthetase and polysialic acid to determine whether polysialic acid is primarily expressed in Müller cells. Although there was partial co-localization with Müller cells, polysialic acid was also observed in other retinal cells and structures. This suggests that polysialic acid may have ubiquitous expression across the retina, indicating that multiple cell types could be affected by decreased sialylation in the retinas of Gne+/- mice. Data are in line with the overall decrease of membrane bound sialic acid observed in different organs of Gne+/- mice, as reported by Gagiannis and colleagues (Gagiannis et al., 2007). In addition, the reduced levels of both trisialic and polysialic acids were consistent to those reported by Klaus et al., in the brain of Gne+/- mice (Klaus et al., 2020). This suggests that the impairment in sialylation may occur in a similar manner in both, the brain and retina of Gne+/- mice.

After confirmation of decreased sialylation in the retinas of adult Gne+/- mice, at 9 and 12 months of age, I aimed to determine whether this sialic acid affectation is present from development or arises later in adult mice. To address this, I stained the retinas of Gne+/- mice at 3 months of age with antibodies for sialic acids. The analysis revealed no significant differences in sialic acid staining between Gne+/- and wildtype (WT) mice at this age. However, a trend toward reduced levels of polysialic acid was observed in Gne+/- mice at 3 months. A limitation of this analysis is the relatively small sample size due to the limited availability of mice at this age; therefore, larger sample sizes would be needed for more robust conclusions in the future. Nonetheless, the available data suggest that sialylation in the Gne+/- mouse model is more significantly affected in adult mice compared to younger mice, indicating that this mouse model is suitable for studying decreased sialylation in aging. Further research on the human retina is needed to determine whether the decreased sialylated gangliosides observed in the human brain (Segler Stahl et al., 1983) also occur in the human retina with advanced age.

Immunostaining of sialic acid in retinal cryosections allows to analyze the expression pattern of sialic acids across the retinal layers and to investigate whether a specific layer is more affected in Gne+/- mice. However, additional methods are required for more precise analysis of decreased sialylation. For example, colorimetric assays like thiobarbituric acid can be used to detect total sialic acids, and bead-based technologies such as AlphaLISA can quantify polysialic acid. Unfortunately, these colorimetric approaches require homogenates of the entire retina, which would require either a large number of animals or result in a limited amount of tissue available for other analyses, i.e., immunostainings on retinal cryosections and thus, these analyses were not performed.

4.3 Microglial response to hyposialylation in the mouse retina

Sialic acids can regulate complement activation and also modulate microglial pro-inflammatory responses through sialic acid-binding immunoglobulin-like lectin (SIGLEC) receptors (Crocker et al., 2007; Shahraz et al., 2022). Microglial cells, as part of the innate immune system, are crucial for monitoring and maintaining retinal homeostasis. However, chronic or dysregulated microglial responses can lead to tissue damage and neuronal loss, contributing to retinal diseases such as glaucoma, retinitis pigmentosa, and AMD (Bosco et al., 2015; Gupta et al., 2003; Karlstetter et al., 2015).

Upon encountering stimuli or insults, common microglial responses include proliferation, migration, and morphological changes. Analysis of stained retinal cryosections in this study revealed that the majority of microglia were located in the plexiform layers (IPL and OPL) and in the ganglion cell layer (GCL), with only a few microglia observed in the outer nuclear layer (ONL) or in the subretinal space in both Gne+/- and WT mice. This distribution suggests that microglia remained in their typical locations, in which can be found under physiological conditions (reviewed in F. Li et al., 2019) and showed no migration towards the outer segments of the retina.

To further investigate microglia across retinal layers, I quantified fluorescence staining of two common microglial markers, Iba1 and CD68. This analysis included not only the microglial cell bodies but also their processes and branches, which are not typically considered in cell density assessments. The results indicated that Iba1 staining intensity was similar between Gne+/- and WT mice at 9 months of age, with only a trend towards

increased intensity at 12 months. On the contrary, the lysophagosomal marker CD68 was elevated in most retinal layers at both 9 and 12 months of age. Despite the increased expression of these microglia markers, the gene transcription analysis with sqRT-PCR of the microglial markers *Aif1*, *CD68*, and *Tmem119* showed no up-regulation in the retinas of 9 months old Gne+/- mice, indicating that there are post-transcriptional modifications and upregulation of these markers at protein level, particularly at 12 months of age.

While Iba1 and CD68 staining in cryosections provided insights into the distribution, localization, and staining intensity of microglial markers, I also performed microglia staining in retinal whole-mounts to assess larger retinal areas to visualize the full extent of microglial cell morphology. Analysis of these retinal whole-mounts showed no significant changes in microglial cell number or skeletal parameters such as ramification index, branch number, or junction count. This suggests that hyposialylation is associated with only a mild microglial response, as indicated by the increase in CD68, which may reflect enhanced phagocytosis by microglia. However, further validation through additional phagocytosis assays is needed to confirm this, which were beyond the scope of this study. According to previous studies, the increased CD68 expression has been interpreted as a marker of microglial activation in the retina and around the optic nerve (Santos et al., 2008; Yuan & Neufeld, 2001).

Microglial activation in the retina is widely recognized as a hallmark of many retinal diseases and has been observed in various rodent models of retinal conditions such as glaucoma, optic nerve damage, (Bosco et al., 2015; Yuan & Neufeld, 2001), photoreceptor degeneration (Gupta et al., 2003), and retinal detachment (Y. Wang et al., 2021). The data presented in this study reveal only minor retinal changes, which may be attributed to the relatively small reduction in sialylation observed in the Gne+/- mice. Unlike the more pronounced physical or chemical interventions used in other rodent models of retinal diseases, the Gne+/- mice in this study did not undergo further manipulations. Nevertheless, even small alterations in retinal sialylation in Gne+/- mice triggered microglial responses. Future studies should explore whether sustained hyposialylation in older mice, such as those at 24 months of age, could result in more pronounced microglial changes.

4.4 Astrocytes and Müller cells response to retinal hyposialylation

Microglial cells are part of the retinal glial cell population alongside macroglia, which include astrocytes and Müller cells. These macroglial cells are crucial for retinal homeostasis, providing structural support, and modulating neuronal activity and immune responses (Iandiev et al., 2006; Inman & Horner, 2007; Newman, 1999; Reichenbach & Bringmann, 2020). The results of this study revealed increased staining intensity for the macroglial marker GFAP (glial fibrillary acidic protein) in the inner retinal layers, specifically the GCL the IPL, in Gne+/- mice at 9 months of age. Elevated GFAP expression, indicative of overall glial activation or gliosis, has been associated with oxidative stress, inflammation, vascular alterations, and loss of photoreceptors and ganglion cells in various animal models (Guttenplan et al., 2020; Iandiev et al., 2006; Inman & Horner, 2007; Nakazawa et al., 2006). Additionally, alterations in astrocytes have been observed in aging retinas and in AMD in humans (Madigan et al., 1994). The data from this study suggest that reduced sialylation in Gne+/- mice retinas trigger macroglial responses, which may reflect a compensatory or protective mechanism. However, this macroglial response could also contribute to local inflammation and retinal damage.

4.5 Bipolar cell loss in the retina of Gne+/- mice

Glial cells in the retina are crucial for maintaining tissue homeostasis. However, chronic activation or over-reactivity of glial cells can be associated with neuronal damage and death (Clayton et al., 2017; Friker et al., 2020; Hanisch & Kettenmann, 2007). This study found that retinal hyposialylation triggers glial responses. To further investigate, I examined the main types of retinal neurons involved in the basic visual circuit: photoreceptors, which capture light stimuli; bipolar cells, which act as interneurons; and ganglion cells, which transmit signals from photoreceptors through bipolar cells.

The ONL, which contains the cell bodies of photoreceptors, was also examined for changes in thickness as an indicator of photoreceptor loss. No significant alterations were observed in the retinas of Gne+/- mice. To specifically assess photoreceptors, I stained the outer segments of rod cells with rhodopsin antibody, but no differences were detected. Given that the smear-like pattern observed in rhodopsin staining was difficult to measure,

I used an antibody against cone arrestin to visualize and quantify individual cone cells. The analysis showed that cone cell density remained unaffected in Gne+/- mice.

Similarly, the number of ganglion cells was comparable between Gne+/- and WT mice. In contrast, the density of rod bipolar cells in the retinas of Gne+/- mice was significantly decreased at 12 months of age, suggesting that these interneurons are more susceptible to changes in sialylation or to the observed microglial response. In line with this, it was also observed an increased transcription of visual system homeobox 2 (*Vsx2*) gene, a marker of retinal progenitors and bipolar cells. Studies in mice have demonstrated that *Vsx2* is critical for the development and differentiation of bipolar cells (Goodso et al., 2020), and mutations in *Vsx2* are associated with the development of microphthalmia in both mice and humans (Reis et al., 2011). Interestingly, organoids of retinal pigment epithelium (RPE) tissue treated with extracellular vesicles (EVs) from human RPE with AMD showed upregulation of retinal progenitor markers such as paired Box 6 (*Pax6*) and *Vsx2*, along with the presence of CRYAB-positive cells as a response to EVs-induced damage (Kurzawa-Akanbi et al., 2022). Consistent with these findings, the data from this study suggest that the upregulation of *Vsx2* transcription may represent a regenerative response to compensate for the bipolar cell loss in the retinas of Gne+/- mice.

Interestingly, in human reports it has been shown that in post mortem retinas of donor without known retinal diseases, the number of bipolar cells starts to decrease already in the third decade and worsen substantially in the seventh decade (Aggarwal et al., 2007). In addition, sialylated gangliosides in humans have been also reported reduced in elderly population (Segler Stahl et al., 1983). Accordingly, further studies of sialic acid levels in the retina of humans at advance age could elucidate whether hyposialylation is associated not only with loss of bipolar cells, but also with other neurodegenerative pathologies such as AD or AMD.

Previous studies have shown that neurons with alteration in the sialylation are phagocytosed via complement pathway involvement (Linnartz-Gerlach et al., 2016; Linnartz et al., 2012). It was also reported opsonization by complement factors of neurons undergoing degeneration prior to removal by microglia (Hong et al., 2016; Werneburg et al., 2020). In addition, a study with brains of new born mice demonstrated that C1q binding to desialylated synapses triggered by sevoflurane exposure, resulted in microglial removal

of these synapses (G. Wang et al., 2024). Despite the loss of bipolar cells in this study was not accompanied by increased expression of C1q in the Gne+/- mouse retina, the transcription of other complement factors such as *C3* and *C4* were increased, suggesting involvement of complement system in the loss of bipolar cells related to hyposialylation. However, more studies are necessary to identify the exact mechanism leading to loss of rod bipolar cells in the hyposialylated retinas. On the other hand, despite oxidative stress damage is often involved in neuronal damage (Boje & Arora, 1992; Kreutzberg, 1996; Zeng et al., 2005), the results of this study did not show increase transcription of oxidative stress markers, the cytochrome b alpha (*Cyba*), and cytochrome b beta (*Cybb*) chain in Gne+/- mice.

Microglia-mediated synaptic removal may occur prior to neuronal loss. To explore this, I performed co-staining for pre-synapses using an antibody against vesicular glutamate transporter 1 (VGLUT1) and for post-synapses using an antibody against postsynaptic density protein 95 (PSD-95). However, the data were excluded, as confocal microscopy revealed a high density of VGLUT1 and a weak PSD-95 signal, making reliable quantification of functional synapses via puncta co-localization analysis impractical. Further studies employing high-resolution imaging are recommended to assess whether retinal hyposialylation leads to synapse loss in the mouse retina.

4.6 Upregulation of gene set hallmarks in Gne+/- mice retinas

Analysis of bipolar cell density revealed loss of these interneurons at 12 months of age. Then, RNA sequencing analysis was performed in whole-retina homogenates at 9 months of age to investigate the underlying transcriptional mechanisms associated to the bipolar cell loss and the microglia response in the hyposialylated retinas of Gne+/- mice. The principal component analysis (PCA) showed only a shift but not a very clear separation of the Gne+/- mice from the WT animals, which could be explained by the heterozygosity of the Gne+/- mice with only one allele with the null *Gne* mutation causing moderate decrease of sialic acid. Nevertheless, the volcano plot of differentially expressed gene (DEG) showed various genes to be up-regulated and also downregulation of *Gne* in the Gne+/- mice. In addition, the gene set enrichment analysis (GSEA) showed significantly

upregulated hallmark genes sets in the Gne+/- mice, indicating important transcriptional changes in Gne+/- mice comparing with WT animals already at 9 months of age.

Notably, several up-regulated hallmarks' gene sets identified with the GSEA in the retinas of Gne+/- mice are either associated to AMD development or are suggested as potential approach for therapy or models for AMD. For example, changes in the epithelial-mesenchymal transition (EMT) hallmark have been proposed as a driving factor for RPE alterations in AMD (Yao et al., 2022). Accordingly, by targeting some components of EMT, fibrosis and oxidative stress associated to AMD can be attenuated by using components such as retinoic acid receptor-γ, or Kallistatin (Kimura et al., 2015; Shen et al., 2023; Tuo et al., 2015). Additionally, the heatmap from the GSEA analysis revealed the upregulation of genes related to EMT, including collagen genes *Col5a2* and *Col16a1*, as well as the tight junction gene *Cldn2*. In this study, it was also observed increased transcription of *Vegfa* using sqRT-PCR, a gene of the EMT closely associated with angiogenesis and abnormal neovascularization. Upregulation of *Vegfa* is a well-known marker of the wet form of AMD (reviewed in L. S. Lim et al., 2012; Uemura et al., 2021). These findings further support the involvement of EMT-related changes in retinal hyposialylation.

Similarly, components of the up-regulated hallmark UV response have been extensively analyzed and associated with the development of AMD, particularly in solar radiation exposition (Prüss-üstün et al., 2006; Sui et al., 2013; Taylor et al., 1990). Another upregulated hallmark identified in the GSEA was the p53 pathway, which has been associated with alterations in RPE cells related to AMD, and also in response to retinal blue light damage. In these contexts, inhibiting or modulating the p53 pathway has been shown to reduce choroidal neovascularization and retinal senescence in AMD models (Bhattacharya et al., 2012; Fietz et al., 2023; Son et al., 2020; Song et al., 2024; Wolfrum et al., 2022).

Regarding the identified genes in the DEG volcano plot, some genes showed up-regulation in the retinas of Gne+/- mice; e.g., *Cryab* and *Crybb1* gene transcripts, which are essential for the transparency and refractivity properties of the lens. Mutations in the crystallin genes have been associated with development of congenital cataracts in both mice and humans (Cohen et al., 2007; Cui et al., 2017; Graw et al., 2017; Willoughby et al., 2005). Additionally, *Cryab* is crucial in anti-apoptotic pathways under stress conditions

throughout the nervous system (J. F. Zhang et al., 2019). *Cryab* also plays a significant anti-inflammatory role by modulating pro-inflammatory macrophages in the nervous system (Hagen et al., 2024; E. M. F. Lim et al., 2021) and by preventing microglia activation, as demonstrated in a mouse model of endotoxin-induced retinal damage (F. Wang et al., 2021). Moreover, mutations in the *Cryab* gene or alterations in crystallin proteins are associated not only with cataract but also with RPE changes linked to retinal degeneration, as seen in AMD. Specifically, crystallins have been shown to protect RPE cells against oxidative stress and microglia-mediated neutrophil activation (Boyce et al., 2022; Christopher et al., 2014; Ghosh et al., 2018; Kannan et al., 2016; Kurzawa-Akanbi et al., 2022). Another up-regulated gene identified in the volcano plot is the *Hormad2*, an essential gene for the control of meiotic prophase by recognizing unsynapsis (Kogo et al., 2012). A meta-analysis of genome-wide association studies in humans with more than 24,000 individuals revealed that among others, *HORMAD2* is a novel loci associated with the morphology of the optic nerve head, and propose that these novel genes, including *HORMAD2,* could have association with glaucoma development and therefore, these loci are clinically relevant (Springelkamp et al., 2015).

4.7 Increased transcription of *Il-1β* and complement factors in Gne+/- mice

Increased expression of microglial CD68, along with GFAP, is widely regarded as an indicator of activation in microglia, astrocytes, and Müller cells. This activation often results in the release of pro-inflammatory cytokines, which can contribute to tissue damage and neuronal death (Guttenplan et al., 2020; Iandiev et al., 2006). Consistent with the increased expression of CD68 and GFAP in glial cells, in this study was also observed elevated gene transcription of factors and cytokines linked to a pro-inflammatory profile. The sqRT-PCR analysis revealed higher levels of the complement components *C3* and *C4*, as well as the pro-inflammatory cytokine *Il-1β*, in the retinas of Gne+/- mice at 9 months of age. Earlier studies have demonstrated that *Il-1β* in the retina is primarily expressed by infiltrating macrophages and activated resident microglia (Eandi et al., 2016; Jiao et al., 2015; Natoli et al., 2017; Rivera et al., 2013). *In vitro* studies have revealed that *Il-1β* is upregulated in response to treatment or challenge with lipofuscin (J. Zhang et al., 2015), oxidative stress (Kauppinen et al., 2012), and complement proteins (Asgari et al., 2013; Laudisi et al., 2013). *In vivo*, light-induced retinal degeneration has been linked

to an early and significant upregulation of *Il-1β* (Jiao et al., 2015). Notably, inhibiting *Il-1β* before photo-oxidative damage prevented microglial activation, macrophage infiltration, and the resulting photoreceptor death (Natoli et al., 2017). Additionally, cultured human and mouse mononuclear phagocytes expressed *Il-1β* and induced cone photoreceptor degeneration in retinal tissue explants (Eandi et al., 2016).

On the other hand, although the complement system is crucial for synaptic pruning and remodelling (Stevens et al., 2007), its activation has also been linked to the development of retinal diseases such as AMD (Armento et al., 2021; Gemenetzi & Lotery, 2016), glaucoma (Rosen & Stevens, 2010), and also observed in mouse models of retinal damage (Katschke et al., 2018; Natoli et al., 2016). A previous report has also documented the deposition of C3 and C5 in post-mortem human retinas from donors with AMD (Nozaki et al., 2006). In contrast, mutations or alterations in complement components such as CFH are associated with complement overactivation and with increased risk of developing AMD. The data presented in this study revealed no changes in the transcription levels of *C1q* and *CFH*. However, sqRT-PCR analysis indicated that *C3* and *C4* transcription was elevated in the retinas of Gne+/- mice, which aligns with the upregulation of the complement hallmark observed in the GSEA hallmark gene set. Notably, *in vivo* and *in vitro* studies, demonstrated that sialylation is associated with the transcription regulation of complement factors and with prevention of neuronal removal by macroglia or macrophages in a complement-dependent manner (Klaus et al., 2020; Linnartz-Gerlach et al., 2016; Shahraz et al., 2022).

Consistent with the aforementioned studies, the data from this study show that the upregulation of *C3* and *C4*, along with the pro-inflammatory cytokine *Il-1β,* in response to reduced retinal sialylation, may contribute to retinal tissue damage.

4.8 Prevention of retinal changes in Gne+/- mice by *C3* deficiency

Activation of the complement system, particularly increased expression of C3, has been linked not only to various retinal degenerative diseases but also to general proinflammatory responses in both the retina and the brain. For example, a cohort study found that elevated levels of C3 were associated with an increased risk of diabetic complications, including retinopathy, neuropathy, and nephropathy (Rasmussen et al.,

2018). Similarly, another study reported that alterations in the N-glycosylation of C3 were observed in patients with severe albuminuria, hypertension, and non-proliferative retinopathy, suggesting that glycosylation analysis of C3 could be useful for assessing disease progression and severity in type 1 diabetes (Šoić et al., 2023). In experimental studies, a mouse model of retinal geographic atrophy induced by sodium iodate (NaIO3) showed increased expression and deposition of complement components C1s, C3, CFH, and CFB, as well as other proinflammatory cytokines like Il-1β. This study suggested that macrophages, microglia, and Müller cells contribute to the local inflammation (Enzbrenner et al., 2021). Additionally, in a model of ischemic damage, rats with hypoxic-ischemic brain damage exhibited *in vivo* and *in vitro* reactivity of astrocytes, along with upregulation of C3, NLR family pyrin domain containing 3 (NLRP3), and GFAP (Jin et al., 2024).

In accordance with the studies discussed above and with the observed increased transcription of *C3* and *C4* in this study. The Gne+/- mice were crossed with *C3*-deficient mice, to investigate the role of C3 in the hyposialylation-related responses in the retina. The analysis of the retinas in Gne+/- mice deficient for *C3* focused mainly on the key findings previously observed in Gne+/- mice. These findings include increased expression of microglial markers and bipolar cell loss, as identified through immunohistochemistry (IHC) at 12 months of age. Additionally, at 9 months, sqRT-PCR analysis revealed elevated transcription of pro-inflammatory and retina-associated markers. The RNAseq analysis further highlighted the upregulation of several hallmarks and genes in these mice.

4.8.1 Prevention of the increased microglial CD68 in Gne+/- mice by *C3* deficiency

This study found that transcription of complement system components was upregulated in the hyposialylated retinas of Gne+/- mice. Previous research has highlighted the role of the complement system in microglial activation (Bodea et al., 2014; Klaus et al., 2020). It was explored whether the increased expression of the microglial marker CD68 could be mitigated by genetic depletion of the critical complement component *C3*. The results revealed that *C3* deficiency not only prevented the elevated CD68 expression in Gne+/- mice retinas but also led to a significant reduction in Iba1 expression. This reduction in microglial CD68 suggests that *C3* deficiency may decrease the phagocytic activity of

microglia towards hyposialylated retinal structures. However, to definitively confirm reduced phagocytic activity, as mentioned in section 4.3, further validation with functional analysis is necessary. Nevertheless, these findings indicate that *C3* deficiency can counteract the microglial responses associated with hyposialylation.

4.8.2 Prevention of bipolar cell loss in Gne+/- mice by *C3* deficiency

In line with previous publications that showed that neuronal loss associated with hyposialylation is mediated by components of the complement system, the results of this study demonstrated that the observed loss of rod bipolar cells in retinas of Gne+/- mice was completely prevented in the Gne+/- mice that were crossed with *C3*-deficient mice. Notably, the number of bipolar cells was even higher in the mice deficient for *C3* (Gne+/-C3-/- and Gne+/+C3-/-) comparing not only to Gne+/-C3+/+ but also to the WT control mice (Gne+/+C3+/+). This higher number of rod bipolar cells in 12 months C3-deficient mice suggest that C3 is apparently involved in deleterious effects for retinas of adult mice. Our results contrast with those published by Hoh Kam and colleagues, who reported that the deficiency of C3, CFH, or both together, was detrimental for the retinal health of 12-month-old mice (Hoh Kam et al., 2013). However, the mice used in this study were apparently healthy without any other genetic intervention. Moreover, retinal bipolar cells or other retinal neurons were not investigated with specific staining in this study (Hoh Kam et al., 2013). In contrast, our findings align with those presented by Gharagozloo et al., that observed high expression of C3 in retinal astrocytes in post-mortem human retinas of patients with multiple sclerosis and loss of retinal ganglion cells (RGC) (Gharagozloo et al., 2021). Gharagozloo and colleagues validated these findings using a mouse model of experimental autoimmune encephalomyelitis (EAE) with optic neuritis, where developmental depletion of C3 resulted in reduced RGC loss and decreased optic nerve injury (Gharagozloo et al., 2021). In the same line, Jiao et al., found that mice with genetic deletion of *C3*, when exposed to photo-oxidative retinal damage, exhibited reduced glial cell reactivity and decreased photoreceptor removal by macrophages (Jiao et al., 2020). Consistent with the aforementioned studies, the data from this research highlight the role of sialic acids in regulating complement activation and innate immune responses in the mouse retina, as well as in preventing removal of retinal neurons.

4.8.3 Prevention of the transcriptomic changes in Gne+/- mice by *C3* deficiency

Analysis of the retinal transcriptome in Gne+/- mice crossed with C3-/- mice revealed that the transcription of specific genes identified by sqRT-PCR, as well as the upregulated genes and pathways observed in the RNAseq analysis, were either fully or partially prevented. As expected, the transcription of *C3* in the *C3*-deficient mice was almost undetectable. Additionally, the increased transcription of *C4* and *Vsx2* in Gne+/-C3+/+ mice was reverted in the Gne+/-C3-/- mice, with *Il-1β* showing a trend towards reversal. Although oxidative stress markers were not upregulated, the transcription levels of *Cyba* and *Cybb* were reduced in *C3*-deficient mice compared to mice with intact *C3* at 9 months of age. Similar results were observed at 12 months, yet the differences between genotype groups were smaller, suggesting that transcriptional changes occur earlier than the observed changes at the protein or cellular level, such as increased microglial markers and bipolar cell loss.

The volcano plot comparing DEG between Gne+/-C3+/+ mice and the other genotype groups revealed several significantly up- and down-regulated genes. Notably, the previously observed up-regulation of *Cryab*, *Crybb1*, and *Hormad2* in Gne+/- mice was no longer evident by C3 deficiency. Additionally, the GSEA heatmap highlighting the top 50 up- and down-regulated genes demonstrated that transcriptional changes in key genes were also prevented. For instance, genes related to immune responses such as *H2-Eb1*, *Lcp1*, and *P2ry10b*, as well as genes involved in tight junctions and collagen formation like *Cldn2*, *Col5a2*, and *Col16a1*, were significantly altered in Gne+/-C3+/+ mice and prevented with the deletion of *C3*. Similarly, *Derl3*, a gene associated with the degradation of misfolded proteins, also showed changes that were prevented by *C3* deficiency. These findings suggest that *C3* deficiency mitigates retinal changes associated with hyposialylation, including alterations in EMT components, immune responses, and the reduced capacity to clear defective proteins.

Thus, the data of this study indicate that in spite of hyposialylation in the mouse retina, the absence of *C3* prevents many of the transcriptional changes in the mouse retina, and highlight the relevance of sialic acids in the regulation of immune responses as shown previously in the brain of different animal models (Klaus et al., 2020; H. Liao et al., 2021).

4.9 Limitations of the Gne+/- and *C3*-deficient mouse models

It was reported that complete *Gne* knock-out (Gne-/-) results in embryonic lethality in mice, while Gne+/- mice develop without apparent phenotypic defects (Schwarzkopf et al., 2002). However, the null *Gne* mutation in only one allele leads to varying degrees of hyposialylation in different mouse organs, making it challenging to control the reduction of sialic acids in a precise manner. Therefore, other approaches, such as pharmacological interventions or conditional Gne knock-out in specific retinal cells, may allow for more targeted interventions to induce a more pronounced retinal phenotype and overcome the limitations of only slight sialic acid reduction. Nevertheless, considering that sialylation levels in the retinas of young Gne+/- mice (3 months of age) were not affected, this Gne+/- mouse model might reflect the reduction of sialylation during aging. However, there is insufficient evidence of a reduction in membrane-bound sialic acid in elderly humans. Thus, additional studies in human retinas are needed to verify the association between hyposialylation, aging, inflammation, and degeneration.

Another challenge lies in determining whether the mild retinal phenotype observed in Gne+/- mice is a local response or if it is linked to systemic changes caused by overall hyposialylation. Similarly, the effect of genetic *C3* deficiency on mitigating the retinal phenotype in Gne+/- mice might also be affected by systemic changes resulting from complete *C3* knockout. Therefore, further analyses are required to explore the mechanisms driving changes in hyposialylated retinas and to better understand the role of the complement system in retinal inflammation and degeneration associated with hyposialylation.

4.10 Future work to elucidate the sialylation role in retinal homeostasis

The data presented in this study showed that Gne+/- mice exhibited only a light phenotype in hyposialylated retinas, characterized by a mild pro-inflammatory profile and slight loss of bipolar cells. While it remains unclear whether the observed bipolar cell loss impacts retinal function, functional analysis of the retina was not pursued in this study due to the mild retinal degeneration, which may not reveal significant changes in functional retinal assessment such as electroretinogram measurements. Therefore, further studies are needed to determine whether hyposialylated retinas, when challenged with factors such

as bright light or increased sensitivity to light stress, may exhibit more pronounced histological and functional changes.

Considering that the retinas analyzed in this study were from mice aged 9 and 12 months, including older mice, e.g., 18 or 24 months of age, may reveal a more pronounced retinal phenotype and provide deeper insights into the role of decreased sialylation in the aging retina. Further investigation in older Gne+/- mice could also replicate more accurately the reported loss of sialylated gangliosides in elderly humans (Segler Stahl et al., 1983).

Accordingly, challenging the retinas of Gne+/- mice to overcome potential compensatory mechanisms activated by slight hyposialylation, and analyzing older mice, could help to identify potential links between hyposialylation and retinal inflammation and degeneration in the aging retina.

4.11 Implications of the findings in the mouse retinas with hyposialylation

As already revised in detail by Wißfeld and colleagues, targeting sialylation has potential applications in mouse diseased models and also in human diseases (Wißfeld et al., 2024). Different types of sialic acids can regulate the complement system by binding to various complement components (Shahraz et al., 2022). Dysregulated and chronic microglial activation, along with complement activation and retinal deposition, have been observed in numerous retinal and ocular diseases, including AMD and glaucoma (reviewed in Armento et al., 2021; Colonna & Butovsky, 2017; Rashid et al., 2019). The findings of this study indicate that reduced sialylation is linked to microglial responses and increased transcription of complement components. Notably, research from four decades ago revealed a significant decline in sialylated gangliosides in the brains of the elderly (Segler Stahl et al., 1983), a population in which neurodegenerative diseases are highly prevalent. Given this observed indirect decline in sialylation and the established role of sialic acids in regulating immune responses, it is possible to hypothesize that hyposialylation may be an underlying contributor to neurodegenerative and inflammatory retinal diseases.

Long chain sialic acids (polySia) have been shown to decrease reactivity of mononuclear phagocytes and overall protection against induced retinal damage in SIGLEC-11 transgenic mice (Karlstetter et al., 2017; Krishnan et al., 2023). In addition, polySia attached to a polymer has been used not only in light-induced retinal degeneration mouse

models to mitigate damage (Krishnan et al., 2023), but it also began being tested in a phase II clinical trial as a therapy for patients with geographic atrophy secondary to AMD (clinical trial identifier NCT05839041). Yet, a study reported that these polymers induced inflammatory responses, which might represent a challenge for long term application (Ramot et al., 2016). Hence, exploring other approaches to administrate sialic acids are necessary to investigate safety, therapeutic effects and potential side effects.

In summary, this study examined the retinas of Gne+/- mice, confirming reduced levels of polysialic and trisialic acids. While sialylation levels in various organs and tissues, including the brains of adult Gne+/- mice, have been previously characterized, the impact of reduced sialylation on the retina had not been previously investigated. The findings revealed that retinal hyposialylation is associated with microglial activation, increased transcription of complement components and pro-inflammatory markers, as well as bipolar cell loss (Fig. 25). Overall, the results demonstrate that, in the mouse retina, sialic acids act as critical regulators of the innate immune system by modulating microglial and complement activation. These data also suggest that sialylation could be a promising therapeutic target for treating degenerative and inflammatory diseases in the aging retina.

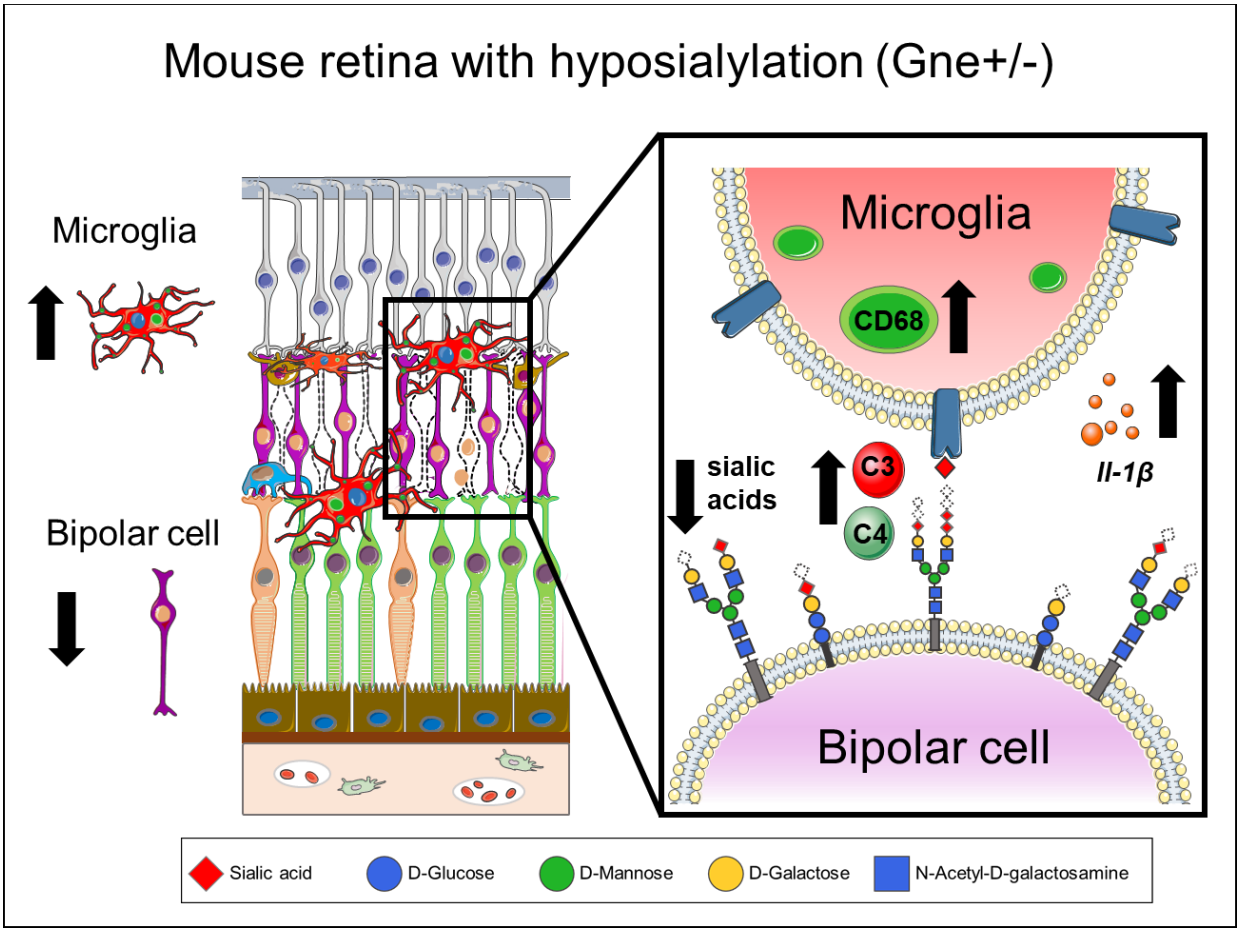

Figure 25. Hyposialylation elicits proinflammation and bipolar cell loss in mouse retinas. Decreased levels of sialic acids (red rhombus) in the membrane glycocalyx of retinal cells lead to increased expression of the lysosomal microglial markers CD68 (green ovals in the red cell), elevated transcription of the complement factors *C3* (red circle) and *C4* (green circle), and the pro-inflammatory cytokine *Il-1β* (orange circles). These hyposialylation-related changes in the retinas of Gne+/- mice are also associated with a reduced number of rod bipolar cells (purple cell). Image created using original or modified images from Servier Medical Art, licensed under CC BY 4.0. (https://creativecommons.org/licenses/by/4.0/).

Finally, the data presented in this study pave the way for further research into sialylation in the human retina and its potential links to retinal pathologies. Moreover, these findings highlight the need to investigate the molecular and cellular mechanisms underlying retinal hyposialylation and its consequences.

5. Abstract

Sialic acids are sugars located at the cell surface on glycoproteins and lipids, and act as check-point inhibitors of the innate immune and complement systems. Sialic acids are abundant throughout the central nervous system, including the retina. Notably, aging is associated with decreased levels of sialylated gangliosides. However, it remains unknown whether reduced sialylation contributes to retinal inflammation and degeneration. Here, I investigated the retina of mice heterozygous for the null mutant of UDP-N-acetylglucosamine 2-epimerase/N-acetylmannosamine kinase GNE (Gne+/-), an enzyme crucial for sialic acid biosynthesis, to determine whether decreased sialic acids levels (hyposialylation) contribute to retinal inflammation and degeneration.

The immunostainings results showed decreased expression of trisialic and polysialic acids in most retinal layers in 9-month-old Gne+/- mice compared to wildtype mice (WT). This hyposialylation was correlated with higher microglial expression of the lysosomal marker CD68. The RNA sequencing analysis and semi-quantitative real-time polymerase chain reaction showed increased gene transcription and pathways related to inflammation, complement system, and retinal-associated functions in retinas of Gne+/- mice compared to WT mice. Principally, increased gene transcription was observed in complement factors *C3* and *C4*, and the pro-inflammatory cytokine interleukin 1-beta in 9-month-old Gne+/- mice. In addition, the number of bipolar cells was reduced in 12-month-old Gne+/- mice in comparison to WT mice, suggesting loss of these interneurons that connect photoreceptors with ganglion cells. Interestingly, the transcriptional changes including increased transcription of *C4*, the higher expression of CD68, as well as the bipolar cell loss were prevented in the Gne+/- mice that were crossed with *C3*-deficient mice.

Overall, the data from this study indicate that hyposialylation is associated with an enhanced lysosomal response in microglia, an increase in pro-inflammatory markers, and loss of bipolar cells. These retinal changes were dependent on complement factor *C3*. Thus, these findings confirm that sialylation serves as a checkpoint for the immune system in the mouse retina and suggest that targeting sialylation could be a potential therapeutic approach for inflammatory and degenerative retinal diseases.

6. List of figures

7. List of tables

8. References

Aggarwal, P., Nag, T. C., & Wadhwa, S. (2007). Age-related decrease in rod bipolar cell density of the human retina: An immunohistochemical study. Journal of Biosciences; 32: 293–298

Ajami, B., Bennett, J. L., Krieger, C., Tetzlaff, W., & Rossi, F. M. V. (2007). Local self-renewal can sustain CNS microglia maintenance and function throughout adult life. Nature Neuroscience; 10: 1538–1543

Al-Zamil, W. M., & Yassin, S. A. (2017). Recent developments in age-related macular degeneration: A review. Clinical Interventions in Aging; 12: 1313–1330

Angata, T., & Varki, A. (2002). Chemical diversity in the sialic acids and related α-keto acids: An evolutionary perspective. Chemical Reviews; 102: 439–469

Armento, A., Ueffing, M., & Clark, S. J. (2021). The complement system in age-related macular degeneration. In Cellular and Molecular Life Sciences; 78: 4487–4505

Asgari, E., Le Friec, G., Yamamoto, H., Perucha, E., Sacks, S. S., Köhl, J., Cook, H. T., & Kemper, C. (2013). C3a modulates IL-1β secretion in human monocytes by regulating ATP efflux and subsequent NLRP3 inflammasome activation. Blood; 122: 3473–3481

Bauer, J., & Osborn, H. M. I. (2015). Sialic acids in biological and therapeutic processes: Opportunities and challenges. In Future Medicinal Chemistry; 7: 2285–2299

Beltran, W. A., Cideciyan, A. V., Guziewicz, K. E., Iwabe, S., Swider, M., Scott, E. M., Savina, S. V., Ruthel, G., Stefano, F., Zhang, L., Zorger, R., Sumaroka, A., Jacobson, S. G., & Aguirre, G. D. (2014). Canine retina has a primate fovea-like bouquet of cone photoreceptors which is affected by inherited macular degenerations. PLoS ONE; 9: 11–17

Bhattacharya, S., Chaum, E., Johnson, D. A., & Johnson, L. R. (2012). Age-related susceptibility to apoptosis in human retinal pigment epithelial cells is triggered by disruption of p53-Mdm2 association. Investigative Ophthalmology & Visual Science; 53: 8350–8366

Bhide, G. P., & Colley, K. J. (2017). Sialylation of N-glycans: mechanism, cellular compartmentalization and function. In Histochemistry and Cell Biology; 147: 149–174

Boatright, J. H., Dalal, N., Chrenek, M. A., Gardner, C., Ziesel, A., Jiang, Y., Grossniklaus, H. E., & Nickerson, J. M. (2015). Methodologies for analysis of patterning in the mouse RPE sheet. Molecular Vision; 21: 40–60

Bodea, L. G., Wang, Y., Linnartz-Gerlach, B., Kopatz, J., Sinkkonen, L., Musgrove, R., Kaoma, T., Muller, A., Vallar, L., Di Monte, D. A., Balling, R., & Neumann, H. (2014). Neurodegeneration by activation of the microglial complement-phagosome pathway. Journal of Neuroscience; 34: 8546–8556

Boje, K. M., & Arora, P. K. (1992). Microglial-produced nitric oxide and reactive nitrogen oxides mediate neuronal cell death. Brain Research; 587: 250–256

Bosco, A., Romero, C. O., Breen, K. T., Chagovetz, A. A., Steele, M. R., Ambati, B. K., & Vetter, M. L. (2015). Neurodegeneration severity can be predicted from early microglia alterations monitored in vivo in a mouse model of chronic glaucoma. DMM Disease Models and Mechanisms; 8: 443–455

Boyce, M., Xin, Y., Chowdhury, O., Shang, P., Liu, H., Koontz, V., Strizhakova, A., Nemani, M., Hose, S., Zigler, J. S., Campbell, M., Sinha, D., Handa, J. T., Kaarniranta, K., Qian, J., & Ghosh, S. (2022). Microglia–Neutrophil Interactions Drive Dry AMD-like Pathology in a Mouse Model. Cells; 11: 3535

Bringmann, A., Pannicke, T., Grosche, J., Francke, M., Wiedemann, P., Skatchkov, S. N., Osborne, N. N., & Reichenbach, A. (2006). Müller cells in the healthy and diseased retina. In Progress in Retinal and Eye Research; 25: 397–424

Carlson, M. (2019). org.Mm.eg.db: Genome wide annotation for Mouse. R Package Version 3.8.2.

Chen, L., Yang, P., & Kijlstra, A. (2002). Distribution, markers, and functions of retinal microglia. In Ocular Immunology and Inflammation; 10: 27–39

Christopher, K. L., Pedler, M. G., Shieh, B., Ammar, D. A., Petrash, J. M., & Mueller, N. H. (2014). Alpha-crystallin-mediated protection of lens cells against heat and oxidative stress-induced cell death. Biochimica et Biophysica Acta - Molecular Cell

Research; 1843: 309–315

Claybon, A., & Bishop, A. J. R. (2011). Dissection of a mouse eye for a whole mount of the retinal pigment epithelium. Journal of Visualized Experiments; 48: 3–7

Clayton, K. A., Van Enoo, A. A., & Ikezu, T. (2017). Alzheimer's disease: The role of microglia in brain homeostasis and proteopathy. In Frontiers in Neuroscience; 11: 680

Cohen, D., Bar-Yosef, U., Levy, J., Gradstein, L., Belfair, N., Ofir, R., Joshua, S., Lifshitz, T., Carmi, R., & Birk, O. S. (2007). Homozygous CRYBB1 deletion mutation underlies autosomal recessive congenital cataract. Investigative Ophthalmology and Visual Science; 48: 2208–2213

Colonna, M., & Butovsky, O. (2017). Microglia function in the central nervous system during health and neurodegeneration. In Annual Review of Immunology; 35: 441–468

Crocker, P. R., Paulson, J. C., & Varki, A. (2007). Siglecs and their roles in the immune system. In Nature Reviews Immunology; 7: 255–266

Cuevas-Rios, G., Tawfik, |, Assale, A., Wissfeld, J., Bungartz, A., Hofmann, J., Langmann, T., & Neumann, H. (2024). Decreased sialylation elicits complement-related microglia response and bipolar cell loss in the mouse retina. GLIA; Epub ahead of print

Cui, X. J., Lv, F. Y., Li, F. H., Zeng, K., & Abdelrahman, K. A. (2017). Correlations of single nucleotide polymorphisms of CRYAA and CRYAB genes with the risk and clinicopathological features of children suffering from congenital cataract. Medicine; 96: e7158

Deng, L., Chen, X., & Varki, A. (2013). Exploration of sialic acid diversity and biology using sialoglycan microarrays. Biopolymers; 99: 650–665

Deng, Y., Qiao, L., Du, M., Qu, C., Wan, L., Li, J., & Huang, L. (2022). Age-related macular degeneration: Epidemiology, genetics, pathophysiology, diagnosis, and targeted therapy. In Genes and Diseases; 9: 62–79

Ding, S. L. S., Kumar, S., & Mok, P. L. (2017). Cellular reparative mechanisms of mesenchymal stem cells for retinal diseases. In International Journal of Molecular

Sciences; 18: 1406

Dobin, A., Davis, C. A., Schlesinger, F., Drenkow, J., Zaleski, C., Jha, S., Batut, P., Chaisson, M., & Gingeras, T. R. (2013). STAR: Ultrafast universal RNA-seq aligner. Bioinformatics; 29: 15–21

Duan, S., & Paulson, J. C. (2020). Siglecs as Immune Cell Checkpoints in Disease. In Annual Review of Immunology; 38: 365–395

Eandi, C. M., Messance, H. C., Augustin, S., Dominguez, E., Lavalette, S., Forster, V., Hu, S. J., Siquieros, L., Craft, C. M., Sahel, J. A., Tadayoni, R., Paques, M., Guillonneau, X., & Sennlaub, F. (2016). Subretinal mononuclear phagocytes induce cone segment loss via IL-1β. ELife; 5: e16490

El Ali, A., & Rivest, S. (2016). Microglia ontology and signaling. In Frontiers in Cell and Developmental Biology; 4: 72

Ennis, S., Gibson, J., Cree, A. J., Collins, A., & Lotery, A. J. (2010). Support for the involvement of complement factor i in age-related macular degeneration. In European Journal of Human Genetics; 18: 15–16

Enzbrenner, A., Zulliger, R., Biber, J., Pousa, A. M. Q., Schäfer, N., Stucki, C., Giroud, N., Berrera, M., Kortvely, E., Schmucki, R., Badi, L., Grosche, A., Pauly, D., & Enzmann, V. (2021). Sodium iodate-induced degeneration results in local complement changes and inflammatory processes in murine retina. International Journal of Molecular Sciences; 22: 9218

Eyo, U. B., Peng, J., Swiatkowski, P., Mukherjee, A., Bispo, A., & Wu, L. J. (2014). Neuronal hyperactivity recruits microglial processes via neuronal NMDA receptors and microglial P2Y12 receptors after status epilepticus. Journal of Neuroscience; 34: 10528–10540

Fan, W., Huang, W., Chen, J., Li, N., Mao, L., & Hou, S. (2022). Retinal microglia: Functions and diseases. In Immunology; 166: 268–286

Fietz, A., Corsi, F., Hurst, J., & Schnichels, S. (2023). Blue Light Damage and p53: Unravelling the Role of p53 in Oxidative-Stress-Induced Retinal Apoptosis. Antioxidants; 12: 2072

Flamendorf, J., Agrón, E., Wong, W. T., Thompson, D., Wiley, H. E., Doss, E. L., Al-Holou, S., Ferris, F. L., Chew, E. Y., & Cukras, C. (2015). Impairments in dark adaptation are associated with age-related macular degeneration severity and reticular pseudodrusen. Ophthalmology; 122: 2053–2062

Fontainhas, A. M., Wang, M., Liang, K. J., Chen, S., Mettu, P., Damani, M., Fariss, R. N., Li, W., & Wong, W. T. (2011). Microglial morphology and dynamic behavior is regulated by ionotropic glutamatergic and GABAergic neurotransmission. PLoS ONE; 6: e15973

Friker, L. L., Scheiblich, H., Hochheiser, I. V., Brinkschulte, R., Riedel, D., Latz, E., Geyer, M., & Heneka, M. T. (2020). β-Amyloid Clustering around ASC Fibrils Boosts Its Toxicity in Microglia. Cell Reports; 30: 3743-3754.e6

Gagiannis, D., Orthmann, A., Danßmann, I., Schwarzkopf, M., Weidemann, W., & Horstkorte, R. (2007). Reduced sialylation status in UDP-N-acetylglucosamine-2-epimerase/N- acetylmannosamine kinase (GNE)-deficient mice. Glycoconjugate Journal; 24: 125–130

Gemenetzi, M., & Lotery, A. J. (2016). Complement pathway biomarkers and age-related macular degeneration. In Eye; 30: 1–14

Gharagozloo, M., Smith, M. D., Jin, J., Garton, T., Taylor, M., Chao, A., Meyers, K., Kornberg, M. D., Zack, D. J., Ohayon, J., Calabresi, B. A., Reich, D. S., Eberhart, C. G., Pardo, C. A., Kemper, C., Whartenby, K. A., & Calabresi, P. A. (2021). Complement component 3 from astrocytes mediates retinal ganglion cell loss during neuroinflammation. Acta Neuropathologica; 142: 899–915

Ghosh, S., Shang, P., Terasaki, H., Stepicheva, N., Hose, S., Yazdankhah, M., Weiss, J., Sakamoto, T., Bhutto, I. A., Xia, S., Zigler, J. S., Kannan, R., Qian, J., Handa, J. T., & Sinha, D. (2018). A role for βA3/A1-crystallin in type 2 EMT of RPE cells occurring in dry age-related Macular degeneration. Investigative Ophthalmology and Visual Science; 59: AMD104–AMD113

Gianchecchi, E., Arena, A., & Fierabracci, A. (2021). Sialic acid-siglec axis in human immune regulation, involvement in autoimmunity and cancer and potential

therapeutic treatments. In International Journal of Molecular Sciences; 22: 5774

Ginhoux, F., Greter, M., Leboeuf, M., Nandi, S., See, P., Gokhan, S., Mehler, M. F., Conway, S. J., Ng, L. G., Stanley, E. R., Samokhvalov, I. M., & Merad, M. (2010). Fate mapping analysis reveals that adult microglia derive from primitive macrophages. Science; 330: 841–845

Goodso, N. B., Kaufma, M. A., Par, K. U., & Brzezinski, J. A. (2020). Simultaneous deletion of Prdm1 and Vsx2 enhancers in the retina alters photoreceptor and bipolar cell fate specification, yet differs from deleting both genes. Development; 147: dev190272

Graw, J., Amarie, O., Kumar, D., Scheideler, A., Hrabé de Angelis, M., Przemeck, G., & Sabrautzki, S. (2017). Mutation in the Crybb1 gene encoding beta-B1-crystallin leads to recessive cataracts in the mouse. Acta Ophthalmologica; 95: S259

Gupta, N., Brown, K. E., & Milam, A. H. (2003). Activated microglia in human retinitis pigmentosa, late-onset retinal degeneration, and age-related macular degeneration. Experimental Eye Research; 76: 463–471

Guttenplan, K. A., Stafford, B. K., El-Danaf, R. N., Adler, D. I., Münch, A. E., Weigel, M. K., Huberman, A. D., & Liddelow, S. A. (2020). Neurotoxic Reactive Astrocytes Drive Neuronal Death after Retinal Injury. Cell Reports; 31: 107776

Hagen, K. M., Gordon, P., Frederick, A., Palmer, A. L., Edalat, P., Zonta, Y. R., Scott, L., Flancia, M., Reid, J. K., Joel, M., & Ousman, S. S. (2024). CRYAB plays a role in terminating the presence of pro-inflammatory macrophages in the older, injured mouse peripheral nervous system. Neurobiology of Aging; 133: 1–15

Haines, J. L., Hauser, M. A., Schmidt, S., Scott, W. K., Olson, L. M., Gallins, P., Spencer, K. L., Shu, Y. K., Noureddine, M., Gilbert, J. R., Schnetz-Boutaud, N., Agarwal, A., Postel, E. A., & Pericak-Vance, M. A. (2005). Complement factor H variant increases the risk of age-related macular degeneration. Science; 308: 419–421

Hanisch, U. K., & Kettenmann, H. (2007). Microglia: Active sensor and versatile effector cells in the normal and pathologic brain. In Nature Neuroscience; 10: 1387–1394

Hansen, J. N., Brückner, M., Pietrowski, M. J., Jikeli, J. F., Plescher, M., Beckert, H., Schnaars, M., Fülle, L., Reitmeier, K., Langmann, T., Förster, I., Boche, D., Petzold,

G. C., & Halle, A. (2022). MotiQ: an open-source toolbox to quantify the cell motility and morphology of microglia. Molecular Biology of the Cell; 33: ar99

Hersi, M., Irvine, B., Gupta, P., Gomes, J., Birkett, N., & Krewski, D. (2017). Risk factors associated with the onset and progression of Alzheimer's disease: A systematic review of the evidence. NeuroToxicology; 61: 143–187

Hildebrandt, H., & Dityatev, A. (2013). Polysialic acid in brain development and synaptic plasticity. Topics in Current Chemistry; 366: 55–96

Hoh Kam, J., Lenassi, E., Malik, T. H., Pickering, M. C., & Jeffery, G. (2013). Complement component C3 plays a critical role in protecting the aging retina in a murine model of age-related macular degeneration. American Journal of Pathology; 183: 480–492

Hong, S., Beja-Glasser, V. F., Nfonoyim, B. M., Frouin, A., Li, S., Ramakrishnan, S., Merry, K. M., Shi, Q., Rosenthal, A., Barres, B. A., Lemere, C. A., Selkoe, D. J., & Stevens, B. (2016). Complement and microglia mediate early synapse loss in Alzheimer mouse models. Science; 352: 712–716

Hoon, M., Okawa, H., Della Santina, L., & Wong, R. O. (2014). Functional architecture of the retina: Development and disease. In Progress in Retinal and Eye Research; 42: 44–84

Horstkorte, R., Nöhring, S., Wiechens, N., Schwarzkopf, M., Danker, K., Reutter, W., & Lucka, L. (1999). Tissue expression and amino acid sequence of murine UDP-N-acetylglucosamine-2-epimerase/N-acetylmannosamine kinase. European Journal of Biochemistry; 260: 923–927

Hume, D. A., Perry, V. H., & Gordon, S. (1983). Immunohistochemical localization of a macrophage-specific antigen in developing mouse retina: Phagocytosis of dying neurons and differentiation in microglial cells to form a regular array in the plexiform layers. Journal of Cell Biology; 97: 253–257

Iandiev, I., Biedermann, B., Bringmann, A., Reichel, M. B., Reichenbach, A., & Pannicke, T. (2006). Atypical gliosis in Müller cells of the slowly degenerating rds mutant mouse retina. Experimental Eye Research; 82: 449–457

Inman, D. M., & Horner, P. J. (2007). Reactive nonproliferative gliosis predominates in a

chronic mouse model of glaucoma. GLIA; 55: 942–953

Ishibashi, T., Hata, Y., Yoshikawa, H., Nakagawa, K., Sueishi, K., & Inomata, H. (1997). Expression of vascular endothelial growth factor in experimental choroidal neovascularization. Graefe's Archive for Clinical and Experimental Ophthalmology; 235: 159–167

Jiao, H., Natoli, R., Valter, K., Provis, J. M., & Rutar, M. (2015). Spatiotemporal cadence of macrophage polarisation in a model of light-induced retinal degeneration. PLoS ONE; 10: e0143952

Jiao, H., Provis, J. M., Natoli, R., & Rutar, M. (2020). Ablation of C3 modulates macrophage reactivity in the outer retina during photo-oxidative damage. Molecular Vision; 26: 679–690

Jin, D., Dai, Z., Zhao, L., Ma, T., Ma, Y., & Zhang, Z. (2024). CYR61 is Involved in Neonatal Hypoxic-ischemic Brain Damage Via Modulating Astrocyte-mediated Neuroinflammation. Neuroscience; 552: 54–64

Kannan, R., Sreekumar, P. G., & Hinton, D. R. (2016). Alpha crystallins in the retinal pigment epithelium and implications for the pathogenesis and treatment of age-related macular degeneration. In Biochimica et Biophysica Acta - General Subjects; 1860: 258–268

Karlstetter, M., Kopatz, J., Aslanidis, A., Shahraz, A., Caramoy, A., Linnartz-Gerlach, B., Lin, Y., Lückoff, A., Fauser, S., Düker, K., Claude, J., Wang, Y., Ackermann, J., Schmidt, T., Hornung, V., Skerka, C., Langmann, T., & Neumann, H. (2017). Polysialic acid blocks mononuclear phagocyte reactivity, inhibits complement activation, and protects from vascular damage in the retina. EMBO Molecular Medicine; 9: 154–166

Karlstetter, M., Scholz, R., Rutar, M., Wong, W. T., Provis, J. M., & Langmann, T. (2015). Retinal microglia: Just bystander or target for therapy? In Progress in Retinal and Eye Research; 45: 30–57

Katschke, K. J., Xi, H., Cox, C., Truong, T., Malato, Y., Lee, W. P., McKenzie, B., Arceo, R., Tao, J., Rangell, L., Reichelt, M., Diehl, L., Elstrott, J., Weimer, R. M., & Van

Lookeren Campagne, M. (2018). Classical and alternative complement activation on photoreceptor outer segments drives monocyte-dependent retinal atrophy. Scientific Reports; 8: 7348

Kauppinen, A., Niskanen, H., Suuronen, T., Kinnunen, K., Salminen, A., & Kaarniranta, K. (2012). Oxidative stress activates NLRP3 inflammasomes in ARPE-19 cells-Implications for age-related macular degeneration (AMD). Immunology Letters; 147: 29–33

Kauppinen, A., Paterno, J. J., Blasiak, J., Salminen, A., & Kaarniranta, K. (2016). Inflammation and its role in age-related macular degeneration. Cellular and Molecular Life Sciences; 73: 1765–1786

Kaur, I., Katta, S., Reddy, R. K., Narayanan, R., Mathai, A., Majji, A. B., & Chakrabarti, S. (2010). The involvement of complement factor B and complement component C2 in an Indian cohort with age-related macular degeneration. Investigative Ophthalmology and Visual Science; 51: 59–63

Kimura, K., Orita, T., Liu, Y., Yang, Y., Tokuda, K., Kurakazu, T., Noda, T., Yanai, R., Morishige, N., Takeda, A., Ishibashi, T., & Sonoda, K. H. (2015). Attenuation of EMT in RPE cells and subretinal fibrosis by an RAR-γ agonist. Journal of Molecular Medicine; 93: 749–758

Kitaoka, Y., Kitaoka, Y., Kwong, J. M. K., Ross-Cisneros, F. N., Wang, J., Rong, K. T., Sadun, A. A., & Lam, T. T. (2006). TNF-α-induced optic nerve degeneration and nuclear factor-κB p65. Investigative Ophthalmology and Visual Science; 47: 1448–1457

Klaus, C., Hansen, J. N., Ginolhac, A., Gérard, D., Gnanapragassam, V. S., Horstkorte, R., Rossdam, C., Buettner, F. F. R., Sauter, T., Sinkkonen, L., Neumann, H., & Linnartz-Gerlach, B. (2020). Reduced sialylation triggers homeostatic synapse and neuronal loss in middle-aged mice. Neurobiology of Aging; 88: 91-107

Klaus, C., Liao, H., Allendorf, D. H., Brown, G. C., & Neumann, H. (2021). Sialylation acts as a checkpoint for innate immune responses in the central nervous system. GLIA; 69: 1619–1636

Klein, R. J., Zeiss, C., Chew, E. Y., Tsai, J. Y., Sackler, R. S., Haynes, C., Henning, A. K., SanGiovanni, J. P., Mane, S. M., Mayne, S. T., Bracken, M. B., Ferris, F. L., Ott, J., Barnstable, C., & Hoh, J. (2005). Complement factor H polymorphism in age-related macular degeneration. Science; 308: 385–389

Koch, K., McLean, J., Segev, R., Freed, M. A., Berry, M. J., Balasubramanian, V., & Sterling, P. (2006). How Much the Eye Tells the Brain. Current Biology; 16: 1428–1434

Kogo, H., Tsutsumi, M., Inagaki, H., Ohye, T., Kiyonari, H., & Kurahashi, H. (2012). HORMAD2 is essential for synapsis surveillance during meiotic prophase via the recruitment of ATR activity. Genes to Cells; 17: 897–912

Kreutzberg, G. W. (1996). Microglia: A sensor for pathological events in the CNS. In Trends in Neurosciences; 19: 312–318

Krishnan, A., Sendra, V. G., Patel, D., Lad, A., Greene, M. K., Smyth, P., Gallaher, S. A., Herron, Ú. M., Scott, C. J., Genead, M., & Tolentino, M. (2023). PolySialic acid-nanoparticles inhibit macrophage mediated inflammation through Siglec agonism: a potential treatment for age related macular degeneration. Frontiers in Immunology; 14: 1237016

Kumar, H., Kawai, T., & Akira, S. (2011). Pathogen recognition by the innate immune system. International Reviews of Immunology; 30: 16–34

Kurzawa-Akanbi, M., Whitfield, P., Burté, F., Bertelli, P. M., Pathak, V., Doherty, M., Hilgen, B., Gliaudelytė, L., Platt, M., Queen, R., Coxhead, J., Porter, A., Öberg, M., Fabrikova, D., Davey, T., Beh, C. S., Georgiou, M., Collin, J., Boczonadi, V., … Lako, M. (2022). Retinal pigment epithelium extracellular vesicles are potent inducers of age-related macular degeneration disease phenotype in the outer retina. Journal of Extracellular Vesicles; 11: 12295

Langmann, T. (2007). Microglia activation in retinal degeneration. Journal of Leukocyte Biology; 81: 1345–1351

Laudisi, F., Spreafico, R., Evrard, M., Hughes, T. R., Mandriani, B., Kandasamy, M., Morgan, B. P., Sivasankar, B., & Mortellaro, A. (2013). Cutting Edge: The NLRP3

Inflammasome Links Complement-Mediated Inflammation and IL-1β Release. The Journal of Immunology; 191: 1006–1010

Lewis, A. L., Chen, X., Schnaar, R. L., & Varki, A. (2022). Sialic Acids and Other Nonulosonic Acids. In Essentials of Glycobiology. Cold Spring Harbor Laboratory Press. New York; Chapter 15

Lewis, A. L., Toukach, P., Bolton, E., Chen, X., Frank, M., Lütteke, T., Knirel, Y., Schoenhofen, I., Varki, A., Vinogradov, E., Woods, R. J., Zachara, N., Zhang, J., Kamerling, J. P., & Neelamegham, S. (2023). Cataloging natural sialic acids and other nonulosonic acids (NulOs), and their representation using the Symbol Nomenclature for Glycans. Glycobiology; 33: 99–103

Li, F., Jiang, D., & Samuel, M. A. (2019). Microglia in the developing retina. In Neural Development; 14: 12

Li, Y., & Chen, X. (2012). Sialic acid metabolism and sialyltransferases: Natural functions and applications. In Applied Microbiology and Biotechnology; 94: 887–905

Liang, K. J., Lee, J. E., Wang, Y. D., Ma, W., Fontainhas, A. M., Fariss, R. N., & Wong, W. T. (2009). Regulation of dynamic behavior of retinal microglia by CX3CR1 signaling. Investigative Ophthalmology and Visual Science; 50: 4444–4451

Liao, H., Klaus, C., & Neumann, H. (2020). Control of innate immunity by sialic acids in the nervous tissue. International Journal of Molecular Sciences; 21: 1–25

Liao, H., Winkler, J., Wißfeld, J., Shahraz, A., Klaus, C., & Neumann, H. (2021). Low molecular weight polysialic acid prevents lipopolysaccharide-induced inflammatory dopaminergic neurodegeneration in humanized SIGLEC11 transgenic mice. GLIA; 69: 2845–2862

Liao, Y., Smyth, G. K., & Shi, W. (2014). FeatureCounts: An efficient general purpose program for assigning sequence reads to genomic features. Bioinformatics; 30: 923–930

Lim, E. M. F., Hoghooghi, V., Hagen, K. M., Kapoor, K., Frederick, A., Finlay, T. M., & Ousman, S. S. (2021). Presence and activation of pro-inflammatory macrophages are associated with CRYAB expression in vitro and after peripheral nerve injury.

Journal of Neuroinflammation; 18: 82

Lim, L. S., Mitchell, P., Seddon, J. M., Holz, F. G., & Wong, T. Y. (2012). Age-related macular degeneration. In The Lancet; 379: 1728–1738

Linnartz-Gerlach, B., Schuy, C., Shahraz, A., Tenner, A. J., & Neumann, H. (2016). Sialylation of neurites inhibits complement-mediated macrophage removal in a human macrophage-neuron Co-Culture System. GLIA; 64: 35–47

Linnartz, B., Kopatz, J., Tenner, A. J., & Neumann, H. (2012). Sialic acid on the neuronal glycocalyx prevents complement c1 binding and complement receptor-3-mediated removal by microglia. Journal of Neuroscience; 32: 946–952

Linnartz, B., & Neumann, H. (2013). Microglial activatory (immunoreceptor tyrosine-based activation motif)- and inhibitory (immunoreceptor tyrosine-based inhibition motif)-signaling receptors for recognition of the neuronal glycocalyx. GLIA; 61: 37–46

Love, M. I., Huber, W., & Anders, S. (2014). Moderated estimation of fold change and dispersion for RNA-seq data with DESeq2. Genome Biology; 15: 1–21

Luna, G., Lewis, G. P., Banna, C. D., Skalli, O., & Fisher, S. K. (2010). Expression profiles of nestin and synemin in reactive astrocytes and Müller cells following retinal injury: A comparison with glial fibrillar acidic protein and vimentin. Molecular Vision; 16: 2511–2523

Lünemann, J. D., von Gunten, S., & Neumann, H. (2021). Targeting sialylation to treat central nervous system diseases. In Trends in Pharmacological Sciences; 42: 998–1008

Ma, W., Zhao, L., Fontainhas, A. M., Fariss, R. N., & Wong, W. T. (2009). Microglia in the mouse retina alter the structure and function of retinal pigmented epithelial cells: A potential cellular interaction relevant to AMD. PLoS ONE; 4: e7945

Madigan, M. C., Penfold, P. L., Provis, J. M., Balind, T. K., & Billson, F. A. (1994). Intermediate filament expression in human retinal macroglia: Histopathologic changes associated with age-related macular degeneration. Retina; 14: 65–74

McCaa, C. S. (1982). The eye and visual nervous system: anatomy, physiology and

toxicology. Environmental Health Perspectives; 44: 1–8

Mootha, V. K., Lindgren, C. M., Eriksson, K. F., Subramanian, A., Sihag, S., Lehar, J., Puigserver, P., Carlsson, E., Ridderstråle, M., Laurila, E., Houstis, N., Daly, M. J., Patterson, N., Mesirov, J. P., Golub, T. R., Tamayo, P., Spiegelman, B., Lander, E. S., Hirschhorn, J. N., … Groop, L. C. (2003). PGC-1α-responsive genes involved in oxidative phosphorylation are coordinately downregulated in human diabetes. Nature Genetics; 34: 267–273

Nadal-Nicolás, F. M., Vidal-Sanz, M., & Agudo-Barriuso, M. (2018). The aging rat retina: from function to anatomy. Neurobiology of Aging; 61: 146–168

Nakazawa, T., Matsubara, A., Noda, K., Hisatomi, T., She, H., Skondra, D., Miyahara, S., Sobrin, L., Thomas, K. L., Chen, D. F., Grosskreutz, C. L., Hafezi-Moghadam, A., & Miller, J. W. (2006). Characterization of cytokine responses to retinal detachment in rats. Molecular Vision; 12: 867–878

Natoli, R., Fernando, N., Madigan, M., Chu-Tan, J. A., Valter, K., Provis, J., & Rutar, M. (2017). Microglia-derived IL-1β promotes chemokine expression by Müller cells and RPE in focal retinal degeneration. Molecular Neurodegeneration; 12: 31

Natoli, R., Jiao, H., Barnett, N. L., Fernando, N., Valter, K., Provis, J. M., & Rutar, M. (2016). A model of progressive photo-oxidative degeneration and inflammation in the pigmented C57BL/6J mouse retina. Experimental Eye Research; 147: 114–127

Neumann, H., Linnartz, B., & Wang, Y. (2010). Microglial immunoreceptor tyrosine-based activation and inhibition motif signaling in neuroinflammation. In International Journal of Alzheimer's Disease; 2010: 58746

Newman, E. A. (1999). Sodium-bicarbonate cotransport in retinal astrocytes and Muller cells of the rat. GLIA; 26: 302–308

Nozaki, M., Raisler, B. J., Sakurai, E., Sarma, J. V., Barnum, S. R., Lambris, J. D., Chen, Y., Zhang, K., Ambati, B. K., Baffi, J. Z., & Ambati, J. (2006). Drusen complement components C3a and C5a promote choroidal neovascularization. Proceedings of the National Academy of Sciences of the United States of America; 103: 2328–2333

Ohsawa, K., Imai, Y., Sasaki, Y., & Kohsaka, S. (2004). Microglia/macrophage-specific

protein Iba1 binds to fimbrin and enhances its actin-bundling activity. Journal of Neurochemistry; 88: 844–856

Paolicelli, R. C., Bolasco, G., Pagani, F., Maggi, L., Scianni, M., Panzanelli, P., Giustetto, M., Ferreira, T. A., Guiducci, E., Dumas, L., Ragozzino, D., & Gross, C. T. (2011). Synaptic pruning by microglia is necessary for normal brain development. Science; 333: 1456–1458

Pearson, A. M. (1996). Scavenger receptors in innate immunity. Current Opinion in Immunology; 8: 20–28

Pillai, S., Netravali, I. A., Cariappa, A., & Mattoo, H. (2012). Siglecs and immune regulation. In Annual Review of Immunology; 30: 357–392

Provis, J. M., Diaz, C. M., & Penfold, P. L. (1996). Microglia in human retina: A heterogeneous population with distinct ontogenies. Perspectives on Developmental Neurobiology; 3: 213–222

Prüss-üstün, A., Zeeb, H., Mathers, C., & Repacholi, M. (2006). Solar Ultraviolet Radiation: Global burden of disease from solar ultraviolet radiation. World Health; 55: 987–999

Purves, D., Augustine, G. J., Fitzpatrick, D., Katz, L. C., LaMantia, A.-S., McNamara, J. O., & Williams, S. M. (2001). The Retina. Neuroscience. Sunderland: Sinauer Associates

Ramot, Y., Haim-Zada, M., Domb, A. J., & Nyska, A. (2016). Biocompatibility and safety of PLA and its copolymers. In Advanced Drug Delivery Reviews; 107: 153–162

Ramprasad, M. P., Terpstra, V., Kondratenko, N., Quehenberger, O., & Steinberg, D. (1996). Cell surface expression of mouse macrosialin and human CD68 and their role as macrophage receptors for oxidized low density lipoprotein. Proceedings of the National Academy of Sciences of the United States of America; 93: 14833–14838

Rashid, K., Akhtar-Schaefer, I., & Langmann, T. (2019). Microglia in retinal degeneration. Frontiers in Immunology; 10: 1975

Rasmussen, K. L., Nordestgaard, B. G., & Nielsen, S. F. (2018). Complement C3 and risk

of diabetic microvascular disease: A cohort study of 95202 individuals from the general population. Clinical Chemistry; 64: 1113–1124

Reichenbach, A., & Bringmann, A. (2020). Glia of the human retina. GLIA; 68: 768–796

Reis, L. M., Khan, A., Kariminejad, A., Ebadi, F., Tyler, R. C., & Semina, E. V. (2011). VSX2 mutations in autosomal recessive microphthalmia. Molecular Vision; 17: 2527–2532

Rivera, J. C., Sitaras, N., Noueihed, B., Hamel, D., Madaan, A., Zhou, T., Honoré, J. C., Quiniou, C., Joyal, J. S., Hardy, P., Sennlaub, F., Lubell, W., & Chemtob, S. (2013). Microglia and interleukin-1β in ischemic retinopathy elicit microvascular degeneration through neuronal semaphorin-3A. Arteriosclerosis, Thrombosis, and Vascular Biology; 33: 1881–1891

Rosen, A. M., & Stevens, B. (2010). The role of the classical complement cascade in synapse loss during development and glaucoma. In Advances in Experimental Medicine and Biology; 703: 75–93)

RStudio Team. (2020). RStudio: Integrated Development Environment for R. RStudio, PBC, Boston, MA. http://www.rstudio.com/

Santos, A. M., Calvente, R., Tassi, M., Carrasco, M. C., Martín-Oliva, D., Marín-Teva, J. L., Navascués, J., & Cuadros, M. A. (2008). Embryonic and postnatal development of microglial cells in the mouse retina. Journal of Comparative Neurology; 506: 224–239

Sato, C., & Kitajima, K. (2013). Disialic, oligosialic and polysialic acids: Distribution, functions and related disease. In Journal of Biochemistry; 154: 115–136

Schmidt, C. Q., Hipgrave Ederveen, A. L., Harder, M. J., Wuhrer, M., Stehle, T., & Blaum, B. S. (2018). Biophysical analysis of sialic acid recognition by the complement regulator factor H. Glycobiology; 28: 765–773

Schnaar, R. L., Gerardy-Schahn, R., & Hildebrandt, H. (2014). Sialic acids in the brain: Gangliosides and polysialic acid in nervous system development, stability, disease, and regeneration. Physiological Reviews; 94: 461–518

Schwarzkopf, M., Knobeloch, K. P., Rohde, E., Hinderlich, S., Wiechens, N., Lucka, L., Horak, I., Reutter, W., & Horstkorte, R. (2002). Sialylation is essential for early development in mice. Proceedings of the National Academy of Sciences of the United States of America; 99: 5267–5270

Segler Stahl, K., Webster, J. C., & Brunngraber, E. G. (1983). Changes in the concentration and composition of human brain gangliosides with aging. Gerontology; 29: 161–168

Shahraz, A., Lin, Y., Mbroh, J., Winkler, J., Liao, H., Lackmann, M., Bungartz, A., Zipfel, P. F., Skerka, C., & Neumann, H. (2022). Low molecular weight polysialic acid binds to properdin and reduces the activity of the alternative complement pathway. Scientific Reports; 12: 5818

Shen, G., Li, Y., Zeng, Y., Hong, F., Zhang, J., Wang, Y., Zhang, C., Xiang, W., Wang, J., Fang, Z., Qi, W., Yang, X., Gao, G., & Zhou, T. (2023). Kallistatin Deficiency Induces the Oxidative Stress-Related Epithelial-Mesenchymal Transition of Retinal Pigment Epithelial Cells: A Novel Protagonist in Age-Related Macular Degeneration. Investigative Ophthalmology and Visual Science; 64: 15

Silverman, S. M., & Wong, W. T. (2018). Microglia in the Retina: Roles in Development, Maturity, and Disease. Annual Review of Vision Science; 4: 45–77

Šoić, D., Štambuk, J., Tijardović, M., Keser, T., Lauc, G., Bulum, T., Lovrenčić, M. V., Rebrina, S. V., Tomić, M., Novokmet, M., Smirčić-Duvnjak, L., & Gornik, O. (2023). Human complement component C3 N-glycome changes in type 1 diabetes complications. Frontiers in Endocrinology; 14: 1101154

Son, Y., Lim, D., Park, S., Song, I. S., Kim, J. H., Shin, S., Jang, H., Liu, K. H., O, Y., Song, G. Y., Kang, W., Cho, Y. seok, Na, M. K., Chung, H., & Oh, S. (2020). Ilimaquinone inhibits neovascular age-related macular degeneration through modulation of Wnt/β-catenin and p53 pathways. Pharmacological Research; 161: 105146

Song, Y., Wei, D., Wang, Q., Guo, J., Zhu, Y., Shang, E., & Duan, J. ao. (2024). Luteoloside mitigates premature age-related macular degeneration by suppressing

p53-p21-Rb1 axis: Insights from transcriptomic analysis, serum metabolomics and gut microbiota analysis. Journal of Pharmaceutical and Biomedical Analysis; 248: 116296

Springelkamp, H., Mishra, A., Hysi, P. G., Gharahkhani, P., Höhn, R., Khor, C. C., Cooke Bailey, J. N., Luo, X., Ramdas, W. D., Vithana, E., Koh, V., Yazar, S., Xu, L., Forward, H., Kearns, L. S., Amin, N., Iglesias, A. I., Sim, K. S., van Leeuwen, E. M., … Zhang, K. (2015). Meta-analysis of Genome-Wide Association Studies Identifies Novel Loci Associated With Optic Disc Morphology. Genetic Epidemiology; 39: 207–216

Stence, N., Waite, M., & Dailey, M. E. (2001). Dynamics of microglial activation: A confocal time-lapse analysis in hippocampal slices. GLIA; 33: 256–266

Stevens, B., Allen, N. J., Vazquez, L. E., Howell, G. R., Christopherson, K. S., Nouri, N., Micheva, K. D., Mehalow, A. K., Huberman, A. D., Stafford, B., Sher, A., Litke, A. M. M., Lambris, J. D., Smith, S. J., John, S. W. M., & Barres, B. A. (2007). The Classical Complement Cascade Mediates CNS Synapse Elimination. Cell; 131: 1164–1178

Stone, J., & Dreher, Z. (1987). Relationship between astrocytes, ganglion cells and vasculature of the retina. Journal of Comparative Neurology; 255: 35–49

Subramanian, A., Tamayo, P., Mootha, V. K., Mukherjee, S., Ebert, B. L., Gillette, M. A., Paulovich, A., Pomeroy, S. L., Golub, T. R., Lander, E. S., & Mesirov, J. P. (2005). Gene set enrichment analysis: A knowledge-based approach for interpreting genome-wide expression profiles. Proceedings of the National Academy of Sciences of the United States of America; 102: 15545–15550

Sui, G. Y., Liu, G. C., Liu, G. Y., Gao, Y. Y., Deng, Y., Wang, W. Y., Tong, S. H., & Wang, L. (2013). Is sunlight exposure a risk factor for age-related macular degeneration? A systematic review and meta-analysis. In British Journal of Ophthalmology; 97: 389–394

Taylor, H. R., Munoz, B., West, S., Bressler, N. M., Bressler, S. B., & Rosenthal, F. S. (1990). Visible light and risk of age-related macular degeneration. In Transactions of the American Ophthalmological Society; 88: 163–178)

Traving, C., & Schauer, R. (1998). Structure, function and metabolism of sialic acids. In

Cellular and Molecular Life Sciences; 54: 1330–1349

Tseng, W. A., Thein, T., Kinnunen, K., Lashkari, K., Gregory, M. S., D'Amore, P. A., & Ksander, B. R. (2013). NLRP3 inflammasome activation in retinal pigment epithelial cells by lysosomal destabilization: Implications for age-related macular degeneration. Investigative Ophthalmology and Visual Science; 54: 110–120

Tuo, J., Wang, Y., Cheng, R., Li, Y., Chen, M., Qiu, F., Qian, H., Shen, D., Penalva, R., Xu, H., Ma, J. X., & Chan, C. C. (2015). Wnt signaling in age-related macular degeneration: Human macular tissue and mouse model. Journal of Translational Medicine; 13: 330

Uemura, A., Fruttiger, M., D'Amore, P. A., De Falco, S., Joussen, A. M., Sennlaub, F., Brunck, L. R., Johnson, K. T., Lambrou, G. N., Rittenhouse, K. D., & Langmann, T. (2021). VEGFR1 signaling in retinal angiogenesis and microinflammation. In Progress in Retinal and Eye Research; 84: 100954

Usui-Ouchi, A., Usui, Y., Kurihara, T., Aguilar, E., Dorrell, M. I., Ideguchi, Y., Sakimoto, S., Bravo, S., & Friedlander, M. (2020). Retinal microglia are critical for subretinal neovascular formation. JCI Insight; 5: e137317

Varki, A. (2008). Sialic acids in human health and disease. In Trends in Molecular Medicine; 14: 351–360

Varki, A., & Gagneux, P. (2012). Multifarious roles of sialic acids in immunity. Annals of the New York Academy of Sciences; 1253: 16–36

Varki, N. M., Strobert, E., Dick, E. J., Benirschke, K., & Varki, A. (2011). Biomedical differences between human and nonhuman hominids: Potential roles for uniquely human aspects of sialic acid biology. Annual Review of Pathology: Mechanisms of Disease; 6: 365–393

Vecino, E., & Acera, A. (2015). Development and programed cell death in the mammalian eye. International Journal of Developmental Biology; 59: 63–71

Völgyi, B., Abrams, J., Paul, D. L., & Bloomfield, S. A. (2005). Morphology and tracer coupling pattern of alpha ganglion cells in the mouse retina. Journal of Comparative Neurology; 492: 66–77

Volland, S., Esteve-Rudd, J., Hoo, J., Yee, C., & Williams, D. S. (2015). A Comparison of Some Organizational Characteristics of the Mouse Central Retina and the Human Macula. PLoS ONE; 10: e0125631

Wang, F., Jiang, Z., Lou, B., Duan, F., Qiu, S., Cheng, Z., Ma, X., Yang, Y., & Lin, X. (2021). αB-Crystallin Alleviates Endotoxin-Induced Retinal Inflammation and Inhibits Microglial Activation and Autophagy. Frontiers in Immunology; 12: 641999

Wang, G., Liu, H. Y., Meng, X. W., Chen, Y., Zhao, W. M., Li, W. T., Xu, H. B., Peng, K., & Ji, F. H. (2024). Complement C1q-mediated microglial synaptic elimination by enhancing desialylation underlies sevoflurane-induced developmental neurotoxicity. Cell and Bioscience; 14: 42

Wang, Y., Zhao, X., Gao, M., Wan, X., Guo, Y., Qu, Y., Chen, Y., Li, T., Liu, H., Jiang, M., Wang, F., & Sun, X. (2021). Myosin 1f-mediated activation of microglia contributes to the photoreceptor degeneration in a mouse model of retinal detachment. Cell Death and Disease; 12: 926

Weidemann, W., Klukas, C., Klein, A., Simm, A., Schreiber, F., & Horstkorte, R. (2010). Lessons from GNE-deficient embryonic stem cells: Sialic acid biosynthesis is involved in proliferation and gene expression. Glycobiology; 20: 107–117

Werneburg, S., Jung, J., Kunjamma, R. B., Ha, S. K., Luciano, N. J., Willis, C. M., Gao, G., Biscola, N. P., Havton, L. A., Crocker, S. J., Popko, B., Reich, D. S., & Schafer, D. P. (2020). Targeted Complement Inhibition at Synapses Prevents Microglial Synaptic Engulfment and Synapse Loss in Demyelinating Disease. Immunity; 52: 167-182.e7

Wickham, M. (2016). ggplot2: Elegant graphics for data analysis. Springer-Verlag

Wiedemann, J., Rashid, K., & Langmann, T. (2018). Resveratrol induces dynamic changes to the microglia transcriptome, inhibiting inflammatory pathways and protecting against microglia-mediated photoreceptor apoptosis. Biochemical and Biophysical Research Communications; 501: 239–245

Willoughby, C. E., Shafiq, A., Ferrini, W., Chan, L. L. Y., Billingsley, G., Priston, M., Mok, C., Chandna, A., Kaye, S., & Héon, E. (2005). CRYBB1 mutation associated with

congenital cataract and microcornea. Molecular Vision; 11: 587–593

Wißfeld, J., Abou Assale, T., Cuevas-Rios, G., Liao, H., & Neumann, H. (2024). Therapeutic potential to target sialylation and SIGLECs in neurodegenerative and psychiatric diseases. Frontiers in Neurology; 15: 1330874

Wolfrum, P., Fietz, A., Schnichels, S., & Hurst, J. (2022). The function of p53 and its role in Alzheimer's and Parkinson's disease compared to age-related macular degeneration. In Frontiers in Neuroscience; 16: 1029473

Xin-Zhao Wang, C., Zhang, K., Aredo, B., Lu, H., & Ufret-Vincenty, R. L. (2012). Novel method for the rapid isolation of RPE cells specifically for RNA extraction and analysis. In Experimental Eye Research; 102: 1–9

Yang, Y., Liu, W., Sun, K., Jiang, L., & Zhu, X. (2019). Tmem30a deficiency leads to retinal rod bipolar cell degeneration. Journal of Neurochemistry; 148: 400–412

Yao, P. L., Parmar, V. M., Choudhary, M., & Malek, G. (2022). NURR1 expression regulates retinal pigment epithelial-mesenchymal transition and age-related macular degeneration phenotypes. Proceedings of the National Academy of Sciences of the United States of America; 119: e2202256119

Young, K., & Morrison, H. (2018). Quantifying microglia morphology from photomicrographs of immunohistochemistry prepared tissue using imagej. Journal of Visualized Experiments; 136: 57648

Yu, G., Wang, L. G., Han, Y., & He, Q. Y. (2012). ClusterProfiler: An R package for comparing biological themes among gene clusters. OMICS A Journal of Integrative Biology; 16: 284–287

Yuan, L., & Neufeld, A. H. (2001). Activated microglia in the human glaucomatous optic nerve head. Journal of Neuroscience Research; 64: 523–532

Zarantonello, A., Revel, M., Grunenwald, A., & Roumenina, L. T. (2023). C3-dependent effector functions of complement. In Immunological Reviews; 313: 120–138

Zeng, H. Y., Zhu, X. A., Zhang, C., Yang, L. P., Wu, L. M., & Tso, M. O. M. (2005). Identification of sequential events and factors associated with microglial activation,

migration, and cytotoxicity in retinal degeneration in rd mice. Investigative Ophthalmology and Visual Science; 46: 2992–2999

Zhang, J., Bai, Y., Huang, L., Qi, Y., Zhang, Q., Li, S., Wu, Y., & Li, X. (2015). Protective effect of autophagy on human retinal pigment epithelial cells against lipofuscin fluorophore A2E: implications for age-related macular degeneration. Cell Death & Disease; 6: e1972

Zhang, J. F., Liu, J., Wu, J. L., Li, W. F., Chen, Z. W., & Yang, L. S. (2019). Progression of the role of CRYAB in signaling pathways and cancers. In OncoTargets and Therapy; 12: 4129–4139

9. Acknowledgements

Although I initially felt insecure about working in a laboratory due to my limited experience, Prof. Dr. Harald Neumann generously offered me the opportunity to work as a student assistant. It was through this position in AG Neumann that I truly began to develop research and practical lab skills. I greatly admire and appreciate Dr. Neumann's ability to remain available despite his many responsibilities. Naturally, projects and human interactions come with challenges, but I have grown to accept and understand the full spectrum of experiences that have shaped my PhD journey. I am especially grateful to Dr. Neumann for his patience and for encouraging me to pursue and complete my PhD.

I also want to thank the members of my PhD committee—Prof. Dr. Herbert Hildebrandt, Prof. Dr. Jochem Walter, and Prof. Dr. Wolfram S. Kunz—for kindly offering their valuable time to guide me and promptly address my questions throughout my PhD.

The AG Neumann members exemplify how kind and supportive colleagues can enhance performance and work atmosphere. I am sincerely grateful with Dr. Christine Klaus, who was an invaluable mentor during the early stages of my master's and PhD projects. I am also thankful to Tawfik Abou Assale, from whom I learned a great deal from experiments and friendship. Special thanks to Jonas Winkler for introducing me to "real" lab work. I would also like to express my gratitude to Rita Jietou, who consistently lifted my spirits and lightened my time in the lab. My thanks extend to all the former and current AG Neumann colleagues who supported me, either with their knowledge or positive attitude.

Alongside my PhD journey, my friends—both here in Bonn and in Mexico—helped me maintain balance by offering fresh perspectives and reminding me of my strengths. I am also deeply grateful to my partner, who, without even trying, provides me with a solid foundation of stability, affection, and healthy patience. Despite our fields of interest are very different, I have learned a great deal from him. Lastly, my love and gratitude go to my family, that by overcoming their own odds, unconsciously broke patterns and enabled me to go beyond what was expected of a humble and shy boy from the remote countryside. Although we sometimes struggle to fully understand each other's worlds, due to our distinct environments, they have always made sacrifices to support me in pursuing ambitions and dreams that even I cannot always fully comprehend.